Synchronization Analysis by Means of Recurrences in Phase Space

Dissertation zur Erlangung des akademischen Grades
Doktor der Naturwissenschaften (Dr. rer. nat.)
in der Wissenschaftsdisziplin Nichtlineare Dynamik

Eingereicht an der
Mathematisch-Naturwissenschaftlichen Fakultät
der Universität Potsdam

von
M. Carmen Romano Blasco

Potsdam, im August 2004

Contents

List of Abbreviations and Notations

PS	Phase Synchronization
LS	Lag Synchronization
ILS	Intermittent Lag Synchronization
GS	Generalized Synchronization
CS	Complete Synchronization
RPs	Recurrence Plots
RQA	Recurrence Quantification Analysis
RR	Recurrence Rate (percentage of recurrent points in the RP)
CRP	Cross Recurrence Plot
JRP	Joint Recurrence Plot
CPR	Correlation of Probability of Recurrence (index for PS)
JPR	Joint Probability of Recurrence (index for GS)
SPR	Similarity of Probability of Recurrence (index for GS)
$\|\cdot\|$	norm
$\Theta(\cdot)$	Heaviside function
ε	threshold for the computation of the RP
σ	standard deviation
$< \cdot >$	average
μ	coupling strength
ν	frequency mismatch
Φ	phase
$P(\tau)$	probability that the trajectory recurs after the time τ

Chapter 1

Introduction

This work deals with the connection between two basic phenomena in Nonlinear Dynamics: synchronization of chaotic systems and recurrences in phase space. Synchronization takes place when two or more systems adapt (synchronize) some characteristic of their respective motions, due to an interaction between the systems or to a common external forcing. The appearance of synchronized dynamics in chaotic systems is rather universal but not trivial. In some sense, the possibility that two chaotic systems synchronize is counterintuitive: chaotic systems are characterized by the sensitivity to different initial conditions. Hence, two identical chaotic systems starting at two slightly different initial conditions evolve in a different manner, and after a certain time, they become uncorrelated. Therefore, at a first glance, it does not seem to be plausible that two chaotic systems are able to synchronize. But as we will see later, synchronization of chaotic systems has been demonstrated.

The study of synchronization goes back to the 17th century and begins with the analysis of synchronization of nonlinear periodic systems. Well known examples are the synchronization of two pendulum clocks that hang on the same beam (it was through this system, that Huygens discovered synchronization), the synchronized flashing of fireflies, or the peculiarities of adjacent organ pipes which can almost annihilate each other or speak in unison. But the research of chaotic synchronization does not begin until the eighties [20, 62, 2, 61], where it was shown that two chaotic systems can become completely synchronized, i. e. their time evolution becomes identical. This finding has had very important consequences for the design of secure communication devices [84, 104, 28]. The synchronized chaotic trajectories can be used to mask messages and prevent their interception. In [2, 78] the notion of complete synchronization of chaotic systems was generalized, allowing the non identity between the coupled systems. And some time later, Rosenblum et al. considered a rather weak degree of synchronization between chaotic oscillators, of which their associated phases become locked, whereas their amplitudes remain almost uncorrelated. Hence, they called this kind of synchronization, phase synchronization [74]. Not only laboratory exper-

iments have demonstrated phase synchronization of chaotic oscillators, such as electronic circuits [58], lasers [3] and electrochemical oscillators [30, 31, 32], but also natural systems can exhibit phase synchronization. For example, the dynamics of the cardiorespiratory system [79], an extended ecological system [11], and the electroencephalographic activity of Parkinsonian patients [88] display synchronization features.

On one hand it is important to investigate the conditions under which synchronization of chaotic systems occurs, and on the other hand, to develop tests for the detection of synchronization. In this work, I concentrate on the second task for the cases of phase synchronization (PS) and generalized synchronization (GS). Several measures have been proposed so far for the detection of PS and GS (see Secs. 5.1 and 5.3). However, difficulties arise with the detection of synchronization in systems subjected to rather large amounts of noise and/or instationarities, which are common when analyzing experimental data. The new measures that will be proposed in the course of this thesis are rather robust with respect to these effects. They hence allow to be applied to data, which have evaded synchronization analysis so far.

The proposed tests for synchronization in this work are based on the fundamental property of recurrences in phase space. The concept of recurrence goes back to Poincaré [67], who proved that after a sufficiently long time, the trajectory of a chaotic system in phase space will return arbitrarily close to any former point of its route with probability one. The concept of recurrence within the framework of chaotic systems was, since then, not considered anymore until the sixties, with Lorenz's discovery of three ordinary differential equations that exhibit chaotic behavior [43]. In [44] Lorenz wrote about "natural occurring analogues", i. e. dynamical states that are very close to states that have happened in the past. Based on this concept, he proposed different algorithms to predict the future evolution of dynamical systems. Later on, Eckmann et al. introduced the method of recurrence plots (RPs), a technique that visualizes the recurrences of a dynamical system and gives information about the behavior of its trajectory in phase space. This method has become rather popular in the last years because of its applicability to rather short and non-stationary time series. Furthermore, a more theoretical study of the relationship between RPs and the properties of dynamical systems has been addressed in [16, 19, 22, 90, 91, 92, 93]. However, there are still open problems: e. g. the extension of the concept of recurrence to study the relationship between interacting systems has not been exhaustively investigated from a theoretical point of view. This is one of the main points that will be addressed here.

In this thesis, the recurrences of two interacting systems are related to the synchronization features of chaotic systems. After an introduction to the method of RPs (Chap. 2), a new method to calculate recurrence plots of multivariate time series is proposed [72], which is called "joint recurrence plots" (Chap. 3). This technique differs substantially from the former method proposed for the analysis

of bivariate time series and allows to estimate joint dynamical invariants of the interacting subsystems, such as the joint Rényi entropy of second order and the cross mutual information. Although this method is suitable for the study of any coupled system, I concentrate on the analysis of synchronization of chaotic systems by means of the joint Rényi entropy (Chap. 4). However, this analysis yields valuable information only when the parameters of the system under consideration can be changed systematically and it is rather time consuming. Hence, in the last part of the thesis four different indices for the analysis of PS and GS are proposed, which are also based on recurrences [73, 42]. They indicate the onset of PS and respectively GS rather well and therefore, they are appropriate as test statistics for the performance of a hypothesis test. They have the advantage, that they are applicable also for systems with a rather strong phase diffusion, such as the paradigmatic Rössler system in the funnel regime. Furthermore, the proposed indices are rather pragmatic, as they allow detecting synchronization for time series, which are strongly corrupted by noise and non-stationarities. An analysis based on these measures is then demonstrated for experimental data from electrochemical oscillators (Chap. 5).

Chapter 2

Recurrence Plots and their Quantification

Recurrence Plots (RPs) were introduced by Eckmann et al. in 1987 to visualize the behavior of trajectories of dynamical systems in phase space [18]. There, they write: *"… recurrence plots are rather easily obtained aids for the diagnosis of dynamical systems. They display important and easily interpretable information about time scales which are otherwise rather inaccessible."*
Later, this tool of data analysis proved to be useful not only as a visualization technique, but also motivated quantification measures for the local rate of divergence, even for data sets with just few hundred values [39, 41]. Furthermore, a set of measures, constituting what is now known as Recurrence Quantification Analysis (RQA) was proposed to quantify systematically the different structures found in RPs [98]. The RQA became very popular and found numerous applications in different fields, especially for natural systems, such as in Physiology [98, 99, 109, 108, 110], in Geology [49, 96] and in Economy [23, 86]. Among these applications, the contributions to the enhancement of the method of RQA by Marwan et al. are outstanding, reflecting the wide applicability of this technique to measured data sets [45, 46, 47, 50].
Moreover, the theoretical relationship between RPs and dynamical invariants, such as the largest Lyapunov exponent, was not given explicitly in the papers cited above. For example, Atay and Alintaş suggest in [8] that the average length of the diagonal lines in the RP is directly related to the inverse of the largest Lyapunov exponent. However, a rigorous derivation of this conjecture was lacking. In [19, 91] it was shown rigorously first, that there is a direct relationship between RPs and some dynamical invariants, so that RPs can be also used to estimate them. Further theoretical results about RPs and nonlinear dynamics were presented in [92, 93, 94].
In this chapter, a short introduction to the methods of RPs and RQA is given and the main theoretical results about recurrences and some properties of dynamical systems are summarized.

2.1   Recurrence Plots

As mentioned above, RPs provide a visual impression of the trajectory of a dynamical system in phase space. Suppose that the time series $\{\mathbf{x}_i\}_{i=1}^{N}$ representing the trajectory of a system in phase space is given, with $\mathbf{x}_i \in \mathcal{R}^d$. The RP is based on the following matrix

$$\mathbf{R}_{i,j} = \Theta(\varepsilon - ||\mathbf{x}_i - \mathbf{x}_j||), \qquad i, j = 1, \ldots, N, \tag{2.1}$$

where $\Theta(\cdot)$ is the Heaviside function, $|| \cdot ||$ denotes a norm and ε is a predefined threshold. We will use the maximum norm throughout this work. Then the value 1 is coded as a black dot and the value 0 as white one in the RP. Hence, we obtain a 2-dimensional $N \times N$ matrix, which is symmetric with respect to the main diagonal $i = j$.

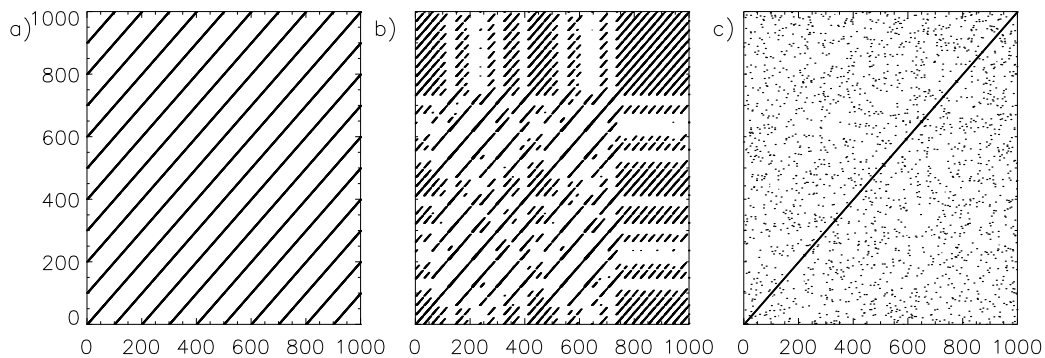In Fig. 2.1 the RPs of three prototypical systems are represented. We observe

Figure 2.1: a) RP of a purely periodic function, b) RP of the Rössler system with standard parameters (see Eq. 2.19), c) RP of a realization of white noise.

that the RP of the purely periodic function (Fig. 2.1 a) consists of uninterrupted diagonal lines separated by the distance T, where T is the period of the function. This is due to the fact, that after one period, the position of the system in phase space is exactly the same, i.e we have identical recurrence and ε could be very small. The RP of white noise (Fig. 2.1 c) is rather homogenous, consisting of mainly single points, indicating the randomness of the system. The RP of a chaotic system (in this case, the Rössler system with standard parameters, Eq. 2.19) is represented in Fig. 2.1 b. The predominant structures here are intermediate between the ones of periodic systems and the ones of purely stochastic systems:

- The distance (in perpendicular direction to the main diagonal) between

diagonal lines is not constant. This is due to the multiple time scales present in chaotic systems.

- The diagonal lines are, due to the exponential divergence of nearby trajectories (the hallmark of chaos), interrupted. When the trajectory of a system recurs to the neighborhood of a former visited point in phase space, the system behaves similarly to the former situation (which is a hallmark of determinism). But due to the sensitivity to slightly different initial conditions, after a certain time, the trajectories separate and hence, the line is interrupted.

We note that the length of the lines is related to the predictability of the system. This is the argument used in [8], among others, to argue that the largest Lyapunov exponent can be estimated by the inverse of the mean length of the diagonals in the RP. However, as will be shown later, this relationship does not hold exactly.

2.2 Recurrence Quantification Analysis

The Recurrence Quantification Analysis (RQA) was introduced in [106, 98] with the aim of quantifying the structures found in RPs and hence, go beyond the purely visual classification. The quantification of diagonal structures is fundamental for the RQA, since they are a key concept for the classification of the different kinds of dynamics. Some of the most important recurrence quantification measures are

- **Recurrence Rate** (RR): it is defined as the percentage of black points in the RP, i. e.

$$RR = \frac{1}{N^2} \sum_{i,j=1}^{N} \Theta(\varepsilon - ||\mathbf{x}_i - \mathbf{x}_j||). \tag{2.2}$$

  Note, that the definition of RR coincides with the definition of the correlation sum [24].

- **Determinism** (DET): it is defined as the the percentage of black points which are part of diagonal lines of at least length l_{min} [48],

$$DET = \frac{\sum_{l=l_{min}}^{N} lP(l)}{\sum_{l=1}^{N} lP(l)}, \tag{2.3}$$

  where $P(l)$ denotes the probability to find a diagonal line of length l in the RP. This measure was introduced to quantify how predictable a system is. For a periodic system, one gets $DET = 1$ and for a purely stochastic system DET tends to zero. However, the results depend crucially on l_{min}, of which the choice is ambiguous [48].

- **Divergence** (DIV): it is defined as

$$DIV = \frac{1}{L_{max}}, \tag{2.4}$$

  where L_{max} is the length of the longest diagonal found in the RP (of course, the main diagonal is not considered). This measure has been used also to estimate the largest Lyapunov exponent [97].

- **Entropy** ($ENTR$): is the Shannon entropy of the frequency distribution of diagonal lines in the plot,

$$ENTR = -\sum_{l=l_{min}}^{N} p(l) \ln p(l), \tag{2.5}$$

  where $p(l) = P(l)/\sum_{l=l_{min}}^{N} P(l)$. This measure is designed to quantify the complexity of the deterministic structure in the system [48].

- **Trend** ($TREND$): it is a linear regression coefficient over the recurrence rate on each diagonal line parallel to the main diagonal,

$$TREND = \frac{\sum_{i=1}^{\tilde{N}}(i - \tilde{N}/2)(RR_i - <RR_i>)}{\sum_{i=1}^{\tilde{N}}(i - \tilde{N})^2}, \tag{2.6}$$

  where $\tilde{N} < N$, to avoid finite size effects [48]. This measure quantifies the non-stationarity of the system.

- **Ratio** ($RATIO$): is the ratio between DET and RR,

$$RATIO = \frac{DET}{RR}. \tag{2.7}$$

  This measure was introduced to determine some transitions between different physiological states, where the RR changes, but not the DET [98].

The measures of RR, DET, DIV and $ENTR$ can be also computed for each diagonal line parallel to the main diagonal. Hence, they can be obtained in dependence on the distance to the main diagonal [47].

The measures introduced up to now quantify efficiently the structures that different dynamical systems generate in RPs. However, the main problem with them is that they depend rather sensitively on the choice of the embedding parameters. Dealing with measured data, one has to embed the time series first to reconstruct the attractor in phase space [87]. But there is some ambiguity in choosing the most appropriate embedding parameters [29]. Slightly different choices of the parameters lead to a different outcome when applying the RQA.

The measures mentioned above are based on the distribution of diagonal lines $P(l)$. Marwan and Kurths introduced three new measures [47], that quantify vertical structures (respectively horizontal, because of the symmetry), which are:

- **Laminarity** (LAM): it is analogously to the DET, defined as the percentage of black points, that belong to vertical lines of at least length l_{min}:

$$LAM = \frac{\sum_{l=l_{min}}^{N} lP_v(l)}{\sum_{l=1}^{N} lP_v(l)}, \quad (2.8)$$

  where $P_v(l)$ denotes the probability to find a vertical line of length l in the RP. LAM quantifies the occurrence of laminar states in a given trajectory.

- **Trapping Time** (TT): it is the mean length of vertical lines

$$TT = \frac{\sum_{l=l_{min}}^{N} lP_v(l)}{\sum_{l=l_{min}}^{N} P_v(l)}, \quad (2.9)$$

  and measures the mean time that the system sticks to a certain state, i. e. how long the trajectory will be trapped.

- **Maximal vertical length** (V_{max}), is analogous to the longest diagonal line in the RP (respectively, its inverse can be considered).

These last measures based on the distribution of vertical lines, allow to identify intermittency and laminar structures, which makes it possible to detect chaos-chaos transitions [45]. Furthermore, they are rather robust against noise. This is a great advantage of these measures with respect to the former RQA ones.

However, because of the uncertainty in the quantification measures of diagonal structures in RPs, it is necessary to introduce new measures, which are invariant with respect to different choices of the embedding parameters. In the next section, I resume the theoretical results about the estimation of dynamical invariants by means of the recurrence matrix found by Thiel et al. [91, 92].

2.3 Dynamical Invariants Estimated by Recurrence Plots

The visual inspection of RPs of different systems (e. g. Fig. 2.1) reveals that diagonal structures play a key role in the codification of the dynamics in the recurrence matrix. Hence, it is plausible to look at the distribution of diagonal lines in the RP in order to see how it depends on the dynamics of the system under consideration. To estimate the distribution of the diagonals in the RP, we start with the correlation sum [25]

$$C(\varepsilon) = \frac{1}{N^2} \times \{\text{number of pairs } (i,j) \text{ with} ||\mathbf{x}_i - \mathbf{x}_j|| < \varepsilon\}, \quad (2.10)$$

where N is assumed to be large but finite [1]. Note that the definition of the recurrence rate RR (Eq. 2.2) coincides with the definition of the correlation sum [90]

$$C(\varepsilon) = \frac{1}{N^2} \sum_{i=1}^{N} \Theta\left(\varepsilon - ||\mathbf{x}_i - \mathbf{x}_j||\right) = RR. \tag{2.11}$$

This fact allows to relate the known results about the correlation integral to the structures in RPs.

Suppose that we have a trajectory $\mathbf{x}(t)$ in the basin of an attractor in the d-dimensional phase space. The state of the system is measured at time intervals τ. Let $\{1, 2, ..., M(\varepsilon)\}$ be a partition of the phase space in boxes of size ε. Then $p(i_1, ..., i_l)$ denotes the joint probability that $\mathbf{x}(\tau)$ is in the box i_1, $\mathbf{x}(2\tau)$ is in the box i_2, ..., and $\mathbf{x}(l\tau)$ is in the box i_l. The order-2 Rényi entropy [71, 26] is then defined as

$$K_2 = -\lim_{\tau \to 0} \lim_{\varepsilon \to 0} \lim_{l \to \infty} \frac{1}{l\tau} \ln \sum_{i_1, ..., i_l} p^2(i_1, \ldots, i_l). \tag{2.12}$$

We can approximate $p(i_1, \ldots, i_l)$ by the probability $P_{t,l}(\mathbf{x}, \varepsilon)$ of finding a sequence of points in boxes of length ε about $\mathbf{x}(t = \tau)$, $\mathbf{x}(t = 2\tau)$, ..., $\mathbf{x}(t = l\tau)$. Assuming that the system is ergodic, which is always the case for chaotic systems as they are mixing, we obtain

$$\sum_{i_1, ..., i_l} p^2(i_1, \ldots, i_l) = \frac{1}{N} \sum_{t=1}^{N} p_t(i_1, \ldots, i_l) \sim \frac{1}{N} \sum_{t=1}^{N} P_{t,l}(\mathbf{x}, \varepsilon), \tag{2.13}$$

where $p_t(i_1, \ldots, i_l)$ represents the probability of being in the box i_1 at time $t = \tau$, in the box i_2 at time $t = 2\tau$, ... and in the box i_l at time $t = l\tau$. Furthermore, we can express $P_{t,l}(\mathbf{x}, \varepsilon)$ by means of the recurrence matrix

$$P_{t,l}(\mathbf{x}, \varepsilon) = \frac{1}{N} \sum_{s=1}^{N} \prod_{m=0}^{l-1} \Theta\left(\varepsilon - ||\mathbf{x}_{t+m} - \mathbf{x}_{s+m}||\right) = \frac{1}{N} \sum_{s=1}^{N} \prod_{m=0}^{l-1} R_{t+m, s+m}. \tag{2.14}$$

Hence, we obtain an estimator for the order-2 Rényi entropy by means of the RP

$$\hat{K}_2(\varepsilon, l) = -\frac{1}{l\tau} \ln \underbrace{\left(\frac{1}{N^2} \sum_{t,s=1}^{N} \prod_{m=0}^{l-1} R_{t+m, s+m} \right)}_{(*)}. \tag{2.15}$$

Note that $(*)$ is the cumulative distribution of diagonal lines $P_\varepsilon^c(l)$ in the RP, i. e. the probability to find a diagonal of at least length l.

On the other hand, we note that for the l-dimensional correlation integral $C_l(\varepsilon)$ [27]

$$C_l(\varepsilon) \sim \varepsilon^\nu \exp(-l\tau K_2) \simeq \sum_{i_1, ..., i_l} p^2(i_1, ..., i_l) \tag{2.16}$$

holds, where ν represents the correlation dimension. Hence, we conclude that

$$P_\varepsilon^c(l) \simeq \varepsilon^\nu \exp(-l\tau K_2). \tag{2.17}$$

Based on this formula, we can estimate two dynamical invariants from RPs:

- the **Rényi entropy of second order** $\hat{K}_2$: representing $P_\varepsilon^c(l)$ in a logarithmic scale versus l we obtain a straight line with slope $-\hat{K}_2(\varepsilon)\tau$ for large l's.

- the **correlation dimension** $\hat{\nu}$: from the vertical distance between $P_\varepsilon^c(l)$ for different ε's, one can derive

$$\hat{\nu}(\varepsilon) = \ln\left(\frac{P_\varepsilon^c(l)}{P_{\varepsilon+\Delta\varepsilon}^c(l)}\right)\left(\ln\left(\frac{\varepsilon}{\varepsilon+\Delta\varepsilon}\right)\right)^{-1}. \tag{2.18}$$

These measures have, among other things the advantage that if only one observable of the system under consideration has been observed, one can calculate them from the reconstructed attractor [1, 87]. In contrast, this does not hold for the measures proposed for the RQA. Furthermore, Thiel et al. have shown in [92], that the estimation of these two dynamical invariants by means of recurrences is independent of the embedding parameters used for the phase space reconstruction. That means, even without any embedding, one gets the correct estimation for K_2 and ν. This is a main advantage of this estimation, as the choice of the appropriate embedding parameters is still a controversial issue.

For the practical application, one has to compute first the cumulative distribution of diagonals for different thresholds ε. The question arises, which values of ε one should consider. As each system has its own amplitude, which may differ from one system to another one, the choice will be different for each case and it is subjected to some arbitrariness. In order to overcome this problem, we can fix the value of RR, because it is normalized, and then calculate the corresponding ε. This can be done by the following algorithm:

1. Compute the distances between each pair of vectors $i = 1, \ldots, N$ and $j = 1, \ldots, i$. Then we obtain the series d_l with $l = 1, \ldots, N^2/2$ (because of the symmetry of the RP, we consider only the half of the matrix. Actually the length of the series of the distances is equal to $N^2/2 - N$, but for large N, we can write $N^2/2$.).

2. Sort the distances d_l in ascending order and denote the rank ordered distances by $\tilde{d}_l$, with $l = 1, \ldots, N^2/2$.

3. For a fixed RR (Eq. 2.2) the corresponding ε is then given by $\tilde{d}_m$, with $m = RR\frac{N^2}{2}$. For example, if $RR = 0.01$, then $\varepsilon = \tilde{d}_{0.01N^2/2}$. We then know that 1% of the distances are less or equal than ε, and hence $RR = 0.01$.

Like this, we avoid the arbitrariness of choosing appropriate values for ε and we can apply the same procedure for all systems.

2.3.1   Application to Three Prototypical Examples

In order to illustrate the estimation of dynamical invariants by means of RPs we compute K_2 for the three prototypical examples presented in Fig. 2.1:

- The sine function: $f(t) = \sin(\omega t)$ (Fig. 2.2). The slope of the logarithmic distribution of diagonals versus the length is almost zero, which is reflected in Fig. 2.2 b. Hence, the estimated value of $\hat{K}_2$ is almost zero, as expected. The fact that it is not exactly zero, is due to the finite size of the plot (in principle, the diagonal lines have infinite length, but they are truncated because of the finite time series we have used).
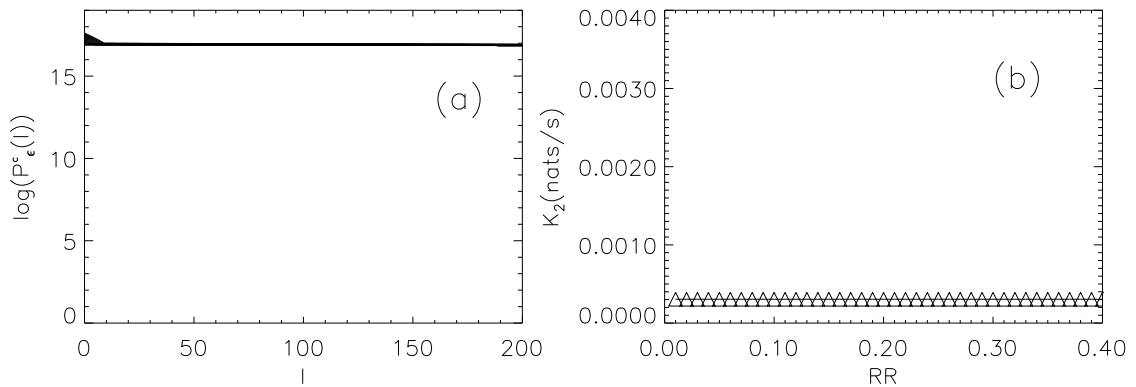

Figure 2.2: (a) Distribution of diagonals in the RP of a sine function. Each line represents the distribution of diagonals for a different RR (Eq. 2.2). Here, the lines corresponding to values of RR from 0.01 to 0.9 are shown. (b) Estimator of the Rényi entropy.

- The Rössler system:

$$\begin{aligned}
\dot{x} &= -y - z \\
\dot{y} &= x + ay \\
\dot{z} &= b + z(x - c),
\end{aligned}$$

(2.19)

with standard parameters $a = b = 0.2$ and $c = 5.7$. In the logarithmic representation of the distribution of diagonals (Fig. 2.3 a) we see two different slopes. The second slope begins at $l = 85$ (which corresponds to 17

s, because the sampling unit is equal to 0.2 s), and as the Rényi entropy is defined for large lengths (Eq. 2.12), this is the slope which is related to K_2. We obtain $\hat{K}_2 = 0.071 \pm 0.001$, which is in excellent accordance with the values given in the literature [4]. The first slope ranges from $l = 0$ to $l = 84$ and is larger than the second one. The dynamical meaning of this first slope is linked to the geometry of the attractor under consideration [91]. The parameters regarded in this example (Eq. 2.19) correspond to a three-band structure in the chaotic attractor, i. e. the trajectory recurs typically to a former neighborhood after three rotations about the fixed point. The length $l = 84$ corresponds to the time (in the sampling units used for the integration) that the trajectory needs to complete three rotations about the fixed point. Varying the parameter c of Eq. 2.19, the structure of the attractor changes, so that we obtain a two-band or a one-band structure. Then, the first slope extends from $l = 1$ to the length corresponding to two, respectively one rotations about the fixed point. Furthermore, the distribution of unstable periodic orbits (UPOs) of the Rössler system with the three-band attractor has a maximum at the period length three.

Hence, the first slope and the length l_{crit}, where the second slope begins, are related to the topology of the attractor. One can interpret the first slope as the short-term predictability of the system: if we do not have enough information about the attractor (the trajectory is shorter than e. g. three rotations), we can predict the evolution of the trajectory worse than if we have a longer trajectory. In the case of the set of parameters $a = b = 0.2$ and $c = 5.7$, the "skeleton" of the attractor consists mainly of a UPO of length three. If the trajectory is longer than three rotations, the attractor has been "scanned" almost completely, and the prediction becomes easier. We also find a scaling law of the first slope with the threshold ε, because the lines in $\log(P_\varepsilon^c(l))$ versus l are parallel for small l's too.

Furthermore, these results coincide with the findings presented by Anishchenko et al. in [5] by an independent method. There, they have related the first slope to the amplitude fluctuations and the second one, to the phase diffusion of the system. This is also related to the nonhyperbolicity of the system under consideration. The traditional estimation of K_2 by means of the correlation sum of the embedded time series [24] does not allow to detect the first slope. Hence, this is an important advantage of the estimation based on RPs.

- Independent white noise: $\{\eta_i\}_{i=1}^N$, with autocorrelation function $C_{i,j} = \delta_{i,j}$. The distribution of diagonal lines, as well as the estimator for K_2 are represented in Fig. 2.4. We observe, that the slope of $\log(P_\varepsilon^c(l))$ versus l is different for each threshold ε, and increases with decreasing ε, i. e. the slope tends to "$-\infty$" as ε tends to zero and therefore, the estimate of K_2 is ∞, as expected.
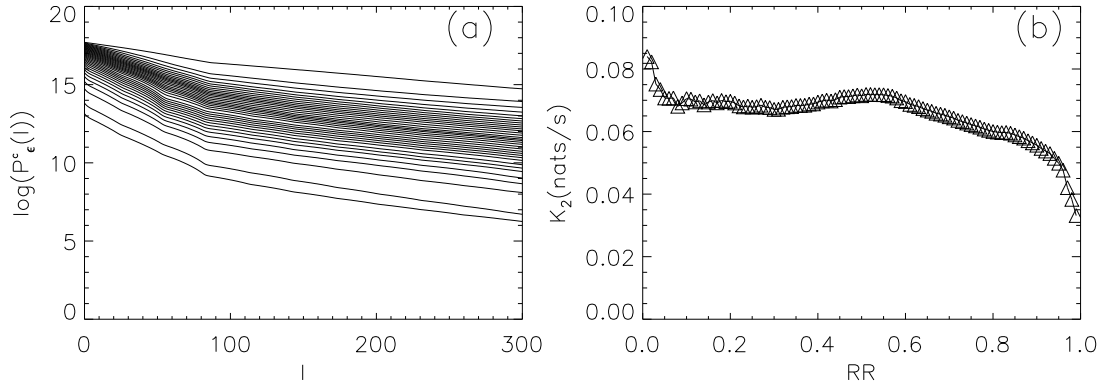
Figure 2.3: (a) Distribution of diagonals in the RP of a Rössler system with standard parameters (Eq. 2.19). Each line corresponds to a different RR. (b) Estimator of the Rényi entropy.

2.4   Information about the System Contained in RPs

One important question from a theoretical point of view is, how much information about the system is lost by mapping the trajectory of the system onto the binary recurrence matrix of Eq. (2.1). Intuitively, one would expect that some properties of the dynamical system are not reflected in the RP anymore, as the trajectory is now represented only by two symbols ("1" and "0"). But Thiel et al. have shown in [93] that it is possible to reconstruct the rank order of a time series, when only its corresponding RP is given. They have proposed an algorithm that reconstructs the time series, except its distribution, only considering the relationship between the neighborhoods of each point.
Furthermore, it is known, that it is possible to calculate the dynamical invariants from the rank ordered time series [9]. Hence, **all relevant information about the dynamics of the system is contained in RP**.

2.5   Cross Recurrence Plots

Cross Recurrence Plots (CRPs) are an extension of RPs and were introduced to analyze the dependencies between two different systems [107, 47]. They can be considered as generalization of the linear cross correlation function. The main advantage of CRPs with respect to other data analysis methods is their appli-
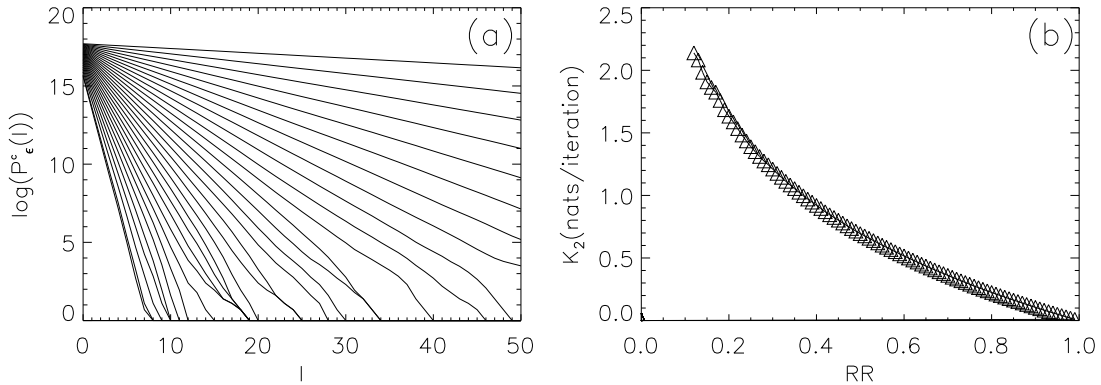
Figure 2.4: (a) Distribution of diagonals in the RP of white noise normally distributed. Each line corresponds to a different RR. (b) Estimator of the Rényi entropy.

cability to non-stationary and rather short time series [47, 18]. They have been successfully applied to observed time series from climate, geological and physiological systems [49, 46, 45, 47, 82].

Suppose we have two dynamical systems, each one represented by the trajectories $\{\mathbf{x}_i\}$ and $\{\mathbf{y}_i\}$ in a d-dimensional phase space for $i = 1, \ldots, N$. Analogously to the RP, the corresponding cross recurrence matrix is defined by

$$CR_{i,j} = \Theta\left(\varepsilon - ||\mathbf{x}_i - \mathbf{y}_j||\right), \qquad i, j = 1, \ldots, N. \tag{2.20}$$

The measures of the RQA can be applied also to this cross recurrence matrix, but they may be misleading for certain applications. For example, if we consider two sine functions in their two dimensional phase spaces with frequencies ω and 2ω we obtain a periodic pattern of lines with slope 2 (see Fig. 2.5) (or 0.5 if the axes are interchanged). Then, even though the relationship between both sine functions is totally deterministic, the value obtained for DET will be rather low because we do not have lines parallel to the main diagonal, i. e. with slope 1. However, a detailed interpretation of diagonal lines in CRPs is given in [51].

  Furthermore, the method of CRPs has some other important drawbacks, mainly due to the calculation of distances between two physically different time series. As the physical units of the two time series are in general different, it makes no sense from a physical point of view to compute the differences. Furthermore, if the dimensions of the systems $\mathbf{x}$ and $\mathbf{y}$ are different, it is not clear how to
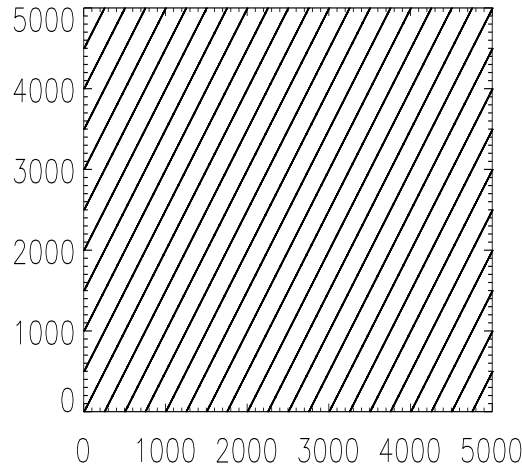
Figure 2.5: CRP of two periodic functions with frequencies ω and 2ω, respectively. The determinism for this example is equal to 0.395.

compute the difference between vectors with a different number of components. Moreover, the CRP is not invariant with respect to an interchange of the order of the components of the systems' vectors: suppose that we have measured $\mathbf{x}_i$ and $\mathbf{y}_i$, for $i = 1, \ldots, N$, with $\mathbf{x}, \mathbf{y} \in \mathcal{R}^3$. If we now interchange the first and the second component in $\mathbf{x}$ and then compute the CRP, the matrix in general changes.

Beyond this, the method of CRPs is not appropriate for the analysis of synchronization of oscillators [1], as demonstrated in the next section.

2.6   Analysis of Phase Synchronization by Means of CRPs

In order to show, that the method of CRPs is not appropriate for the analysis of synchronization of oscillators, we consider two mutually coupled Rössler systems

$$
\begin{aligned}
\dot{x}_1 &= -(1+\nu)x_2 - x_3 + \mu(y_1 - x_1), & \dot{y}_1 &= -(1-\nu)y_2 - y_3 + \mu(x_1 - y_1), \\
\dot{x}_2 &= (1+\nu)x_1 + 0.15x_2, & \dot{y}_2 &= (1-\nu)y_1 + 0.15y_2, \\
\dot{x}_3 &= 0.2 + x_3(x_1 - 10), & \dot{y}_3 &= 0.2 + y_3(y_1 - 10), & (2.21)
\end{aligned}
$$

---

[1] for a definition of the different kinds of synchronization, see Chapter 4

where the parameter ν governs the detuning of the frequencies and where the coupling is diffusive and proportional to the coupling strength μ. The system is integrated using the Runge-Kutta integrator of fourth order. The integration step is $h = 0.01$ and the sampling time $s = 20$, so that the time interval between two consecutive points is $\Delta t = 0.2$ s.

We regard the phase synchronized (PS) and non-phase synchronized (non-PS) regimes. First we compute the CRP between the first components of each Rössler subsystem for both cases. We rescale the original time series, to have the same amplitude scale in both signals [82]

$$\tilde{x}_i = \frac{x_i - \bar{x}}{\sigma_x}, \tag{2.22}$$

where $\bar{x}$ denotes the mean and σ_x the standard deviation of $\{x_i\}_{i=1}^{N}$. Then we use embedding parameters $d = 6$ and $\tau = 8$ according to the methods of false nearest neighbors and first zero of autocorrelation function [29]. We choose the threshold ε, such that the recurrence rate RR is almost the same for both PS and non-PS cases in order to compare better the other quantification measures (RR is set to approximately 3%, following the indications given in [82]). The resulting CRPs are illustrated in Fig. 2.6. At a first glance it seems that in both plots there are
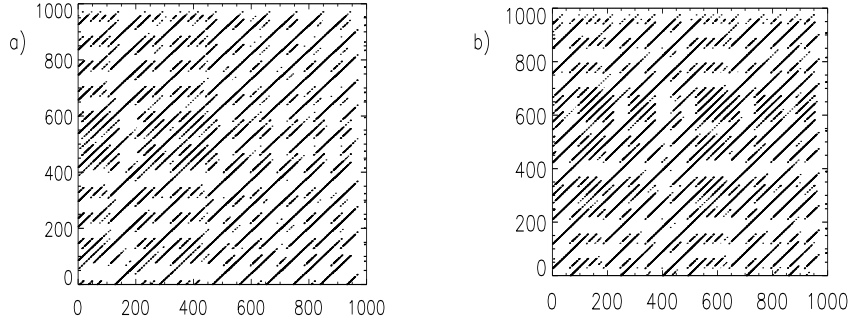

Figure 2.6: CRPs for the first component of each Rössler subsystem of Eqs. 2.21. a) $\mu = 0.01$, non-PS, b) $\mu = 0.04$, PS.

lines, which are parallel to the main diagonal. To quantify this visual impression, we calculate some of the RQA measures. We compute 100 different trajectories corresponding to 100 different initial conditions for the mutually coupled Rössler systems, and calculate the mean value and the standard deviation for each measure.

We see that all computed measures are very similar for the non-PS and PS cases, and hence they are not appropriate to distinguish between both regimes (Tab. 2.1)

[2]. Hence, the CRP method does not seem to be suitable for the detection of small

Measure	**Non-phase synchronized**	**Phase synchronized**
RR	0.0298 ± 0.000138	0.0293 ± 0.000169
$DET(l_{\min} = 2)$	0.963 ± 0.000188	0.958 ± 0.000303
$ENTR(l_{\min} = 2)$	0.0461 ± 0.000233	0.0408 ± 0.000203
$RATIO$	32.346 ± 0.147	32.747 ± 0.180
MAX_LINE	146.03 ± 0.585	146.80 ± 0.372

Table 2.1: RQA measures for the CRPs (mean values over 100 different initial conditions and standard deviations) calculated for two coupled Rössler systems.

changes in the coupling strength, and especially the transition from non-PS to PS, despite the qualitatively different behavior of the coupled systems.
Therefore, we propose in the next chapter a new approach to calculate multivariate recurrence plots, that avoids all the above mentioned problems. Moreover, our new method enables to estimate invariants of the dynamics and information measures, analogously to the RPs.

---

[2]We do not calculate the $TREND$, as it does not make sense for this system, since the percentage of recurrence points in dependence on the distance to the main diagonal oscillates periodically.

Chapter 3

Joint Recurrences

As shown in Sec. 2.5, the definition of CRPs (Eq. 2.20) has some drawbacks. On the other hand, the method of RPs has been applied very successfully in many different fields [45, 50, 49, 98]. Hence, the following question arises:

How can we exploit the concept of recurrence in phase space to analyze the relationship between interacting systems?

The new definition of multivariate RPs which is proposed in this chapter, is based on the idea of **joint recurrence**. That means, that **the probability that both systems recur simultaneously to the neighborhood of a formerly visited point in their respective phase space** is considered. We demonstrate that by this new definition all problems mentioned in Sec. 2.5 are overcome. Moreover, in Chap. 4 it will be shown that the new method is also appropriate for the analysis of complex synchronization, in contrast to the one given by (Eq. 2.20).

The idea of joint recurrence can be easily introduced based on the concept of the mutual information. Hence, I recall in the next section the definition of the cross mutual information as a motivation for the new approach to compute and analyze multivariate RPs.

3.1   Mutual Information by Means of Recurrences

The mutual information quantifies the amount of information that we obtain from the measurement of one variable on another. Hence, it has become a widely applied measure to quantify linear and nonlinear dependencies within or between time series (auto respectively cross mutual information) [69]. Suppose, that we have two dynamical systems represented by the orbits $\mathbf{x}_i$ and $\mathbf{y}_i$, with $i = 1, \ldots, N$. We can associate both systems with probability distributions $\{p_m\}_{m=1}^M$ and $\{q_l\}_{l=1}^L$, where p_m (respectively q_l) denotes the probability that the system is located in the box m of the partition of the phase space (respectively the box l). Furthermore, we can assign to both systems the joint probability distribution $\{p_{m,l}\}_{m,l=1}^{M,L}$ [10]. Then, the generalized mutual information of second

order [68] is given by

$$I_2(\mathbf{x}, \mathbf{y}) = H_2(\mathbf{x}) + H_2(\mathbf{y}) - H_2(\mathbf{x}, \mathbf{y}), \tag{3.1}$$

where H_2 denotes the Rényi information of second order [10], which is defined by

$$H_2(\mathbf{x}) = -\log \sum_{m=1}^{M} p_m^2. \tag{3.2}$$

Substituting (3.2) in Eq. (3.1) we obtain

$$I_2(\mathbf{x}, \mathbf{y}) = -\log \sum_{m=1}^{M} p_m^2 - \log \sum_{l=1}^{N} q_l^2 + \log \sum_{m,l=1}^{M,L} p_{m,l}^2. \tag{3.3}$$

Analogously to the considerations in Sec. 2.3, one can estimate H_2 by means of the recurrence matrix in the following way:
Due to the ergodicity of the system, we can state first that

$$\sum_{m=1}^{M} p_m^2 = \frac{1}{N} \sum_{t=1}^{N} p_{m(t)},$$

where $p_{m(t)}$ represents the probability of the system occupying the box m of the partition at time t. Furthermore, we can approximate $p_{m(t)}$ by

$$p_{m(t)} \simeq \frac{1}{N} \sum_{s=1}^{N} \Theta(\varepsilon^{\mathbf{x}} - ||\mathbf{x}_t - \mathbf{x}_s||) = \frac{1}{N} \sum_{s=1}^{N} R_{t,s}^{\mathbf{x}},$$

where in spite of considering a fixed partition of the phase space, we allow the "boxes" to move along the trajectory: each point of the orbit is the center of one box, and therefore, the boxes are allowed to overlap.
Hence, we can claim that

$$H_2(\mathbf{x}) \simeq -\log \frac{1}{N^2} \sum_{t,s=1}^{N} R_{t,s}^{\mathbf{x}}, \tag{3.4}$$

i. e. that it is possible to estimate the Rényi information of second order by means of RPs. But in order to compute the mutual information I_2 we also have to estimate the joint Rényi information $H_2(\mathbf{x}, \mathbf{y})$. Analogously to the Rényi information of a single system [91], we state

$$\sum_{m,l=1}^{M,L} p_{m,l}^2 = \frac{1}{N} \sum_{t=1}^{N} p_{m(t),l(t)},$$

where $p_{m(t),l(t)}$ is the probability that the system $\mathbf{x}$ is situated in the box m at time t and the system $\mathbf{y}$ is located in the box l also at time t. Furthermore, we can make the following approximation:

$$p_{m(t),l(t)} \simeq \frac{1}{N} \sum_{s=1}^{N} \Theta(\varepsilon^{\mathbf{x}} - ||\mathbf{x}_t - \mathbf{x}_s||)\Theta(\varepsilon^{\mathbf{y}} - ||\mathbf{y}_t - \mathbf{y}_s||) = \frac{1}{N} \sum_{s=1}^{N} R_{t,s}^{\mathbf{x}} R_{t,s}^{\mathbf{y}},$$

where $R_{t,s}^{\mathbf{x}}$ and $R_{t,s}^{\mathbf{y}}$ represent the single recurrence matrices of both systems. As we compute a joint probability, both conditions $||\mathbf{x}_t - \mathbf{x}_s|| < \varepsilon^{\mathbf{x}}$ and $||\mathbf{y}_t - \mathbf{y}_s|| < \varepsilon^{\mathbf{y}}$ must be fulfilled simultaneously, and this is expressed by the multiplication of the Heaviside functions. Hence, we find

$$H_2(\mathbf{x}, \mathbf{y}) \simeq -\log \frac{1}{N^2} \sum_{t,s=1}^{N} R_{t,s}^{\mathbf{x}} R_{t,s}^{\mathbf{y}}. \tag{3.5}$$

Substituting Eq. (3.4) and Eq. (3.5) in Eq. (3.3), we obtain

$$\hat{I}_2(\mathbf{x}, \mathbf{y}) = -\log \frac{1}{N^2} \sum_{t,s=1}^{N} R_{t,s}^{\mathbf{x}} - \log \frac{1}{N^2} \sum_{t,s=1}^{N} R_{t,s}^{\mathbf{y}} + \log \frac{1}{N^2} \sum_{t,s=1}^{N} R_{t,s}^{\mathbf{x}} R_{t,s}^{\mathbf{y}}. \tag{3.6}$$

Analogously, we can estimate the auto-mutual information by means of the recurrence matrix. The auto-mutual information quantifies the amount of information about $\mathbf{x}(t)$ than can be obtained from $\mathbf{x}(t + \tau)$, and is defined as

$$I_2(\mathbf{x}(t), \mathbf{x}(t + \tau)) = 2H_2(\mathbf{x}) - H_2(\mathbf{x}(t), \mathbf{x}(t + \tau)). \tag{3.7}$$

Hence, the estimator of the auto-mutual information by means of recurrences is given by

$$\hat{I}_2(\mathbf{x}(t), \mathbf{x}(t + \tau)) = -2\log \frac{1}{N^2} \sum_{t,s=1}^{N} R_{t,s}^{\mathbf{x}} + \log \frac{1}{N^2} \sum_{t,s=1}^{N} R_{t,s}^{\mathbf{x}} R_{t+\tau,s+\tau}^{\mathbf{x}}. \tag{3.8}$$

This measure for the Rössler system with standard parameters (Eq. 2.19) is represented in Fig. 3.1. The estimation of I_2 by means of RPs is independent of the norm used to compute the distances (solid line), whereas the estimation of I_2 by the usual algorithm (e. g. presented in [29]) depends on the norm used: the Euclidean norm corresponds to the dashed line and the maximum norm to the solid line.

Moreover, this leads to the introduction of the delayed cross mutual information

$$\hat{I}_2(\mathbf{x}(t), \mathbf{y}(t + \tau)) = -\log \frac{1}{N^2} \sum_{t,s=1}^{N} R_{t,s}^{\mathbf{x}} - \log \frac{1}{N^2} \sum_{t,s=1}^{N} R_{t,s}^{\mathbf{y}} + \log \frac{1}{N^2} \sum_{t,s=1}^{N} R_{t,s}^{\mathbf{x}} R_{t+\tau,s+\tau}^{\mathbf{y}}, \tag{3.9}$$
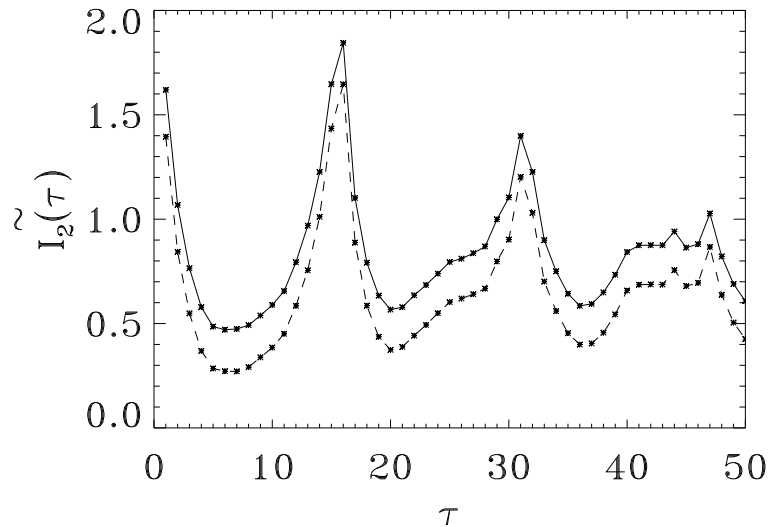
Figure 3.1: (Auto)-mutual information of the Rössler system with standard parameters (Eq. 2.19). The estimation of I_2 by means of RPs is independent of the norm used to compute the distances (solid line), whereas the estimation of I_2 by the usual algorithm (e. g. presented in [29]) depends on the norm used: Euclidean norm (dashed line), maximum norm (solid line).

which quantifies the amount of information that we obtain from the measurement of one variable at time t on another variable at time $t + \tau$.

In summary, we have shown that it is possible to estimate the mutual information (auto, cross and cross-delayed) by means of the recurrence matrices of the corresponding systems.

3.2   Joint Recurrence Matrix

We have seen in Sec. 3.1 that in order to estimate the mutual information it is necessary to consider the two matrices $R_{i,j}^{\mathbf{x}}$ and $R_{i,j}^{\mathbf{y}}$ separately, i. e. we do not *mix* the phase spaces of $\mathbf{x}$ and $\mathbf{y}$, in contrast to the definition of the CRP (Eq. 2.20). We rather extend the phase space to $\mathcal{R}^{d_1+d_2}$, where d_1 and d_2 are the phase space dimensions of the corresponding (sub)systems, which are in general different. Furthermore, we consider a different threshold for each system ($\varepsilon^{\mathbf{x}}$ and $\varepsilon^{\mathbf{y}}$), so that we can apply the criteria to choose them separately [90, 91, 108], respecting the natural measure of both systems. Hence, it is intuitive to introduce the following **joint recurrence matrix**

$$JR_{i,j}^{\mathbf{x},\mathbf{y}} = \Theta\left(\varepsilon^{\mathbf{x}} - ||\mathbf{x}_i - \mathbf{x}_j||\right)\Theta\left(\varepsilon^{\mathbf{y}} - ||\mathbf{y}_i - \mathbf{y}_j||\right), \qquad i,j = 1,\ldots,N, \quad (3.10)$$

i. e.

$$JR_{i,j}^{\mathbf{x},\mathbf{y}} = \begin{cases} 1, & \text{if} \quad ||\mathbf{x}_i - \mathbf{x}_j|| < \varepsilon^{\mathbf{x}} \quad \text{and} \quad ||\mathbf{y}_i - \mathbf{y}_j|| < \varepsilon^{\mathbf{y}} \\ 0, & \text{else.} \end{cases}$$

The graphical representation of the matrix $JR_{i,j}^{\mathbf{x},\mathbf{y}}$ is called **Joint Recurrence Plot** (JRP). Note, that the definition (Eq. 2.1) of an RP is a special case of the definition of Eq. 3.10 if we have only one system, which is an important advantage with respect to CRPs (Eq. 2.20).

The problems mentioned in Sec. 2.5 are also overcome: if both systems have different dimensions d_1 and d_2, the joint recurrence is still well defined, as well as in the case of having different physical units of each component. Additionally, the JRP is invariant under permutation of the coordinates, and the lines of slope 1 are still directly related to the predictability of the system.

In this approach a recurrence takes place if one point of the trajectory $\mathbf{x}_j$ for $j = 1, 2, \ldots$ returns to the neighborhood of a former point $\mathbf{x}_i$ in phase space, and **simultaneously** one point of the trajectory $\mathbf{y}_j$ for $j = 1, 2, \ldots$ returns to the neighborhood of a former point $\mathbf{y}_i$. That means, that we consider the joint probability that both recurrences happen simultaneously in their respective (sub-)phase spaces. In contrast, in CRPs one cannot interpret the matrix $CR_{i,j}$ as a "real" recurrence in the physical sense.

A more direct comparison between CRPs and JPRs is illustrated in Fig. 3.2: in (a) and (b) the RPs of two mutually coupled Rössler systems are represented (Eqs. 2.21). There, the coupling strength between both systems is still not large enough to yield synchronization (see Chap. 4). In Fig. 3.2 c the JRP of the whole system is represented. It is almost "empty", except for the main diagonal. This is because both oscillators are not in PS, and hence the probability of having a joint recurrence is rather small. In Fig. 3.2 d the CRP of both oscillators is represented. By means of this plot, it is much harder to draw some conclusions about the interaction between both oscillators, because there is almost no difference between the CRP for the oscillators in PS and the CRP for the non-PS regime (see Sec. 2.6).

Moreover, one can easily consider the delayed version of the joint recurrence matrix

$$JR_{i,j}^{\mathbf{x},\mathbf{y}}(\tau) = \Theta\left(\varepsilon^{\mathbf{x}} - ||\mathbf{x}_i - \mathbf{x}_j||\right)\Theta\left(\varepsilon^{\mathbf{y}} - ||\mathbf{y}_{i+\tau} - \mathbf{y}_{j+\tau}||\right), \qquad i, j = 1, \ldots, N - \tau, \tag{3.11}$$

which can be useful for the analysis of interacting delayed systems (and also for the study of lag synchronization [75, 83]), or even for systems with feedback.

3.3 Quantification of Joint Recurrence Plots

Analogously to Sec. 2.3 and 3.1, we can estimate the joint Rényi entropy of second order if we consider the joint probability of recurrence instead of the probability
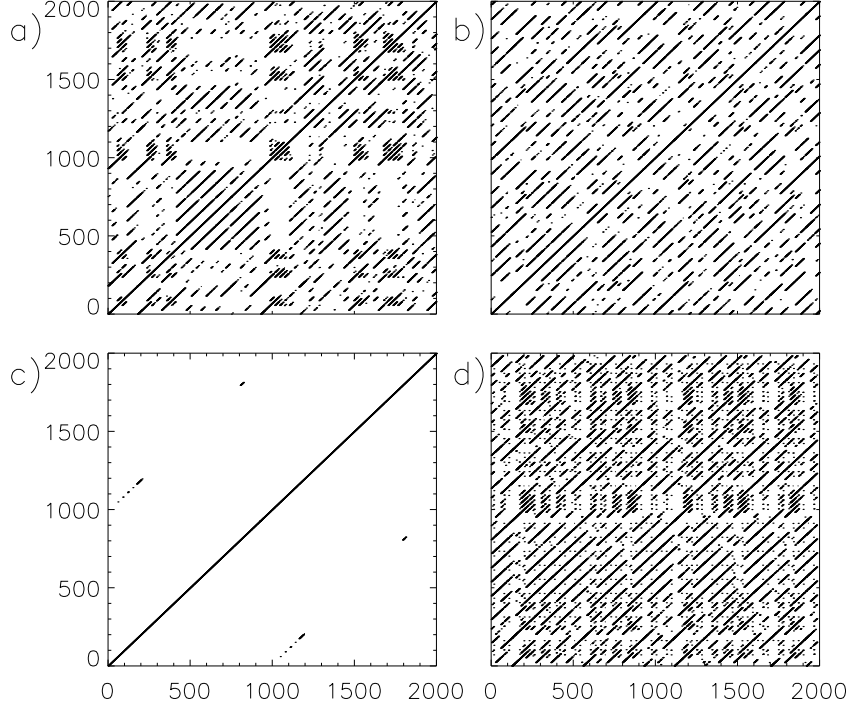
Figure 3.2: a) and b) RPs of two mutually coupled Rössler oscillators (Eqs. 2.21). c) JRP of both oscillators, d) CRP of both oscillators.

of recurrence of a single system. This is an extension of the estimator presented in [91, 92], which is useful for the analysis of two or more interacting systems, as will be shown in Chap. 4.

The **joint Rényi entropy of second order** is defined as

$$JK_2 = -\lim_{\tau \to 0} \lim_{\varepsilon \to 0} \lim_{l \to \infty} \frac{1}{l\tau} \log \sum_{i_1,\ldots,i_l,j_1,\ldots,j_l} p^2(i_1,\ldots,i_l,j_1,\ldots,j_l), \qquad (3.12)$$

where $p(i_1, i_2, \ldots, i_l, j_1, j_2, \ldots, j_l)$ is the joint probability that $\mathbf{x}(\tau)$ is in box i_1, $\mathbf{x}(2\tau)$ is in box i_2, ..., $\mathbf{x}(l\tau)$ is in box i_l and **simultaneously** $\mathbf{y}(\tau)$ is in box j_1, $\mathbf{y}(2\tau)$ is in box j_2, ..., and $\mathbf{y}(l\tau)$ is in box j_l. Similarly to Sec. 2.3, using the ergodicity of the system, we can state

$$\sum_{i_1,\ldots,i_l,j_1,\ldots,j_l} p^2(i_1,\ldots,i_l,j_1,\ldots,j_l) = \frac{1}{N} \sum_{t=1}^{N} p_t(i_1,\ldots,i_l,j_1,\ldots,j_l)$$

On the other hand, we can make the following approximation

$$p_t(i_1, \ldots, i_l, j_1, \ldots, j_l) \simeq \frac{1}{N} \sum_{s=1}^{N} \prod_{m=0}^{l-1} \Theta(\varepsilon^{\mathbf{x}} - ||\mathbf{x}_{t+m} - \mathbf{x}_{s+m}||)\Theta(\varepsilon^{\mathbf{y}} - ||\mathbf{y}_{t+m} - \mathbf{y}_{s+m}||).$$

Then, substituting this expression in Eq. 3.12, we get

$$\widehat{JK_2}(\varepsilon^{\mathbf{x}}, \varepsilon^{\mathbf{y}}, l) = -\frac{1}{l\tau} \log \left(\underbrace{\frac{1}{N^2} \sum_{t,s=1}^{N} \prod_{m=0}^{l-1} JR_{t+m,s+m}}_{*} \right). \tag{3.13}$$

Note, that $*$ is the cumulative distribution of diagonals $P^c_{\varepsilon^{\mathbf{x}},\varepsilon^{\mathbf{y}}}(l)$ in the JRP, i.e the probability to find a diagonal of at least length l in the JRP. Hence, representing it logarithmically versus l, one obtains a straight line for small thresholds $\varepsilon^{\mathbf{x}}, \varepsilon^{\mathbf{y}}$ and long lines, whose slope is equal the joint Rényi entropy multiplied with the sampling time interval.

Another measure for the quantification of JRPs is related to the **recurrence rate RR** or probability of occurrence of a black point in an RP. After choosing the thresholds $\varepsilon^{\mathbf{x}}$ and $\varepsilon^{\mathbf{y}}$ for the RPs of both subsystems so, that $RR^{\mathbf{x}} = RR^{\mathbf{y}} = RR$ (see algorithm presented in Sec. 2.3), we plot $RR^{\mathbf{x},\mathbf{y}}$ versus RR. If there is no statistical dependence between $\mathbf{x}$ and $\mathbf{y}$, then one can calculate the probability to find a recurrence point in the JRP as the product of the probability to find a recurrence point in the RP of $\mathbf{x}$ with the probability to find a recurrence point in the RP of $\mathbf{y}$

$$RR^{x,y} = RR^x RR^y = RR^2, \qquad \text{if } \mathbf{x} \text{ and } \mathbf{y} \text{ are independent.} \tag{3.14}$$

The opposite case is that $\mathbf{x}$ depends strongly on $\mathbf{y}$. Suppose that $\mathbf{x}$ and $\mathbf{y}$ are identical, i. e. $x_i = y_i \quad \forall i$. In this case, we obviously have

$$RR^{x,y} = RR^x = RR^y = RR \qquad \text{if } \mathbf{x} \text{ and } \mathbf{y} \text{ are completely synchronized.} \tag{3.15}$$

If the systems are anticorrelated we expect a curve that is below the parabola given by Eq. (3.14). Then the plot of $RR^{x,y}$ versus RR yields a first insight into the statistical dependence between $\mathbf{x}$ and $\mathbf{y}$.

3.4 Application of the Quantification Measures of JRPs

We consider again two mutually coupled Rössler systems (Eqs. 2.21) to show the practical application of the theory presented in the upper sections. First, in order to estimate the joint Rényi entropy, we compute the distribution of

diagonal lines in the JRP for 99 different values of $\varepsilon^{\mathbf{x}}$ and $\varepsilon^{\mathbf{y}}$ and using $10,000$ data points. Analogously to Sec. 2.3.1, we use the algorithm to compute the thresholds corresponding to the fixed values of RR, varying from 0.01 to 0.99. In this way, we do not have to take the different amplitudes of both oscillators into account and we are sure, that each pair of ($\varepsilon^{\mathbf{x}}$ and $\varepsilon^{\mathbf{y}}$) corresponds to a very similar partition of each sub-"phase space".

The distribution of diagonals in the JRP for the non-PS ($\mu = 0.005$, $\nu = 0.015$ in Eqs. 2.21) and the PS case ($\mu = 0.045$, $\nu = 0.015$ in Eqs. 2.21) are represented logarithmically versus the length in Fig. 3.3 a, respectively 3.4 a. We observe two main slopes. The first slope for small lengths has the same origin than the one in the distribution of diagonals of a single RP (Sec. 2.3.1). As the joint Rényi entropy is defined for large lengths (see Eq. 3.12), we must concentrate on the second slope in order to estimate JK_2.

The estimator of JK_2 is represented in Figs. 3.3 b and 3.4 b, respectively. From Fig. 3.3 b we estimate $\widehat{JK_2} = 0.1798 \pm 0.004$ nats/s and from Fig. 3.4 b, we can estimate $\widehat{JK_2} = 0.0838 \pm 0.005$ nats/s. Hence, the joint Rényi entropy for the non-PS case is larger than in the case of PS. This is expected, because if both subsystems are synchronized, it is easier to predict the whole system than if they are not in PS.
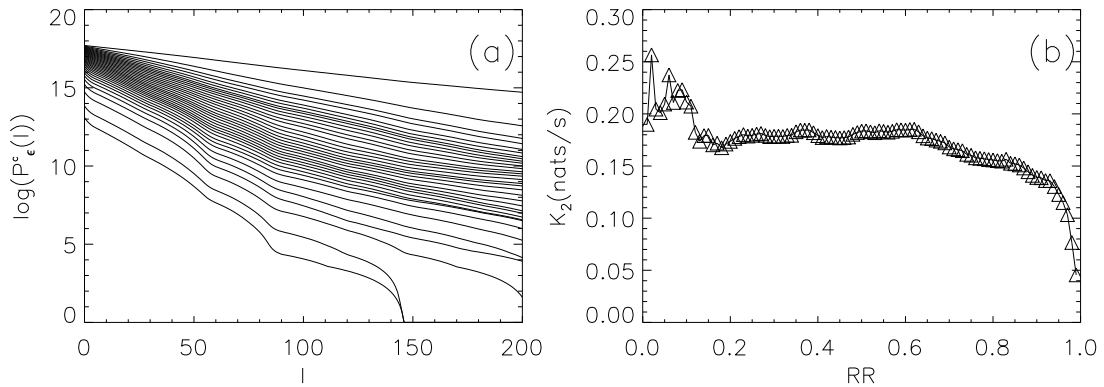

Figure 3.3: (a) Distribution of diagonal lines for two coupled Rössler systems (Eqs. 2.21) in non-PS regime. The different lines correspond to different RR, varying from 0.01 to 0.99 (only each third line is represented). (b) Estimator of K_2 in dependence on RR. We see a pronounced plateau from $RR = 0.11$ to $RR = 0.63$, approximately.

Finally, we calculate the recurrence rate of each subsystem given by Eqs. 2.21 (RR^x and RR^y) in dependence on the recurrence rate of the whole system $RR^{x,y}$,
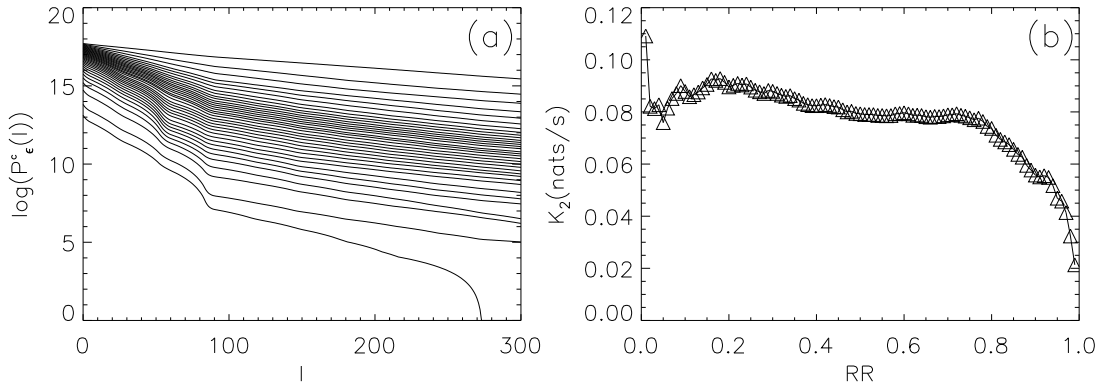
Figure 3.4: (a) Distribution of diagonal lines for two coupled Rössler systems (Eqs. 2.21) in PS regime. The different lines correspond to different RR, varying from 0.01 to 0.99. (b) Estimator of K_2 in dependence on RR. We see a plateau from $RR = 0.06$ to $RR = 0.7$, approximately.

using $RR^x = RR^y = RR$. Fig. 3.5 shows $RR^{x,y}$ versus RR for the PS regime (c)($\mu = 0.04$, $\nu = 0.015$) and non-PS regime (b) ($\mu = 0.01$, $\nu = 0.015$), as well as in the non-coupled case (a) ($\mu = 0.0$, $\nu = 0.015$). For the PS regime, the curve $RR^{x,y}$ versus RR is between the parabola $RR^{x,y} = RR^2$ (which indicates independency) and the main diagonal (which indicates "total" dependence) (see Fig. 3.5 c). Hence, this measure reflects the dependency between both oscillators when they undergo PS. In the non-coupled case, as well as in non-PS, the representation of the recurrence rate corresponds to the parabola $RR^{x,y} = RR^2$ (Fig. 3.5 a, b). This measure does not differentiate between independent oscillators and weakly coupled oscillators, that are not in PS yet. Hence, this measure detects rather well the onset of PS.
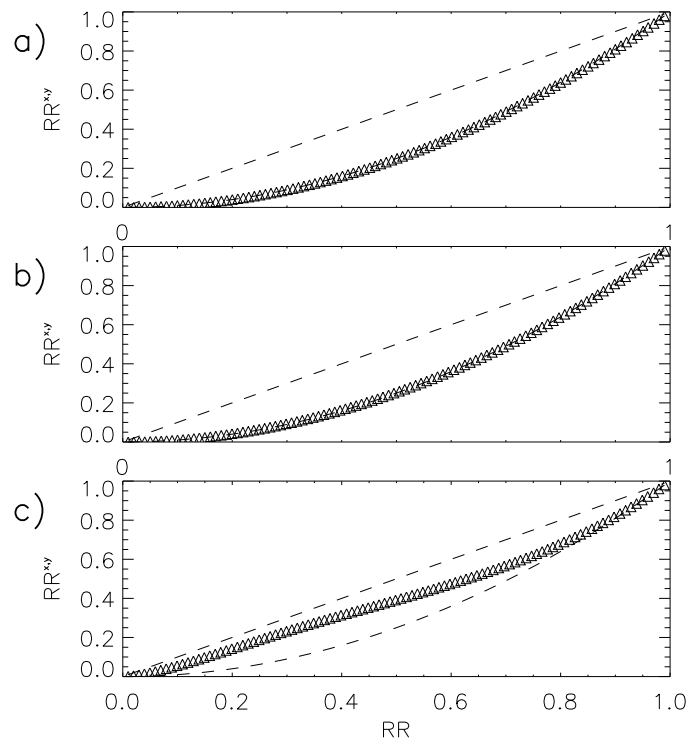
Figure 3.5: $RR^{x,y}$ versus RR for $\mathbf{x}, \mathbf{y}$ non-coupled (a), non-phase synchronized (b) and phase synchronized (c) two coupled Rössler systems (Eq. 2.21).

Chapter 4

Joint Entropy and Synchronization

In the last chapter, the Joint Recurrence Plots (JRPs) have been introduced and it has been shown that they have some advantages with respect to the formerly considered Cross Recurrence Plots (CRPs) for the analysis of the relationship between two or more interacting systems. This was illustrated for the example of two mutually coupled Rössler systems (Eqs. 2.21), which undergo phase synchronization when the coupling strength is sufficiently increased (Secs. 2.6 and 3.4). In Fig. 3.2 we observe that JRPs allow to visually detect synchronization between both oscillators, whereas it is much harder to recognize PS by means of CRPs. Furthermore, by means of the joint Rényi entropy JK_2, we can also quantify the interaction between both oscillators (Sec. 3.4).

Hence, we have seen by the examples presented before, that there exists a relationship between joint recurrences and the synchronization of oscillators.

On the other hand, it is well known, that the synchronization of oscillators can be characterized by means of the Lyapunov spectrum [66]. Moreover, there exists a formal relationship between K_2 and the Lyapunov exponents: Ruelle has shown in [77], that in the general case, the following relationship holds,

$$K_{KS} \leq \sum_{\lambda_i > 0} \lambda_i, \tag{4.1}$$

where λ_i denote the Lyapunov exponents and K_{KS} is the Kolmogorov-Sinai entropy. That means, the sum of the positive Lyapunov exponents is an upper bound of the Kolmogorov-Sinai entropy. Beyond this, the Rényi entropy of first order K_1 coincides with the Kolmogorov-Sinai entropy [10] and furthermore, it can be proven for the Rényi entropies [10], that

$$K_\beta \leq K_{\beta'}, \quad \text{with} \quad \beta' \leq \beta. \tag{4.2}$$

Hence, we can state that

$$K_2 \leq \sum_{\lambda_i > 0} \lambda_i. \tag{4.3}$$

As one can consider two coupled systems as a single whole system, the joint Rényi entropy corresponds to the "single" Rényi entropy of the whole system. Therefore, the upper formula is also valid for JK_2, considering the sum over the positive Lyapunov exponents of both subsystems.

Due to these two aspects, we concentrate in this chapter on the characterization of synchronization of complex oscillators by means of K_2. The algorithm presented in Sec. 3.3 will be automatized, so that we can estimate JK_2 at each point of the parameter space. Moreover, we compare the so obtained results with the ones obtained by means of the Lyapunov exponents and identify new transitions to phase and lag synchronization.

But first of all, a short introduction to the synchronization of chaotic oscillators is given.

4.1   Synchronization of Chaotic Systems

As mentioned in Chap. 1, chaotic systems defy synchronization due to the high sensitivity to slightly different initial conditions. However, it has been demonstrated that this kind of systems are able to synchronize.

The first studies about synchronization of chaotic systems deal with **complete synchronization (CS)**. In this case, coupled identical chaotic systems which start at different initial conditions, but driven by the same forcing, evolve on the same trajectory [20, 2, 61]. There are different coupling schemes that lead to CS, e. g. the Pecora and Carroll method, the active-passive decomposition, diffusive bidirectional coupling, etc. The appearance and robustness of synchronization by these coupling schemes has been analyzed [102]. CS is associated with the transition of the largest conditional Lyapunov exponent [1] of the synchronization manifold ($\mathbf{x} = \tilde{\mathbf{x}}$, with $\tilde{\mathbf{x}}$ denoting a copy of $\mathbf{x}$ with the same forcing but starting at different initial conditions) from positive to negative values.

However, under experimental conditions it is difficult to have two fully identical systems. Usually, there is some mismatch between the parameters of the systems under consideration. Hence, synchronization between nonidentical systems has been studied. Starting with two uncoupled nonidentical oscillators and increasing the coupling strength, a rather weakly degree of synchronization may occur, where the phases and frequencies of the chaotic oscillators become locked, whereas their amplitudes remain almost uncorrelated. This is the so called **phase synchronization (PS)**. In this case, the dynamics of the coupled systems are restricted to a manifold which is in general very complicated. There are several approaches to calculate the phase of chaotic oscillators (see Sec. 5.1). Furthermore, the phase of a chaotic oscillator is closely related to the zero Lyapunov exponent in the autonomous chaotic system. The zero Lyapunov exponent cor-

---

[1]The conditional or transversal Lyapunov exponents are the Lyapunov exponents of the response system under the action of the driver system.

responds to the translation along the chaotic trajectory. Hence, a perturbation in this direction neither decays nor grows. This property makes the adjustment of the phases of two chaotic oscillators (or of one oscillator and the force) possible. If two chaotic oscillators are not coupled, the two zero Lyapunov exponents are linked to the individual phases. Increasing the coupling strength, PS can be manifested by the transition of one of the zero Lyapunov exponents to negative values, indicating the establishment of a relationship between the phases [66].

Moreover, PS of chaotic systems can be studied in terms of the unstable periodic orbits (UPOs) embedded in the attractor [64, 65]. An UPO of period N has a "real" period of $T \simeq T_0 N$, where T_0 is the average return time of the period one periodic orbit. For different periodic orbits, T_0 fluctuates around the average return time of the chaotic oscillations. Due to these fluctuations, each periodic orbit has its individual phase locking region (Arnold tongue [40]) under the periodic external forcing. Hence, the region of phase synchronization is given by the overlapping region of the Arnold tongues of all UPOs [65, 13].

Furthermore, the distribution of the time scales of the system under consideration plays an important role in the synchronization behavior. For example, the variation of the return times (see [66] for a formal definition) or "periods" of rotation for the chaotic Rössler oscillator with standard parameters (Eq. 2.19) is relatively small. Hence, it can be easily synchronized by an external weak forcing with a period close to the average return time. In contrast, the Lorenz system [111] has a broad distribution of time scales, which is reflected in the broad distribution of frequencies of different UPOs [105]. Due to this, the phase locking regions of the UPOs do not overlap to produce a full synchronization region of the chaotic attractor. Therefore, an external signal with a given frequency is not able to entrain all the characteristic time scales of the system. As a consequence, phase slips occur and **imperfect synchronization (IS)** is observed.

Beyond this, the question arises what happens when the coupling strength between nonidentical chaotic oscillators is further increased. It has been demonstrated that a strong dependence between the amplitudes is then established, so that the states of both oscillators are almost identical but shifted in time, i. e. $\mathbf{x}(t) \simeq \mathbf{y}(t + \tau)$ [75]. This regime is called **lag synchronization (LS)**. The transition to LS has also been related to the transition of a positive Lyapunov exponent to negative values. Actually, LS sets in after the zero crossing of the Lyapunov exponent. In the interval between the transition of the Lyapunov exponent and the onset of LS, **intermittent lag synchronization (ILS)** is observed. There, LS is interrupted by intermittent bursts of large synchronization errors $\mathbf{e}(t) = \mathbf{x}(t) - \mathbf{y}(t + \tau)$ [75]. After the onset of LS, a further increase of the coupling strength leads to a decrease of the time lag τ between the trajectories of the oscillators. Hence, the oscillators tend to be **almost synchronized**, i.e $\mathbf{x}(t) \simeq \mathbf{y}(t)$.

The above description of synchronization transitions and their connection with the changes in the Lyapunov spectrum is valid for phase coherent oscillators,

for which a phase can be defined as a monotonously increasing function of time. However, for non-phase coherent chaotic oscillators, this definition may not be possible and the crossing of the zero Lyapunov exponent to negative values may not be an indicator for the onset of PS [13]. We will concentrate on this problem in Chap. 5.

The question about synchronization of coupled systems which are essentially different has been addressed first in [2, 78]. In this case, there is in general no trivial manifold in the phase space which attracts the systems' trajectories. It has been shown, that these systems can synchronize in a more general way, namely $\mathbf{y} = \psi(\mathbf{x})$, where ψ is a transformation which maps asymptotically the trajectories of $\mathbf{x}$ into the ones of the attractor $\mathbf{y}$. This kind of synchronization is called **generalized synchronization (GS)**. The properties of the function ψ depend on the features of the systems $\mathbf{x}$ and $\mathbf{y}$, as well as on the attraction properties of the synchronization manifold $\mathbf{y} = \psi(\mathbf{x})$ [60]. In most cases, evidence of GS has been provided for unidirectional coupling schemes. However, examples of bidirectionally coupled systems that undergo GS are e. g. given in [36, 12]. Kocarev and Parlitz have given the necessary and sufficient conditions for the occurrence of GS in unidirectionally coupled systems [38]. As in the case of CS, the notion of GS is equivalent to the asymptotic stability of the response system. Furthermore, there exists a weaker notion of GS, in which the drive and response are not related by a function. In this case GS occurs if the response system is asymptotically stable with respect to the driving signal. The difference with respect to the former case, is that it is not assumed that the complete synchronization manifold is contained in the basin of synchronization. Hence, the case of subharmonic entrainment of periodic orbits where several basins coexist is included. For example, if a periodic orbit of the drive entrains a stable periodic orbit of the response with twice its period, then any point of the attractor of the drive is mapped to two points on the response orbit. In this case, the transformation ψ is not a function [60].

Moreover, GS in structurally nonequivalent systems, i. e. systems generating chaotic attractors with high and different fractal dimensions has been reported in [12]. There, GS was exemplified for two symmetrically coupled Mackey-Glass systems with two different delays, which generate high-dimensional chaotic signals.

CS and GS have been demonstrated in laboratory experiments for electronic circuits [61, 17, 34] and laser systems [101, 54]. Furthermore, CS and GS have found applications for the the design of communication devices [35, 102, 15, 37, 59] and model verification and parameter estimations from time series [14, 57]. PS of chaotic oscillators has been demonstrated in plasmas [95], lasers [3], electrochemical oscillators [30, 31, 32], etc. Synchronization has been studied also in nature. For example, the dynamics of the cardiorespiratory system [79], an extended ecological system [11], and the electroencephalographic activity of Parkinsonian patients display synchronization features [88].

In the next sections we characterize the transitions to PS and LS by means of

the joint Rényi entropy in the example of two coupled Rössler systems.

4.2 Detection of Synchronization Transitions by Means of the Joint Entropy

In this section we estimate JK_2 by means of JRPs for the prototypical chaotic case of two mutually coupled Rössler oscillators (Eqs. 2.21). We analyze the range of parameters $\nu \in [-0.04, 0.04]$ and $\mu \in [0.0, 0.12]$, for which the two oscillators undergo transitions to phase synchronization.

In Fig. 4.1 the difference of the mean frequencies $\Delta\Omega = \Omega_1 - \Omega_2$ of the two oscillators shows the well-known Arnold tongue [2]. Now we estimate the JK_2
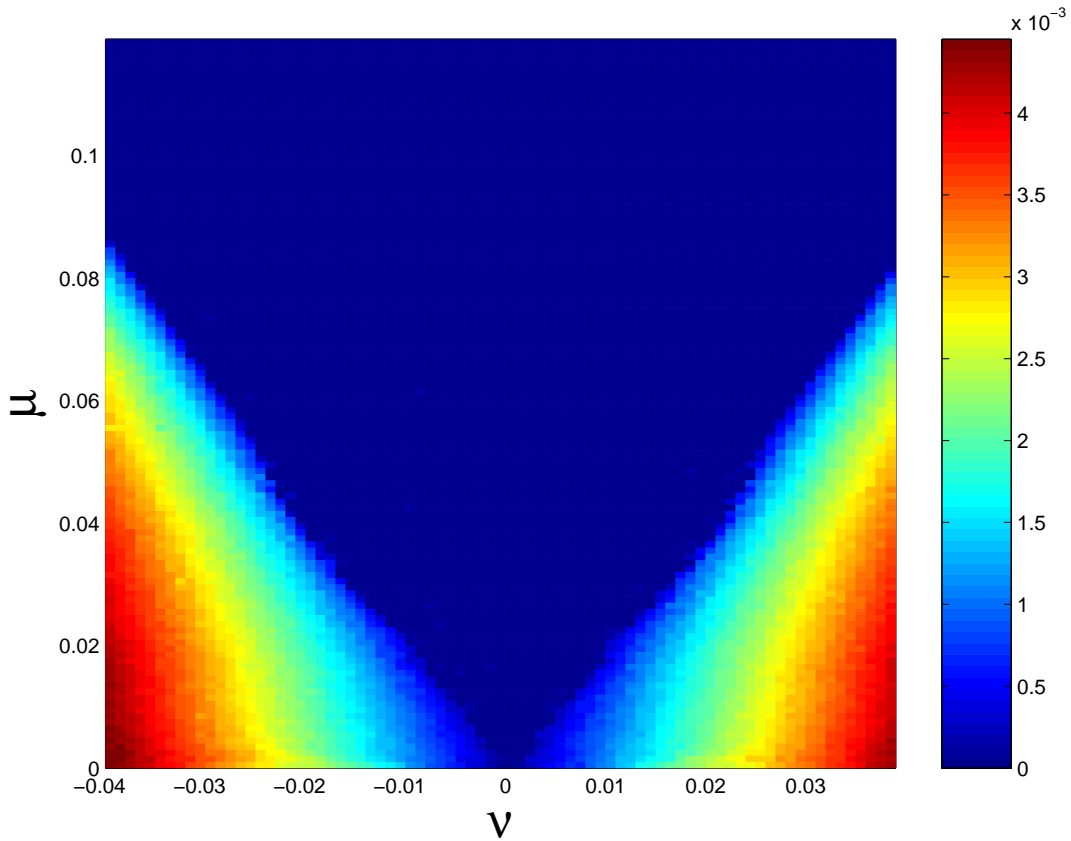
Figure 4.1: Difference $|\Delta\Omega|$ between the mean frequencies of the two Rössler oscillators (Eq.(2.21)) in dependence on the frequency mismatch and coupling strength.

based on JRPs in the same parameter range (for a detailed description of the

---

[2]the mean frequencies Ω_1 and Ω_2 were calculated as proposed in [66]

computation, see the Appendix). The results, represented in Fig. 4.2, also reflect the Arnold tongue, but they exhibit more details than Fig. 4.1:
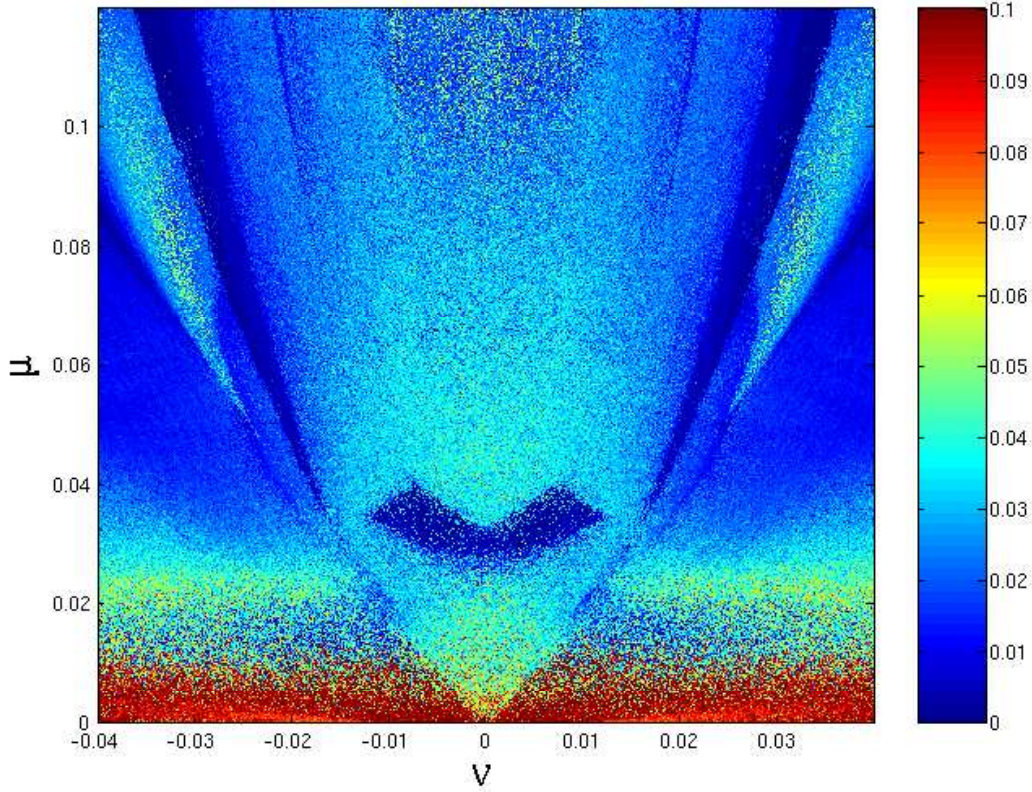
Figure 4.2: Joint Rényi entropy $\widehat{JK_2}$ of the two Rössler oscillators (Eqs. 2.21) in dependence on the frequency mismatch and coupling strength.

- First, we note two "borders" in the upper part of Fig. 4.2 ($\mu > 0.04$): the outer ones correspond to the border of the Arnold tongue, i. e. inside this border the oscillators are in PS, whereas outside they are not. Both borders have very low values of $\widehat{JK_2}$, i. e. the behavior of the system is rather regular there, even periodic in small regions on both borders. This is a remarkable fact, because it means that for relatively high coupling strengths the transition to PS is a chaos-period-chaos one, since inside the tongue $\widehat{JK_2} > 0$, indicating a chaotic regime.

- Inside the Arnold tongue, for coupling strengths μ between approximately 0.025 and 0.04, we find a region (which looks like two eyes), where the value of $\hat{K}_2$ is (almost) 0, i. e. the region is periodic or quasiperiodic.

- For $\mu \geq 0.03$ the region inside the Arnold tongue is "more chaotic" (larger $\hat{K}_2$) than outside the tongue. This is surprising, as one would expect that if both oscillators are synchronized, the behavior of the whole system becomes more and more regular for increasing coupling.

Hence, we have found new characteristics of the transition to PS by means of JK_2, which have to be investigated from a theoretical point of view.

4.3   Comparison between the Sum of the Positive Lyapunov Exponents and JK_2

In order to validate the results obtained in the last section, we calculate the Lyapunov spectrum of the whole system based on Eqs. 2.21, i. e. it is **not** estimated from the time series, but using the equations. As JK_2 is bounded from above by the sum of the positive Lyapunov exponents, we should obtain qualitatively the same structures plotting $\sum_{\lambda_i > 0} \lambda_i$ in the considered parameter space as in Fig. 4.2. Indeed, the structures in Fig. 4.3 are reproduced in Fig. 4.2. It is noteworthy, that K_2 was estimated from time series with $10{,}000$ data points and a sampling rate corresponding to 30 data points per oscillation (see Appendix for the details of the computation), whereas for the computation of the sum of the positive Lyapunov exponents, Eqs. 2.21 were used. As we are interested in a method for data analysis, where the equations governing the system are usually not known, the technique to estimate the predictability of the system in parameter space based on JRPs is quite appropriate and yields robust and reliable results.

Note that one can observe one qualitative difference between Fig. 4.2 and Fig. 4.3: for $\mu \in [0, 0.006]$ one cannot distinguish the tip of the Arnold tongue only by considering the sum of the positive Lyapunov exponents (see Fig. 4.5), whereas taking into account $\widehat{JK_2}$, one can (Fig. 4.4). This is due to the fact, that the relationship $K_2 = \sum_i \lambda_i^+$ holds only for hyperbolic systems but the 6-dimensional system (Eq. (2.21)) is not a hyperbolic one. For non-hyperbolic systems, $K_2 \leq \sum_i \lambda_i^+$ holds [77]. This shows that JK_2 can provide important complementary information to the sum of the positive Lyapunov exponents.

In the next section the transitions to PS and LS are investigated by the transitions in the Lyapunov spectrum.

4.4   Different Types of Transitions to PS

By means of joint recurrences we have detected different transitions to PS for the two coupled Rössler systems in dependence on the coupling strength and frequency mismatch (Fig. 4.2).
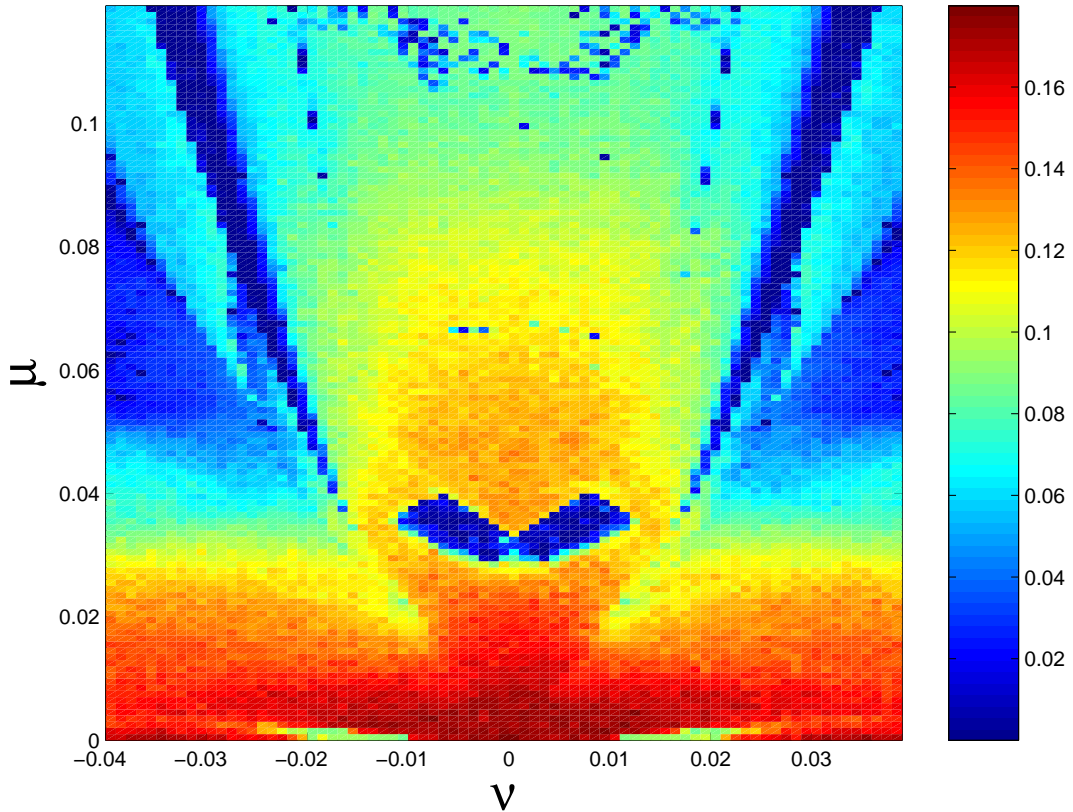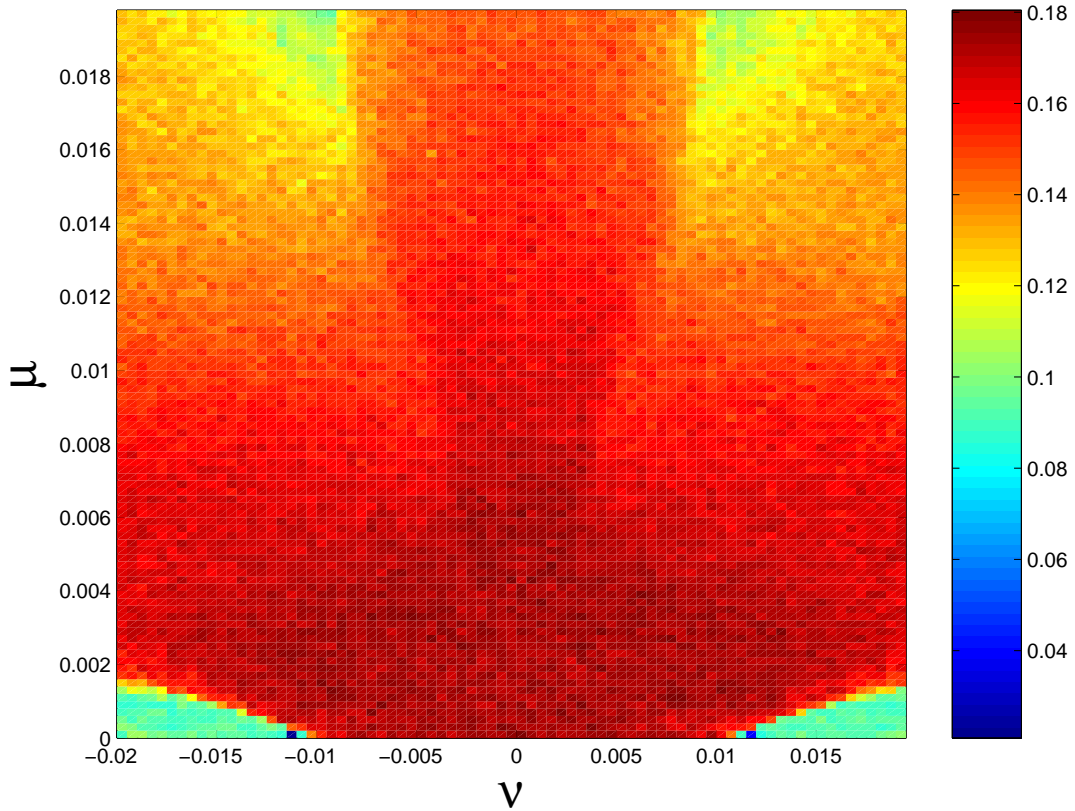
Figure 4.3: Sum of the positive Lyapunov exponents of the two Rössler oscillators (Eqs. 2.21) in dependence on the frequency mismatch and coupling strength.

In the literature, the transitions between different types of synchronization have been related to the changes in the Lyapunov spectrum [75, 53]: for rather low values of the coupling strength, one has the following configuration: $\{\lambda_1 > 0, \lambda_2 > 0, \lambda_3 \sim 0, \lambda_4 \sim 0, \lambda_5 < 0, \lambda_6 < 0\}$. The two zero Lyapunov exponents correspond to the two independent phases; although there is a coupling between both oscillators, both phases can be shifted [66]. Increasing the coupling strength μ, λ_4 becomes negative, indicating the transition to PS. If one continues to increase μ, then $\lambda_2 \sim 0$ and $\lambda_3 < 0$, indicating that the amplitudes become correlated. This has been interpreted as generalized synchronization (GS) in [53]. Indeed, two nonidentical chaotic oscillators bidirectionally coupled undergo transitions from phase to lag synchronization (LS). Furthermore, LS can be considered as an special case of GS [75].

In order to relate these results with ours obtained by means of JK_2 in the case of Eqs. (2.21), we encode the different configurations of the Lyapunov spectrum
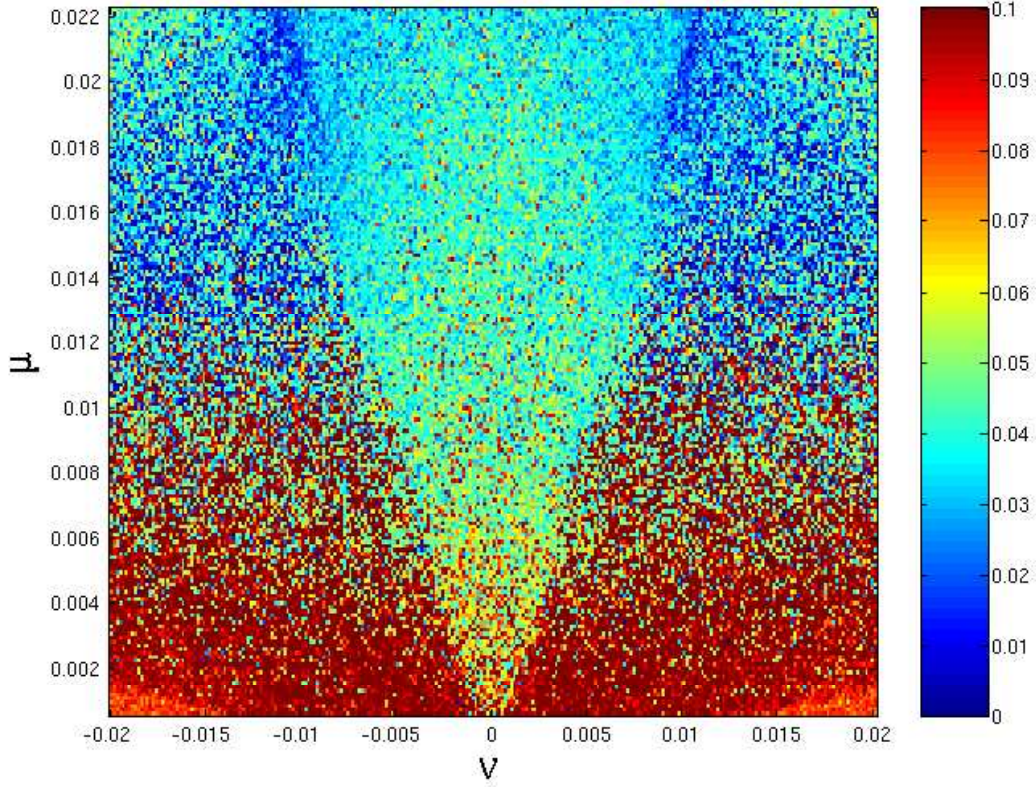
Figure 4.4: Magnification of the joint Rényi entropy $\hat{K}_2$ of the two Rössler oscillators (Eqs. 2.21) in dependence on the frequency mismatch for low values of the coupling strength.

in colors (Fig. 4.6):

- Dark blue: $\{\lambda_1 > 0, \lambda_2 > 0, \lambda_3 \sim 0, \lambda_4 \sim 0\}$, which corresponds to **non-PS**.

- Light blue: $\{\lambda_1 > 0, \lambda_2 > 0, \lambda_3 \sim 0, \lambda_4 < 0\}$, which corresponds to **PS**.

- Yellow: $\{\lambda_1 > 0, \lambda_2 \sim 0, \lambda_3 < 0, \lambda_4 < 0\}$, which corresponds to **strong correlated amplitudes**.

- Red: $\{\lambda_1 \sim 0, \lambda_2 < 0, \lambda_3 < 0, \lambda_4 < 0\}$, which corresponds to **periodicity**.

The conclusions we can draw from Fig.4.6 are:

1. For $0.031 < \mu < 0.055$ the transition to PS is not reflected any more by the change of λ_4 to negative values. In this region λ_4 is negative also outside the Arnold tongue (we take Fig. 4.1 as reference). This means, that for these values of μ, the phases of both subsystems are not independent any

Figure 4.5: Magnification of the sum of the positive Lyapunov exponents of the two Rössler oscillators (Eqs. 2.21) in dependence on the frequency mismatch for low values of the coupling strength.

more, even for large frequency mismatch. However this dependency is still weak, so that both subsystems are not in PS for large frequency mismatch.

2. For $0.055 < \mu < 0.1$ we observe that only one Lyapunov exponent remains positive for large values of the frequency mismatch. This happens outside and on the edge of the Arnold tongue. Decreasing the frequency mismatch (moving in the horizontal direction towards the middle), the correlation between the amplitudes decreases and inside the tongue we only have the configuration of the Lyapunov exponents corresponding to PS. This is in accordance with the upper part of Figs. 4.2 and 4.3, where inside the tongue, the whole system is more chaotic than outside.

3. We see two "borders" of the Arnold tongue (red points): the inner one is nearly periodic and the outer one is exactly periodic only for μ larger than
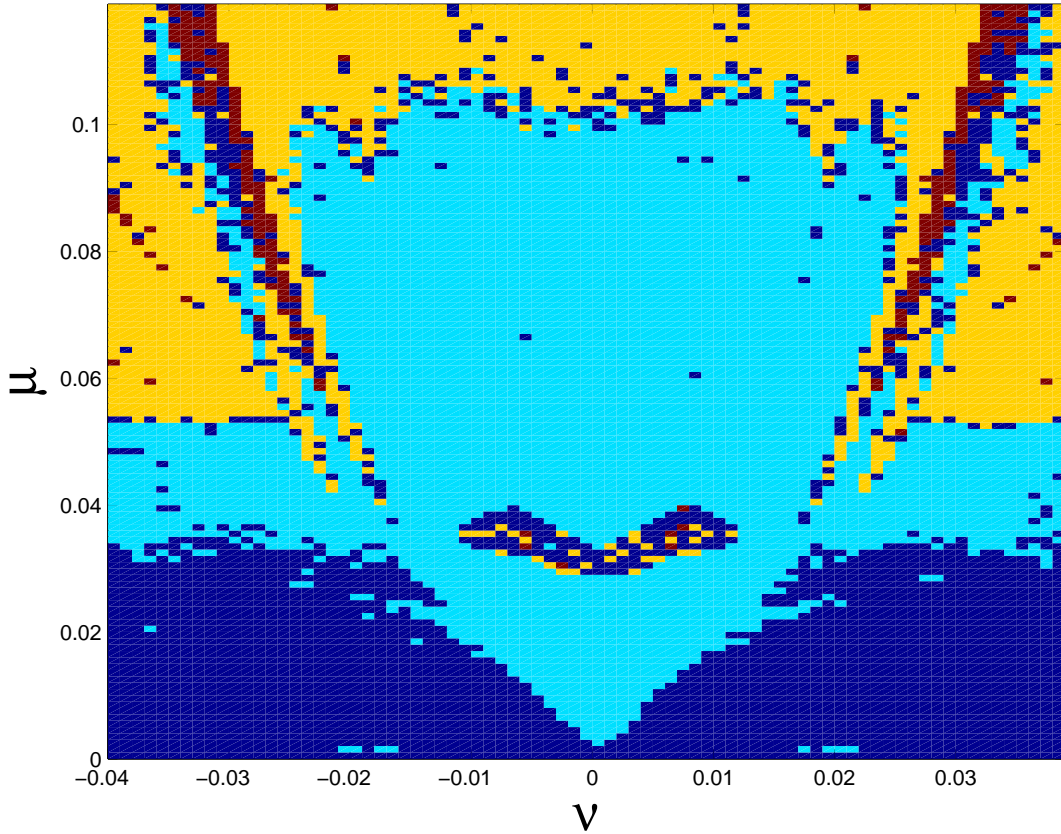
Figure 4.6: Different configurations of the Lyapunov spectrum are coded with different colors: dark blue: $\{\lambda_1 > 0, \lambda_2 > 0, \lambda_3 \sim 0, \lambda_4 \sim 0\}$, light blue: $\{\lambda_1 > 0, \lambda_2 > 0, \lambda_3 \sim 0, \lambda_4 < 0\}$, yellow: $\{\lambda_1 > 0, \lambda_2 \sim 0, \lambda_3 < 0, \lambda_4 < 0\}$ and red: $\{\lambda_1 \sim 0, \lambda_2 < 0, \lambda_3 < 0, \lambda_4 < 0\}$.

about 0.8. This also in accordance with the results of Fig. 4.2.

4. We recognize inside the tongue for $\mu \sim 0.03$ the "eyes", also seen in Figs. 4.2 and 4.3. The color there does not correspond to the periodic regime (red). This might be due to the finite sampling rate or to quasiperiodicity. However, we know from Fig. 4.3 that the sum of the positive Lyapunov exponents is very small there, and hence it is almost periodic.

4.5 Transition to Phase Synchronization for Large Frequency Mismatch

In Fig. 4.2 we have not distinguished between LS and states with the following configuration: $\{\lambda_1 > 0, \lambda_2 \sim 0, \lambda_3 < 0, \lambda_4 < 0\}$ (yellow). In order to do so, the

following similarity index for LS can be calculated in the parameter space [75]:

$$S^2(\tau) = \frac{< [x_1(t+\tau) - y_1(t)]^2 >}{[< x_1^2(t) >< y_1^2(t) >]^{1/2}} \qquad (4.4)$$

and search for its minimum $\sigma = min_\tau S(\tau)$. If the signals are in LS, then the function $S(\tau)$ almost vanishes for a τ different from zero [75]. This similarity index is shown in Fig. 4.7 for the considered parameter space. We see, that outside
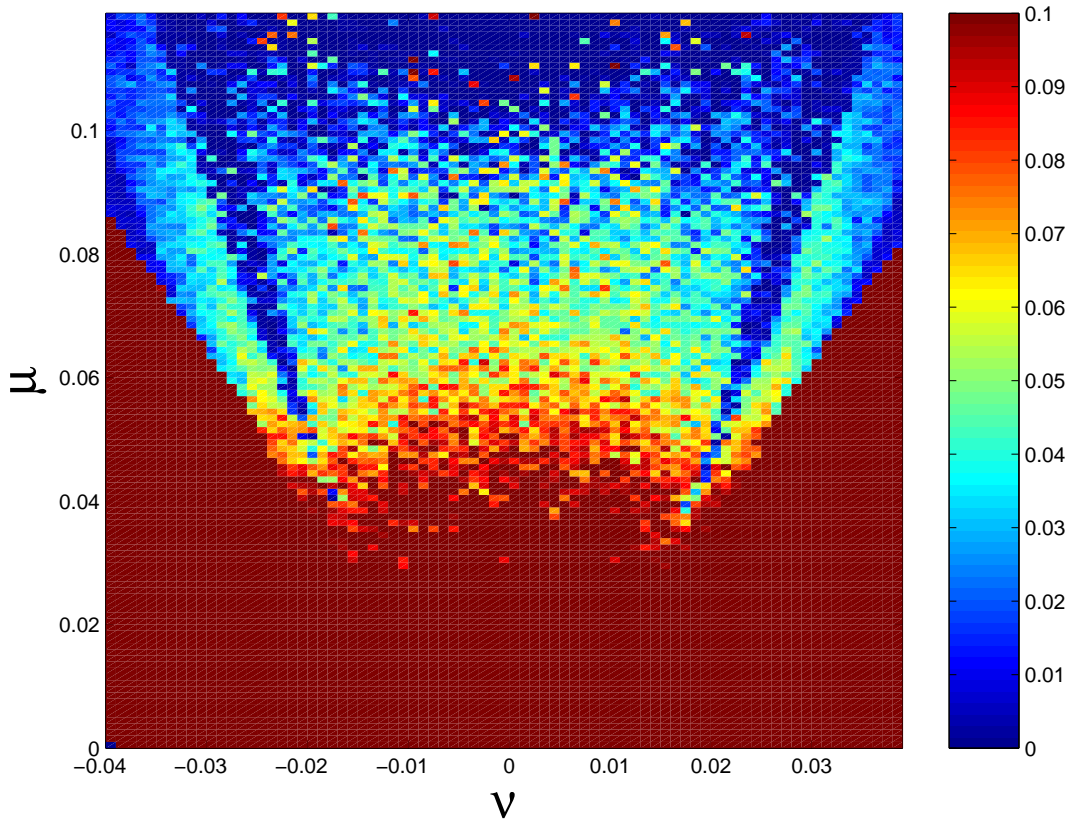

Figure 4.7: Index σ for LS. Values greater than 0.1 are coded with dark red.

the Arnold tongue, there is no LS. Only in the upper part of the Arnold tongue and on the inner "border", we recognize very small values of σ, which indicate LS (dark blue). Hence, for large frequency mismatch (approximately $|\nu| > 0.03$) there is a direct transition to LS (imagine a vertical section in Fig. 4.6 for a large value of $|\nu|$). That means that the amplitudes of the signals become more and more correlated with increasing coupling strength (transition from dark blue to light blue to yellow), without becoming phase synchronized, until they become

LS.

In order to analyze the correlations in the amplitudes in this region of the parameter space, we compute the amplitude of each oscillator in the following way: $A_x(t) = (x_1(t)^2 + x_2(t)^2)^{1/2}$, and analogously for A_y, using the coordinates of Eqs. 2.21. Then we fix the frequency mismatch at $\nu = -0.04$ and take three different values of the coupling strength: $\mu = 0.01$ (dark blue), $\mu = 0.04$ (light blue) and $\mu = 0.07$ (yellow)[3]. The scatter plots A_x versus A_y for the different coupling strengths are represented in Fig. 4.8. We see that for coupling $\mu = 0.01$
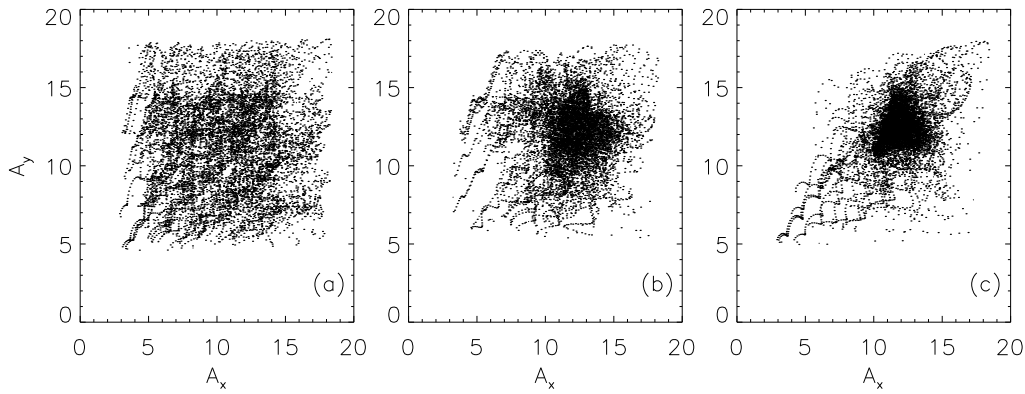
Figure 4.8: Scatter plot of A_x versus A_y for $\nu = -0.04$ and three different coupling strengths: $\mu = 0.01$ (a), $\mu = 0.04$ (b) and $\mu = 0.07$ (c) (Eqs. 2.21).

the amplitudes are almost uncorrelated. For $\mu = 0.04$ a certain correlation can be seen, and for $\mu = 0.07$ we observe that the points are accumulated near the diagonal, indicating a strong correlation of the amplitudes A_x and A_y. The cross correlation coefficient $c = < (A_x(t)- < A_x >)(A_y- < A_y >) > /\sigma_1\sigma_2$ between both amplitudes is summarized in Tab. 4.1 for the three different values of μ. We clearly see, that for $\mu = 0.07$ the correlation between the amplitudes of both oscillators is rather strong, although they are not in PS.

---

[3]these colors refer to Fig. 4.6

μ	c
0.01	0.048
0.04	0.053
0.07	0.478

Table 4.1: Cross correlation c of the amplitudes A_x and A_y for different values of the coupling strength μ.

4.6   Discussion

In this chapter we have estimated the joint Rényi entropy of second order JK_2 based on the joint recurrence matrix introduced in Chap. 3 for the paradigmatic system of two bidirectionally coupled Rössler oscillators (Eqs. 2.21). We have detected three different types of transitions to phase synchronization (see Sec. 4.2). To validate this result, we have compared the estimated JK_2 with the sum of the positive Lyapunov exponents. Qualitatively, we have obtained the same structures in the parameter space. However, for rather small coupling strengths, JK_2 can detect, due to the nonhyperbolicity of the considered system, the transition to PS, whereas the sum of the positive Lyapunov exponents cannot. Hence, the estimate of JK_2 by means of JRPs is a powerful tool for the analysis of the mean predictability of dynamical systems, especially when no model equations of the underlying system are available.

Moreover, we have calculated the Lyapunov spectrum $\{\lambda_i\}$ for the whole range of parameters considered. Coding the different configurations of $\{\lambda_i\}$ with different colors, we have seen that for intermediate coupling strengths, outside the Arnold tongue one zero Lyapunov exponent has passed to negative values. That means, in this range of parameters the phases become already weakly correlated, although they are not locked. Furthermore, the transition to synchronization for large frequency mismatch goes directly from non-synchronized to LS. The amplitudes of both oscillators become more and more correlated, without becoming phase synchronized, until LS sets on. These findings challenge for an extension of the theory of complex synchronization.

Chapter 5

Recurrence and Synchronization

In Chap. 4 we have established a relationship between the concept of recurrence in phase space and the synchronization of chaotic oscillators by means of the joint Rényi entropy JK_2 estimated from JPRs.

However, the computation of $\widehat{JK_2}$ (Eq. 3.12) yields only valuable information, when it is possible to compare the obtained result with different coupling strengths or different natural frequencies of the oscillators (the so called "active experiments" [66]). Therefore, the characterization of synchronization by means of $\widehat{JK_2}$ is of theoretical interest but not the most appropriate one if only two experimental time series are available, from which one wants to determine the degree of synchronization.

Hence, in this chapter four new indices for PS and GS are introduced, which make use of the link between recurrence in phase space and synchronization in a more pragmatic way. They indicate rather well the onset of synchronization and hence, they are appropriate test statistics for the performance of a hypothesis test. On one hand, the establishment of a direct relationship between recurrences and synchronization is of theoretical interest. On the other hand, the quantification measures proposed in this chapter overcome some open problems in the synchronization analysis of experimental systems:

- With the new indices we can quantify the degree of synchronization in the case of non-phase coherent, complex systems, with inherent multiple time scales. Therefore, they are applicable to a wide class of dynamical systems.

- The proposed measures are also appropriate for the analysis of non-stationary data.

- They allow to detect very easily clusters of phase synchronized oscillators in a network.

First, these indices are introduced and the applicability of the algorithm is illustrated for various examples, such as the paradigmatic chaotic Rössler system in

the funnel regime. Furthermore, it is demonstrated for simulated and experimental data, that the method can easily detect phase and generalized synchronization in non-phase coherent and even non-stationary time series. The robustness of the presented technique against observational noise is also discussed.

5.1 Detection of Phase Synchronization of Chaotic Systems

As we have seen in Sec. 4.1, two systems are said to be phase synchronized when their respective frequencies and phases are locked. To study PS of chaotic signals, one has to identify a well defined phase variable in both coupled systems. If the flow of the chaotic oscillators has a proper rotation around a certain reference point, the phase can be defined in a straightforward way. For example, for the Rössler system with standard parameters (Eq. 2.19) the projection of the chaotic attractor on the (x, y) plane looks like a smeared limit cycle. Hence, the phase can be defined as

$$\Phi(t) = \arctan(y(t)/x(t)). \tag{5.1}$$

A more general approach to define the phase in chaotic oscillators, is the analytic signal approach introduced in [21]. The analytic signal $\chi(t)$ is given by

$$\chi(t) = s(t) + i\tilde{s}(t) = A(t)e^{i\Phi(t)}, \tag{5.2}$$

where $\tilde{s}(t)$ denotes the Hilbert transform of the observed scalar time series s(t)

$$\tilde{s}(t) = \frac{1}{\pi} P.V. \int_{-\infty}^{\infty} \frac{s(t')}{t - t'} dt', \tag{5.3}$$

where *P.V.* stands for the Cauchy principal value for the integral [66].
The phase of a chaotic oscillators can also be defined based on an appropriate Poincare' section which the chaotic trajectory crosses once for each rotation. Each cross of the orbit with the Poincare' section corresponds to an increment of 2π of the phase, and the phase in between two crosses is linearly interpolated,

$$\Phi(t) = 2\pi k + 2\pi \frac{t - t_k}{t_{k+1} - t_k}, \quad (t_k < t < t_{k+1}), \tag{5.4}$$

where t_k is the time of the kth crossing of the flow with the Poincare' section.
For phase coherent chaotic oscillators, i. e. for flows which have a proper rotation around a certain reference point, the phases calculated by these different ways are in good agreement [13]. However, we often meet non-coherent attractors with rather broad band power spectra. In these cases, in general a single characteristic time scale does not exist. For this kind of systems it is difficult or impossible to find a proper center of rotation, around which the trajectory oscillates. Hence,

it is also intricated to find a Poincare' section that is crossed transversally by all trajectories of the chaotic attractor. Therefore, the definitions of the phase given above, are not longer applicable. Indirect criteria, e. g. based on the amplitude of the ensemble average of the system, have been proposed to detect PS of chaotic oscillators without coherent phase dynamics [63]. If the systems are in PS the mean field is an oscillating function of time with the locked frequency and a large amplitude. In the absence of PS the mean field fluctuates about zero. In this case, an ensemble of replicas of the chaotic system, or a very long chaotic signal is needed, and this is not always available when dealing with experimental data. Another indirect criterion is based on the increment of the intensity of the spectral component at the driving frequency in the phase synchronized regime. However, the threshold value for PS cannot be uniquely determined from the spectrum [58].

Rosenblum et al. have proposed a method for the determination of a characteristic oscillation frequency for a broad class of chaotic oscillators generating complex signals in [76]. There, an ensemble of uncoupled limit cycle oscillators with natural frequencies distributed in some interval is considered. Each oscillator of the ensemble is driven by a common complex signal. This signal "synchronizes" those elements of the ensemble which have frequencies close to the characteristic frequency of the complex driving signal. Plotting the frequencies Ω_k of the driven limit cycle oscillators versus the natural frequencies ω_k, synchronization manifests itself in the appearance of a horizontal plateau, where the frequency of the entrained limit cycles is equal to the unknown frequency. With this technique synchronization has been detected between systems, which do not allow an estimation of their frequencies by means of a direct application of e. g. the Hilbert transformation. However, the authors state that for chaotic systems with very complicated topology, the plateau may be not seen at all and hence the frequency may be not found. Moreover, the proposed method defines the frequency of a signal and hence, the estimation of the frequency for a different observable may yield different results.

On the other hand, Osipov et al. have recently proposed another definition of the phase based on the general idea of the curvature of an arbitrary curve [53]. For any two-dimensional curve $\mathbf{r} = (u, v)$ the angle velocity at each point is

$$\nu = (ds/dt)/R, \tag{5.5}$$

where $ds/dt = \sqrt{\dot{u}^2 + \dot{v}^2}$ is the speed along the curve and $R = (\dot{u}^2 + \dot{v}^2)^{3/2}/(\dot{v}\ddot{u} - \ddot{v}\dot{u})$ is the radius of the curvature. If $R > 0$ at each point, then

$$\nu = \frac{d\Phi}{dt} = \frac{\dot{v}\ddot{u} - \ddot{v}\dot{u}}{\dot{u}^2 + \dot{v}^2} \tag{5.6}$$

is always positive and hence the variable

$$\Phi = \int \nu dt = \arctan \frac{\dot{v}}{\dot{u}} \tag{5.7}$$

is a monotonically growing angle function of time and can be considered as the phase of the oscillator. These definitions of frequency and phase are general for any dynamical system if the projection of the phase trajectory on some plane is a curve with a positive curvature. For the non-phase coherent Rössler system in funnel regime (Eq. 2.19 with $a = 0.3$, $b = 0.4$ and $c = 7.5$), the projections of chaotic trajectories on the plane $(\dot{x}, \dot{y})$ always rotate around the origin, and the phase can be defined as $\Phi = \arctan \dot{y}/\dot{x}$. By means of this definition, three possible types of transition to PS in dependence on the coherence properties of the motions have been found [53].

However, in the definition of Eq. 5.7 for the phase, derivatives of the components are used. This can be problematic when dealing with time series that are subjected to rather high noise levels. Furthermore, for high dimensional chaotic systems, it is not clear whether an appropriate plane can be always found, on which the projected trajectories rotate around the origin.

In the next section we introduce a criterion for the detection of PS in chaotic oscillators based on recurrences in phase space. This index for PS is applicable to high dimensional systems and it is rather robust against noise influence and non-stationarities, as we will demonstrate. Further, it is defined for the whole system under consideration and not only for one component of it. Hence, the proposed PS index does not depend on the observable which is available.

5.2 Recurrence Based Index for PS

In order to link the concept of recurrences to PS, we concentrate on the probability $P^{(\varepsilon)}(\tau)$ that the system returns to the neighborhood of a former point $\mathbf{x}_i$ of the trajectory after τ time steps [47] (the neighborhood is defined as a box of size ε centered at $\mathbf{x}_i$, as we use the maximum norm). This probability can be estimated directly from the RP as follows [1]

$$\hat{P}^{(\varepsilon)}(\tau) = \frac{1}{N-\tau} \sum_{i=1}^{N-\tau} \Theta(\varepsilon - ||\mathbf{x}_i - \mathbf{x}_{i+\tau}||) = \frac{1}{N-\tau} \sum_{i=1}^{N-\tau} R_{i,i+\tau}^{(\varepsilon)}. \qquad (5.8)$$

$\hat{P}^{(\varepsilon)}(\tau)$ is a **generalized autocorrelation function**, as it also describes higher order correlations between the points of the trajectory in dependence on τ. A further advantage with respect to the linear autocorrelation function, is that $\hat{P}^{(\varepsilon)}(\tau)$ is determined for a trajectory in phase space and not only for a single observable of the system's trajectory. As it is a probability, it assumes values between 0 and 1.

For a periodic system in a 2-dimensional phase space, which is a circle or an

---

[1]Note, that $\hat{P}^{(\varepsilon)}(\tau)$ is just the rate of black points per line parallel to the main diagonal.

ellipse, it can be easily shown that

$$P(\tau) = \lim_{\varepsilon \to 0} \hat{P}^{(\varepsilon)}(\tau) = \begin{cases} 1 & : \quad \tau = kT, \quad \text{with} \quad k \in \mathcal{N} \\ 0 & : \quad \text{otherwise} \end{cases}$$

where T denotes the period of the system. Note that the RP of periodic trajectories in phase space consists of non-interrupted diagonal lines separated by $\tau = T$ time steps (see Fig. 2.1). This reflects the fact, that after one rotation in phase space, the probability that the trajectory recurs to its starting point is equal to one. However, for chaotic systems the diagonal lines (except the main one) in the RP are interrupted due to the exponential divergence of chaotic trajectories, i. e. two trajectories with similar initial conditions evolve similarly, but after some time, they diverge. However, a certain regularity remains in the RP of chaotic systems, especially if they are phase coherent, like the Rössler system for standard parameters (Eq. 2.19). The probability that the trajectory recurs after one or more rotations around the fixed point is rather high, but clearly less than one (see Fig. 5.1).

This is expressed by $\hat{P}^{(\varepsilon)}(\tau)$ (Fig. 5.2), where strong local maxima at multiples of the mean period of the chaotic system occur. (From now on, we omit (ε) and $\hat{}$ in $\hat{P}^{(\varepsilon)}(\tau)$ to simplify the notation.)

Now we show how to connect $P(\tau)$ to PS and demonstrate that this approach overcomes the problem present in non-phase coherent systems.

Originally, a phase Φ is assigned to a periodic trajectory $\mathbf{x}$ in phase space, projecting the trajectory onto a plane and choosing an origin, around which the whole trajectory oscillates. Then an increment of 2π is assigned to Φ, when the point of the trajectory has returned to its initial position, i. e. when $\mathbf{y}(t+T) - \mathbf{y}(t) = \mathbf{0}$, where $\mathbf{y}$ represents the trajectory which is projected on the plane. This concept of phase can be extended to more complex non-periodic trajectories, e. g., the chaotic Rössler system for standard parameters (Eq. 2.19). In this case, the trajectory is projected on the (x, y) plane and the fixed point $(0, 0)$ is chosen as an appropriate origin. Then, the phase can be estimated as $\Phi(t) = \tan^{-1}(y(t)/x(t))$ (see Sec. 5.1). However, there are many systems, such as the Rössler in the funnel regime, where it is difficult or impossible to find an origin on the projection plane around which all points of the trajectory oscillate.

Our approach, which is based on the probability of recurrence in phase space, offers an alternative to assign an increment of 2π to the phase, avoiding the problem of choosing an origin and a projection plane. Analogously to the case of a periodic system, we can ascribe an increment of 2π to Φ to a complex non-periodic trajectory $\mathbf{x}(t)$, when $||\mathbf{x}(t+T) - \mathbf{x}(t)|| \sim \mathbf{0}$, or equivalently when $||\mathbf{x}(t+T) - \mathbf{x}(t)|| < \varepsilon$, where ε is a predefined threshold. That means, a black point in the RP at the coordinates $(t, t + \tau)$ can be interpreted as an increment of 2π of the phase in the time interval τ (of course, τ must be greater than the correlation time of the system, or equivalently, greater than the Theiler window [89]). In this way, we neither have to choose an origin nor a projection plane.
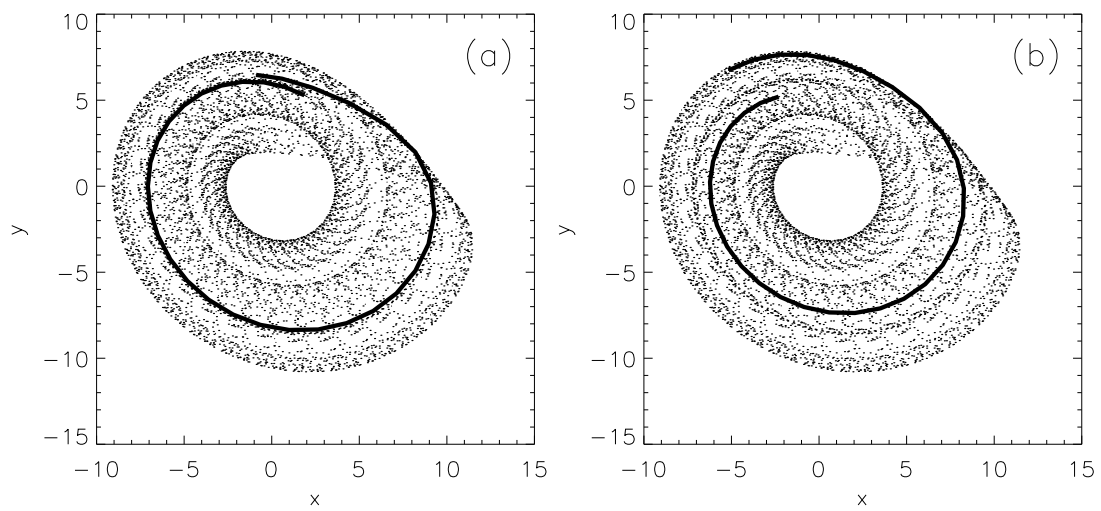
Figure 5.1: After one rotation around the fixed point it is quite probable to recur to its starting point (a). Nevertheless, this is not always the case (b). Hence, the probability to recur after one rotation around the fixed point is less than one.
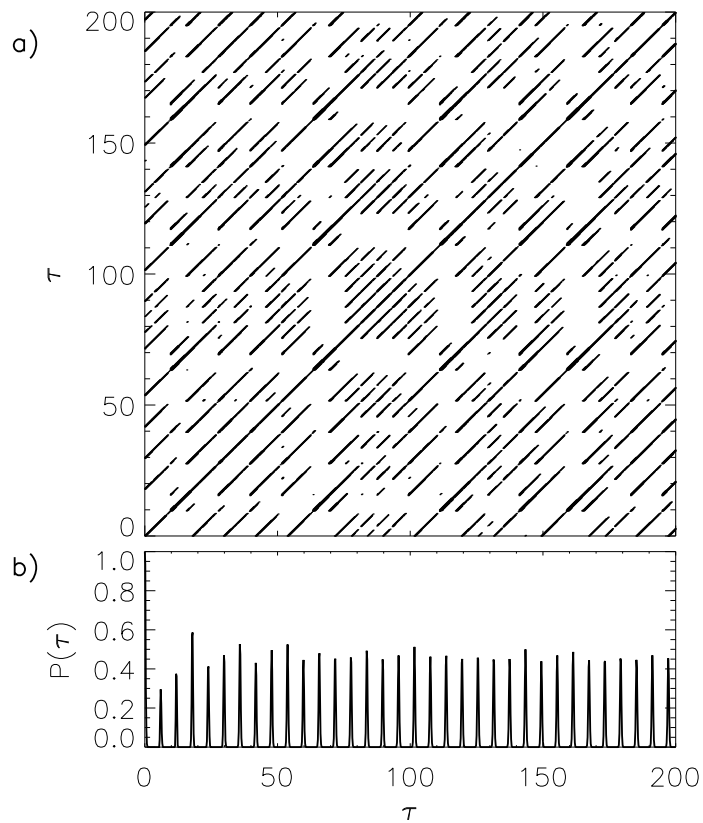
Figure 5.2: a) RP of the Rössler system in phase-coherent regime (Eq. 2.19). b) Corresponding probability of recurrence $\hat{P}^{(\varepsilon)}(\tau)$ (Eq. 5.8).
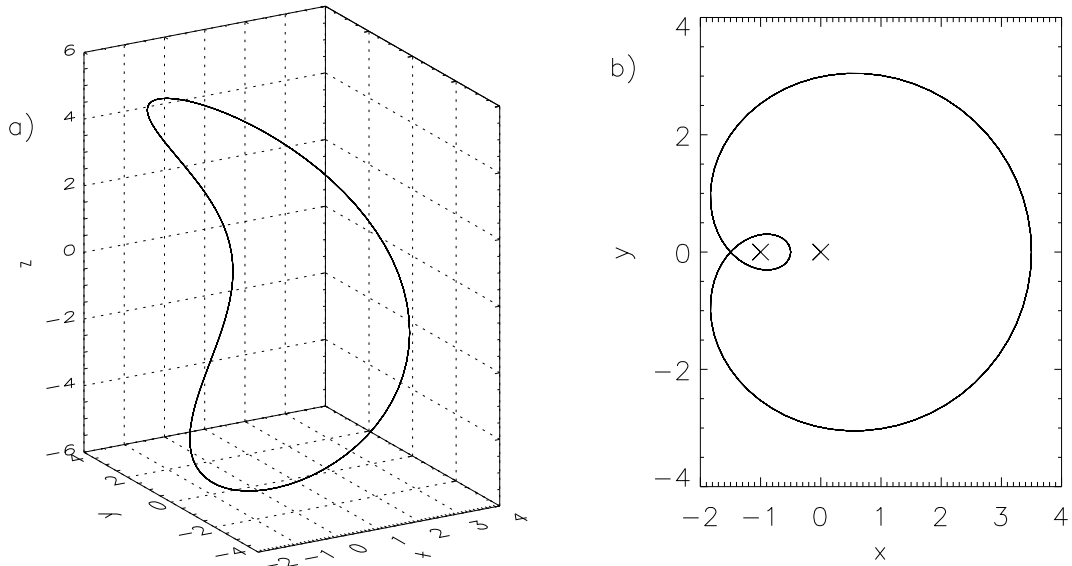
Figure 5.3: a) 3-dimensional periodic trajectory in phase space. b) Corresponding projection on the (x, y) plane. Two reasonable choices for the origin are marked with crosses.

Another problem linked to the definition of the phase based on a projection onto an appropriate plane, is the appearance of false neighbors. This idea is illustrated in Fig. 5.3, where a periodic function lying in a 3-dimensional Cartesian space is represented in phase space (a) and its projection on the (x, y) plane (b). In the projection (Fig. 5.3 b), there is some ambiguity by choosing an origin, and depending on this choice, the obtained phase is strongly different [66]. But from the representation of the trajectory in phase space (Fig. 5.3 a), we see that it is topologically equivalent to a circle, where there is no problem with the choice of the origin. Using the "recurrence" approach, we consider that the phase has increased by 2π, when the trajectory recurs to its initial point in the 3-dimensional phase space, i. e. when $R_{t,t+\tau}^{(\varepsilon)} = 1$. This is equivalent in this case to fixing the origin in the middle of the circle in the 3-dimensional phase space. Moreover, for higher dimensional phase spaces our approach would be still valid, whereas the trajectory on the projection plane may be rather complicated, as consisting of two or more kinds of orbits.

This interpretation of the recurrent points with respect to the phase, can be

extended to arbitrary complex trajectories, especially to chaotic ones. As each chaotic trajectory can be considered as jumping from one unstable periodic orbit (UPO) to another one [55], we will find a recurrence every time when the trajectory has completed a turn about one UPO. On the other hand, a turn about one UPO corresponds to an increment of 2π for Φ in the original phase space, but not necessarily in the projection.

$P(\tau)$ can be considered as a statistical measure about how often Φ has increased by 2π or multiples of 2π within the time τ in the original phase space. If two systems are in PS, their phases increase on average by $k \cdot 2\pi$, where k is a natural number, within the same time interval τ. Hence, looking at the coincidence of the positions of the maxima of $\hat{P}^{(\varepsilon)}(\tau)$ for both systems, we can quantitatively identify PS. A recurrence to a neighborhood after τ time steps does not occur with the same probability for the two systems, but the conditional probability that a recurrence in the second system occurs given that the first system has not returned yet is almost 0, because of the equality of their frequencies. Therefore, we introduce as the first criterion for phase synchronization the cross correlation between $P_1(\tau)$ and $P_2(\tau)$ to quantify PS ($P_1(\tau)$ represents the probability of recurrence of the first system, and $P_2(\tau)$ of the second one):

$$CPR = \frac{< \bar{P}_1(\tau)\bar{P}_2(\tau) >}{\sigma_1 \sigma_2}, \qquad (5.9)$$

where $\bar{P}_{1,2}$ means that the mean value has been subtracted and σ_1 and σ_2 are the standard deviations of $P_1(\tau)$ respectively. $P_2(\tau)$. We call this index **CPR (Correlation of Probability of Recurrence)**. CPR is defined between -1 and 1, because it is a "cross correlation" between two time series. If both systems are in PS, the probability of recurrence is maximal at the same time τ and $CPR \simeq 1$. In contrast, if the systems are not in PS, the maxima of the probability of recurrence do not occur simultaneously. Then we observe a drift (Fig. 5.6 b) and hence expect rather low values of CPR.

5.2.1 Examples for PS

In this section we exemplify the application of the index CPR for PS to four prototypical examples. The number of data points used for the analysis presented here is $5,000$.

- We start with the periodically driven Rössler system [66]:

$$
\begin{aligned}
\dot{x} &= -y - z + \mu \cos(\omega t) \\
\dot{y} &= x + 0.15y \\
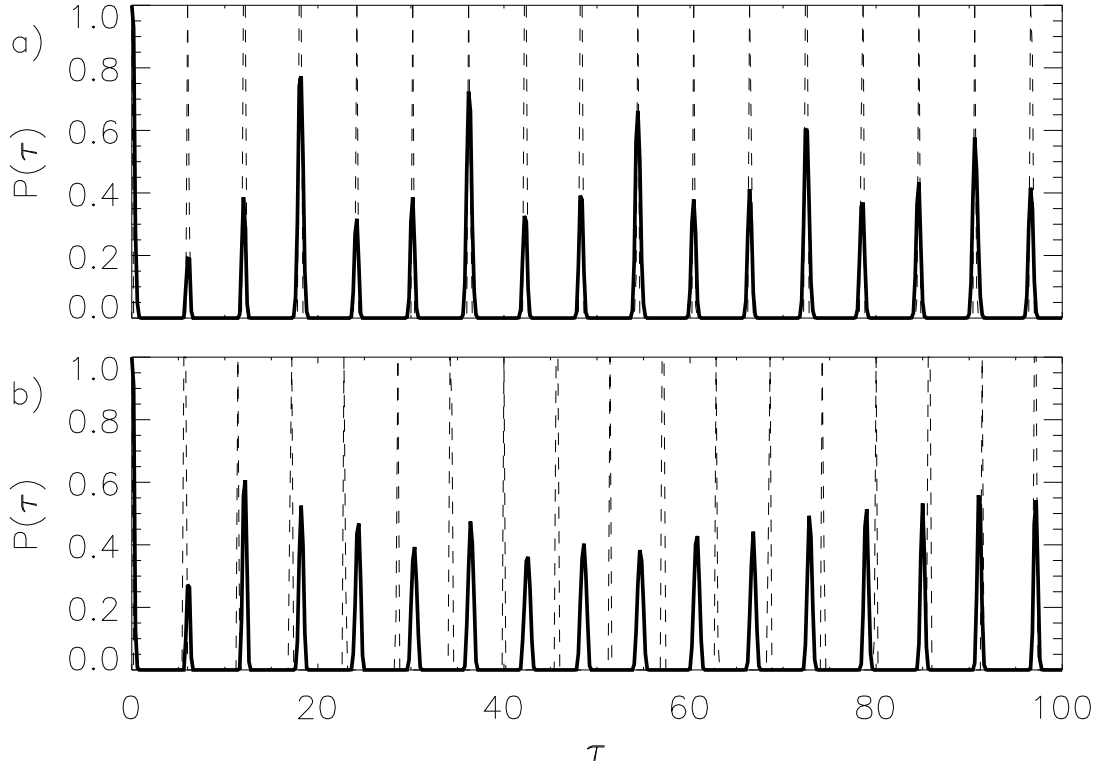\dot{z} &= 0.4 + z(x - 8.5)
\end{aligned}
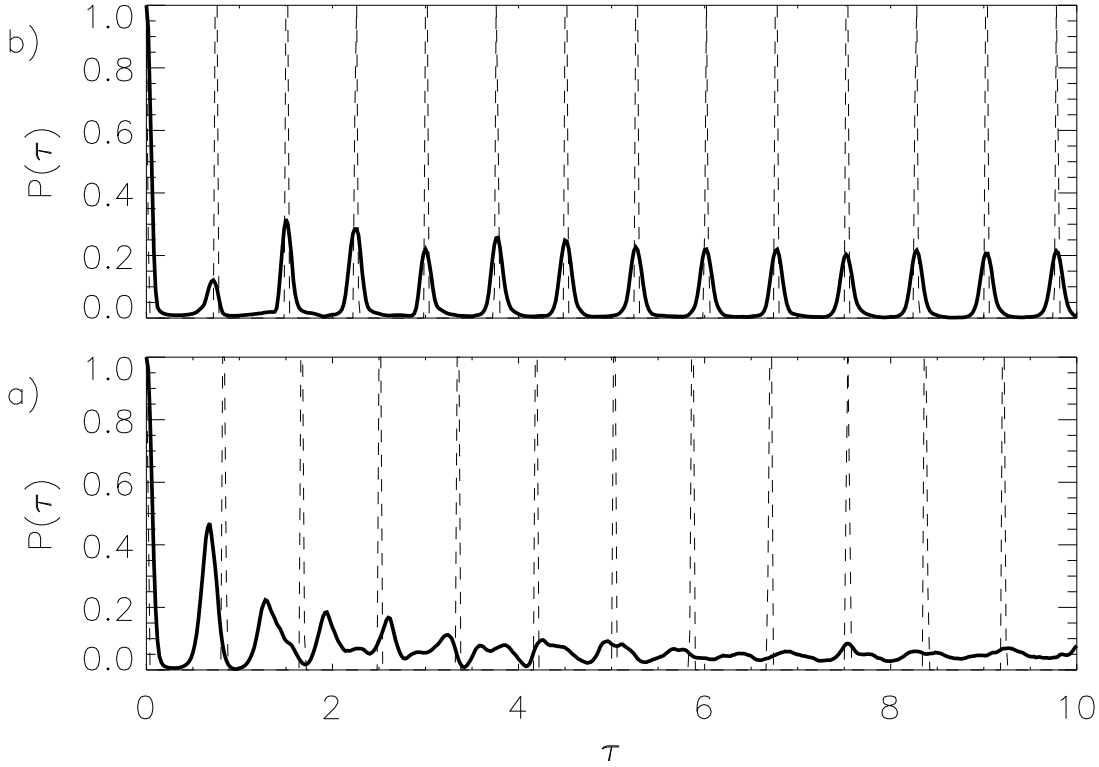\qquad (5.10)
$$

Figure 5.4: $P(\tau)$ for a periodically driven Rössler (Eqs. 5.10) in PS (a) and in non-PS (b). Solid line: $P(\tau)$ of the driven Rössler, dashed line: $P(\tau)$ of the periodic forcing.

For the frequency $\omega = 1.04$ and coupling strength $\mu = 0.16$, the periodic forcing locks the frequency of the Rössler system. This can be clearly seen in Fig. 5.4 a: the position of the maxima coincide. The value of the recurrence based PS index is $CPR = 0.862$.

For the parameters $\omega = 1.1$ and $\mu = 1.1$, the periodic forcing does not synchronize the Rössler system. Hence, the joint probability of recurrence is very low, which is reflected in the drift of the corresponding $P(\tau)$ (Fig. 5.4 b). In this case, $CPR = -0.00241$.

- We continue our considerations with the periodically driven Lorenz system:

$$\begin{aligned}
\dot{x} &= 10(y - x) \\
\dot{y} &= 28x - y - xz \\
\dot{z} &= -8/3z + xy + \mu \cos(\omega t)
\end{aligned} \qquad (5.11)$$

In Fig. 5.5 a the probabilities of recurrence $P(\tau)$ in the PS case ($\mu = 10$, $\omega = 8.35$) are represented: we see, that the position of the local maxima of the

Figure 5.5: $P(\tau)$ for a periodically driven Lorenz in PS (a) and in non-PS (b). Solid line: $P(\tau)$ of the driven Lorenz, dashed line: $P(\tau)$ of the periodic forcing.

Lorenz oscillator coincide with the ones of the periodic forcing. However, the local maxima are not as high as in the case of the Rössler system, and they are broader. This reflects the effective noise intrinsic in the Lorenz system [13]. Because of this, the phase synchronization is not perfect: an exact frequency locking between the periodic forcing and the driven Lorenz cannot be observed [56]. In this case, we obtain $CPR = 0.667$. In the non-PS case ($\mu = 10$, $\omega = 7.5$), we obtain $CPR = 0.147$ (Fig. 5.5 b).

- Now we consider the case of two mutually coupled Rössler systems in the phase coherent regime:

$$\begin{aligned}
\dot{x}_{1,2} &= -\omega_{1,2}y_{1,2} - z_{1,2} \\
\dot{y}_{1,2} &= \omega_{1,2}x_{1,2} + 0.16y_{1,2} + \mu(y_{2,1} - y_{1,2}), \\
\dot{z}_{1,2} &= 0.1 + z_{1,2}(x_{1,2} - 8.5)
\end{aligned} \qquad (5.12)$$

According to [53], for $\omega_1 = 0.98, \omega_2 = 1.02$ and $\mu = 0.05$ both systems are in PS. We observe that the local maxima of P_1 and P_2 occur at $\tau = n \cdot T$, where T is the mean period of both Rössler systems (Fig. 5.6 a). The
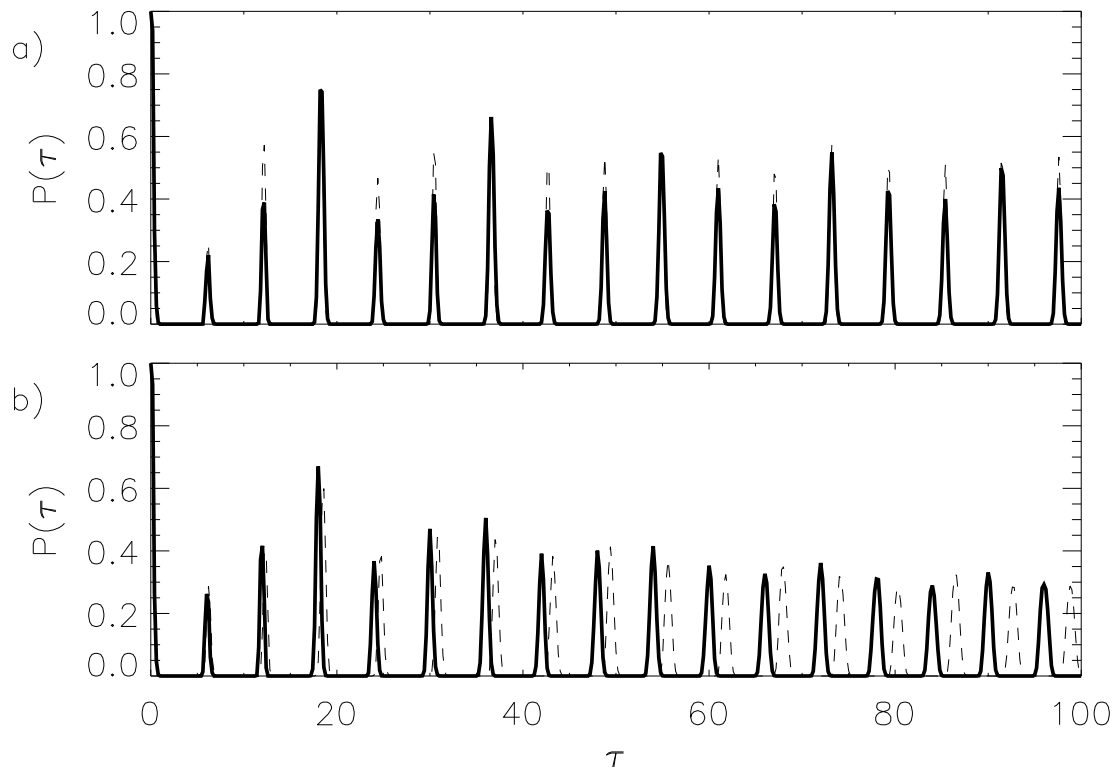
Figure 5.6: $P(\tau)$ for two mutually coupled Rössler systems (Eqs. 5.12) a) in phase coherent regime for $\mu = 0.05$ (b) and for $\mu = 0.02$.

heights of the local maxima are in general different for both systems if they are only in PS and not in GS, as we will see later. But the positions of the local maxima of $P(\tau)$ coincide. In this case, we obtain $CPR = 0.998$.

For $\mu = 0.02$ the systems are not in PS and the positions of the maxima of $P(\tau)$ do not coincide anymore (Fig. 5.6 b), clearly indicating that the frequencies are not locked. In this case, we obtain $CPR = 0.115$.

- As last example with simulated data, we analyze the challenging case of two mutually coupled Rössler systems in the funnel regime:

$$
\begin{aligned}
\dot{x}_{1,2} &= -\omega_{1,2}y_{1,2} - z_{1,2} \\
\dot{y}_{1,2} &= \omega_{1,2}x_{1,2} + 0.2925y_{1,2} + \mu(y_{2,1} - y_{1,2}), \\
\dot{z}_{1,2} &= 0.1 + z_{1,2}(x_{1,2} - 8.5),
\end{aligned}
\tag{5.13}
$$

where $\omega_1 = 0.98$ and $\omega_2 = 1.02$. We consider two different coupling strengths: $\mu = 0.2$ and $\mu = 0.05$. We observe that the structure of $P(\tau)$ in the funnel regime (Fig. 5.7) is rather different from the one in the phase coherent Rössler system (Fig. 5.6). The peaks in $P(\tau)$ are not as well pronounced as in the coherent regime, reflecting the different time scales that play a relevant role and the broad band power spectrum of this system. However, we see that for $\mu = 0.2$ the locations of the local maxima coincide for both oscillators (Fig. 5.7 a), indicating PS, whereas for $\mu = 0.05$ the positions of the local maxima do not coincide anymore (Fig. 5.7 b), indicating non-PS. These results are in accordance with [53].

In the PS case, we obtain $CPR = 0.988$, and in the non-PS case, $CPR = 0.145$. Note, that the positions of the first peaks in Fig. 5.7 b coincide, although the oscillators are not in PS. This is due to the small frequency mismatch ($|\omega_1 - \omega_2| = 0.04$). However, by means of the index CPR we can distinguish rather well between both regimes.

In Sec. 5.5 the transition to PS for this system will be analyzed exhaustively in terms of the index CPR. We will see, that the transition to PS for non-phase coherent systems is different from the one for phase coherent oscillators [53].

5.2.2 Influence of Noise

Dealing with experimental time series, one is always confronted with measurement errors. Hence, it is necessary to analyze the influence of noise on the index CPR (correlation of probability of recurrence) for PS.

We consider here additive or observational noise. We use Eqs. 5.12 as an example for two different coupling strengths, so that we can compute the deviation which is caused by noise in the non synchronized and in the synchronized case.

We add independent Gaussian noise with standard deviation $\sigma_{noise} = \alpha\sigma_j$ to each
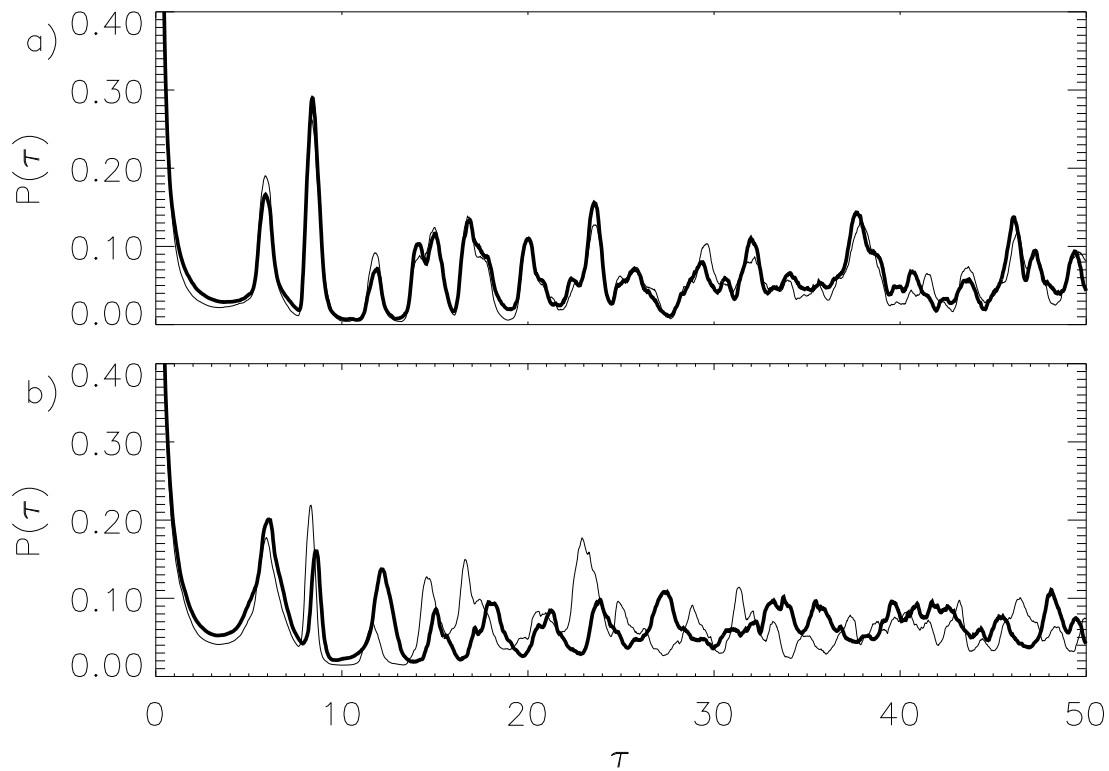
Figure 5.7: $P(\tau)$ for two mutually coupled Rössler systems in funnel regime (Eqs. 5.13) for $\mu = 0.2$ (a) and for $\mu = 0.05$ (b). Bold line: $P_1(\tau)$, solid line: $P_2(\tau)$,
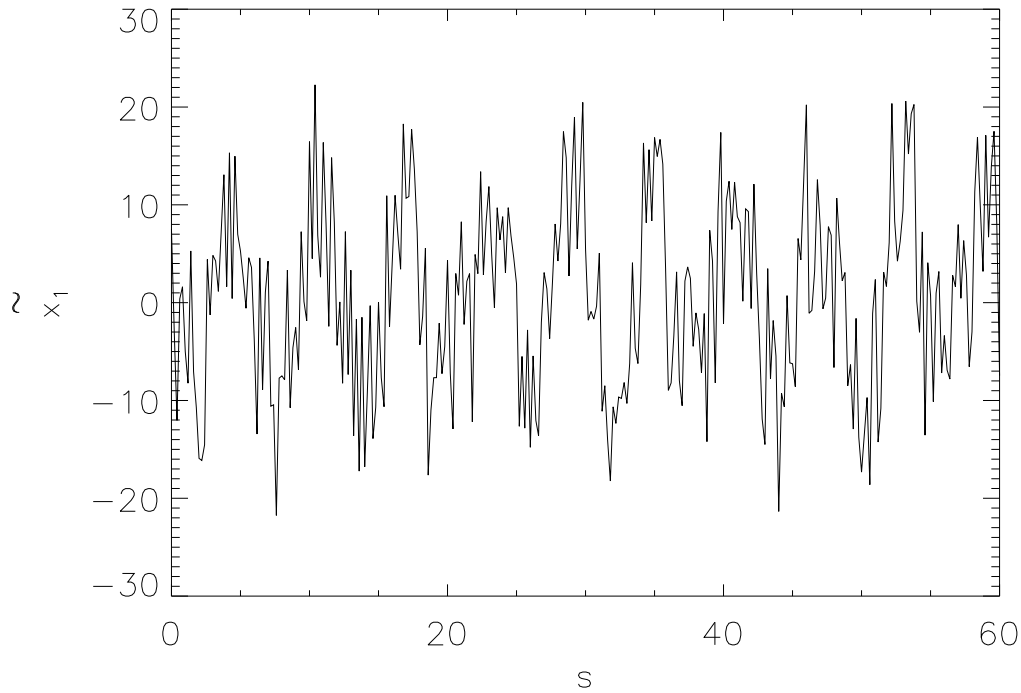
Figure 5.8: First component x_1 of Eqs. 5.12 with 80% independent Gaussian noise (for $\mu = 0.05$). From the figure it is clearly recognizable, that it is difficult to compute the phase by means of e. g. the Hilbert transformation.

coordinate j of the system, where σ_j is the standard deviation of the component j and α is the noise level. In Fig. 5.8 the "corrupted " x-component of the first Rössler subsystem $\tilde{x}_1(t) = x_1(t) + \alpha\sigma_1\eta(t)$, where $\eta(t)$ is a realization of Gaussian noise and $\alpha = 0.8$, is represented. From this figure it is clearly recognizable, that it is difficult to compute the phase by means of e. g. the Hilbert transformation for such a high noise level without filtering.

The choice of ε for the computation of $P_1(\tau)$ and $P_2(\tau)$ in the presence of noise is automatically taken by fixing a determined RR (see Eq. 2.2 and algorithm described in Sec. 2.3). The results presented below were computed for $RR = 0.1$, but the results are rather independent on the choice of RR. However, RR should not be chosen too small if the level of noise is very high.

 In order to compute the index CPR for the noisy oscillators, we calculate first the probabilities of recurrence $P_1(\tau)$ and $P_2(\tau)$ for coupling strengths $\mu = 0.05$ (PS, Fig. 5.9) and $\mu = 0.02$ (non-PS, Fig. 5.10).   We note, that the peaks in $P_1(\tau)$ and $P_2(\tau)$ become lower and broader (Figs. 5.9 b and 5.10 b) compared with the noise free case, as expected (Figs. 5.9 a and 5.10 a). However, despite of
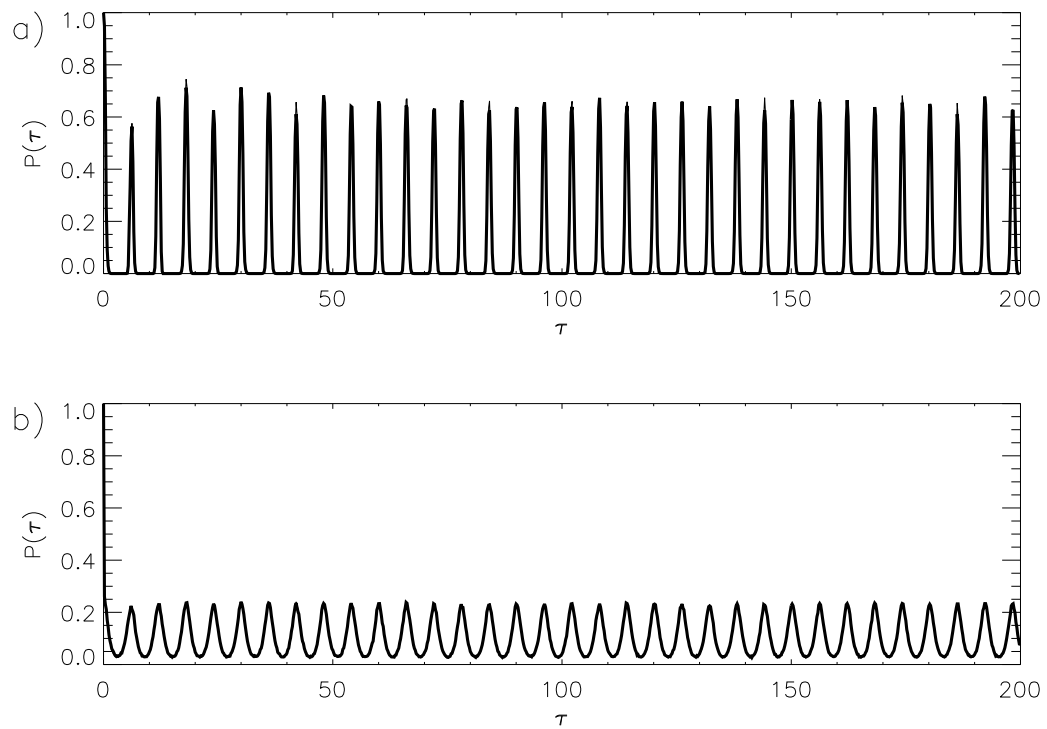
Figure 5.9: Probabilities of recurrence for two coupled Rössler systems (Eqs. 5.12) in PS ($\mu = 0.05$) without noise (a) and with 80% Gaussian observational noise (b). Bold line: subsystem 1, solid line: subsystem 2. Note, that the position of the peaks of $P_1(\tau)$ and $P_2(\tau)$ coincide in both cases, and hence the solid line is hidden by the bold one.
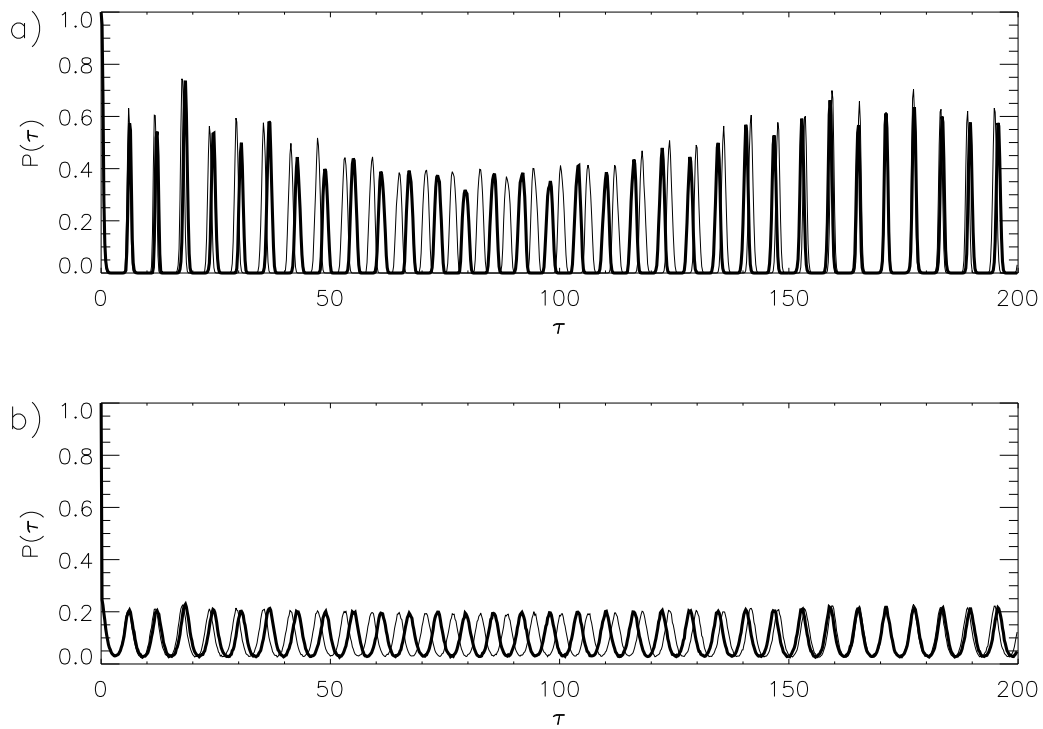
Figure 5.10: Probabilities of recurrence for two coupled Rössler systems (Eqs. 5.12) in non-PS ($\mu = 0.02$) without noise (a) and with 80% Gaussian observational noise (b). Bold line: subsystem 1, solid line: subsystem 2.

μ	$CPR(80\%$ **noise**)	$CPR(\textbf{without noise})$
0.02 (non-PS)	0.149	0.115
0.05 (PS)	0.998	0.998

Table 5.1: Index CPR index for PS calculated for two coupled Rössler systems (Eqs. 5.12) with observational noise and without noise, for comparison.

the large level of noise, the positions of the local maxima coincide in the PS case, and they drift away in the non-PS case. This a convenient result, because we can still decide whether the oscillators are synchronized or not. This is reflected in the obtained values for the CPR index: with 80% noise, in the PS case the obtained value for CPR is exactly the same with and without noise, and in the non-PS case is nearly the same (see Tab. 5.1). This shows that the index CPR for PS is very robust against observational noise. Also in the case of dynamical noise we can expect this method to work, due to its averaging.

5.2.3   Influence of Non-stationarity

Experiments are in general not only contaminated by some noise, but they are also often subjected to instationarities (e. g. drifts). Sometimes, especially when the system evades experimental manipulation (e. g. in the case of physiological data), it may be difficult to avoid or suppress this. Hence, beyond the analysis of the influence of noise, it is important to study the effect of non-stationarity on the CPR index, as well.

In order to do so, we add three different trends to one of the coupled oscillators, then compute the (modified index) CPR and compare with the value obtained without trend at all. We choose again the two mutually coupled Rössler systems (Eqs. 5.12) to exemplify our procedure.

- First, we add a **linear trend** to each component of the first oscillator: $\tilde{x}_1(t) = x_1(t) + at + b$, with $a = 0.01$ and $b = 25.0$ (y_1 and z_1 are modified in the same way as x_1). We compute the modified index CPR for the coupling strengths $\mu = 0.02$ (non-PS) and $\mu = 0.05$ (PS). Tab. 5.2 shows that the deviation of CPR from the case without trend is rather small for both PS and non-PS cases.

- We add next a **periodic trend** to each component of the first oscillator: $\tilde{x}_1(t) = x_1(t) + b\cos(2\pi at)$, with $a = 0.001$ and $b = 10.0$ (again, y_1 and z_1 are modified in the same way as x_1). The results for $\mu = 0.02$ (non-PS) and $\mu = 0.05$ (PS) are summarized in Tab. 5.2. The deviation from the case without trend for $\mu = 0.05$ is larger than for the other kinds of trends considered. However, the value obtained for CPR is still rather high.
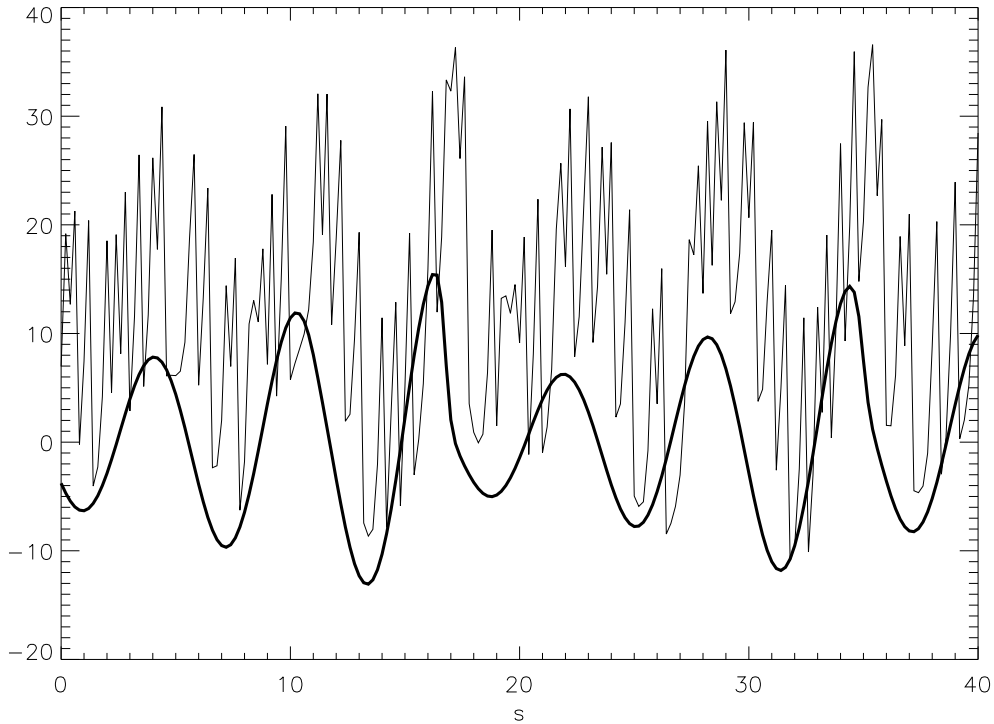
Figure 5.11: $\tilde{x}_1$ (solid line) and x_2 (bold line) of Eqs. 5.12 for $\mu = 0.05$. Despite of the nonlinear trend added to x_1, we can detect the PS by means of the recurrence based index CPR.

- We now add a **nonlinear trend** to each component of the first oscillator: $\tilde{x}_1(t) = x_1(t) + b\nu(t)$, where $b = 25.0$ and $\nu(t)$ is a realization of the logistic map ($\nu(t + 1) = a\nu(t)(1 - \nu(t))$) with $a = 4.0$. As usual, y_1 and z_1 are transformed analogously. Fig. 5.11 shows a segment of $\tilde{x}_1$ (x_2 is also plotted as reference). Fig. 5.12 represents the probabilities of recurrence $P_1(\tau)$ and $P_2(\tau)$ in the PS ($\mu = 0.05$) and non-PS ($\mu = 0.02$) case. We see, that despite of the nonlinear trend, we can clearly recognize in Fig. 5.12 a that the oscillators are in PS, since the position of the local maxima of the probability of recurrence coincide for both oscillators (analogously in the non-PS case). This is reflected by the values obtained for CPR (see Tab. 5.2).

The robustness of the index CPR against non-stationarities is another important advantage for the synchronization analysis of experimental data with respect to other methods, such as the Hilbert transformation, which does not work properly for non-stationary data sets [66].
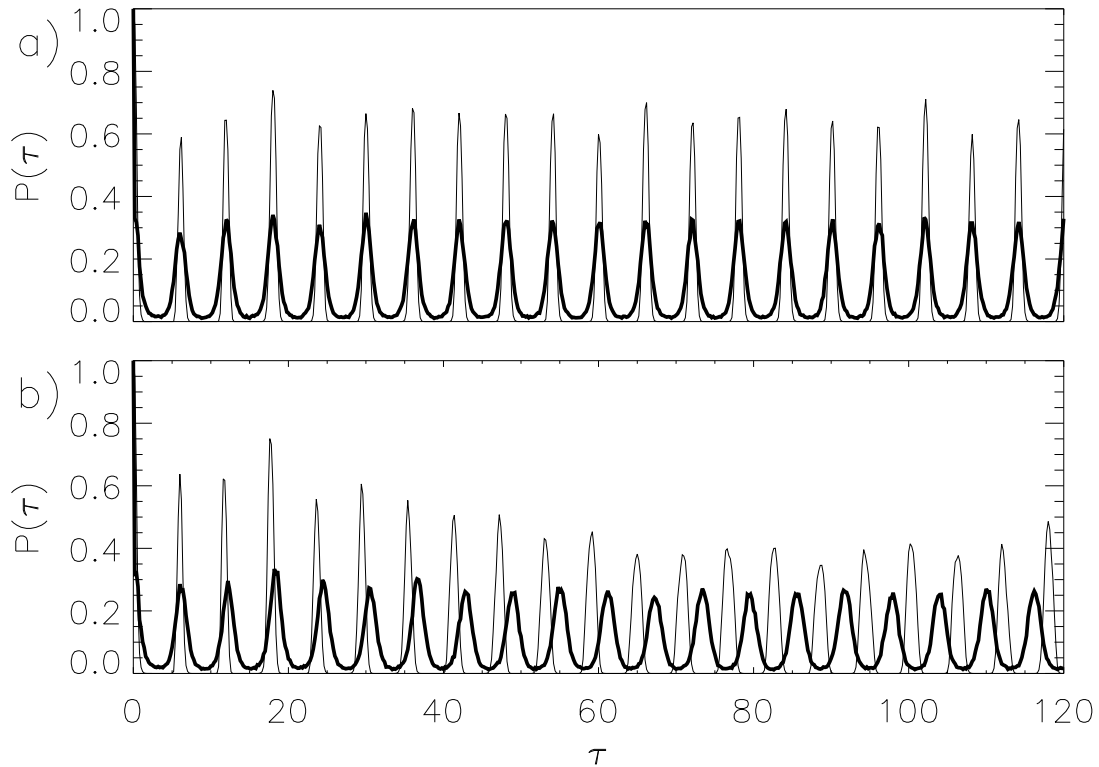
Figure 5.12: Probabilities of recurrence with nonlinear trend: $\mu = 0.05$ (a) and $\mu = 0.02$ (b). Bold line: subsystem 1, solid line: subsystem 2.

Coupling strength	linear	periodic	nonlinear	without trend
0.02 (non-PS)	-0.0327	0.182	-0.0378	0.115
0.05 (PS)	0.793	0.652	0.894	0.998

Table 5.2: Index CPR for PS calculated for two mutually coupled Rössler systems (Eqs. 5.12) with a linear trend, with a periodic trend and with a nonlinear trend. The values for CPR without trend are also given for comparison.

5.3 Detection of Generalized Synchronization

As discussed in Sec. 4.1, two (sub)systems in GS are connected by the relationship $\mathbf{y} = \psi(\mathbf{x})$. Some statistical measures have been introduced for the detection of GS. Most of them are based on the following idea, expressed by Rulkov et al. in [78]: "*When trajectories in the phase spaces of driving and response systems are connected by* $\mathbf{y}(t) = \psi(\mathbf{x}(t))$, *two close states in the phase space of the response system correspond to two close states in the space of the driving system*". There, the method of mutual false nearest neighbors was introduced based on this idea. Other variations of the method have been proposed and analyzed in [6, 70, 81], which are based on the squared mean distance and conditional distance between mutual nearest neighbors.

A few other methods are based on the mutual predictability for detecting dynamical interdependence [80]. There, the nearest neighbors of each subsystem are computed separately in its (sub)state space. This idea has been enhanced in [100], where the nearest neighbors are computed in the mixed state space. Since the nearest neighbors in the subspaces of $\mathbf{x}$ or $\mathbf{y}$ may be false nearest neighbors in the whole space, the prediction may be improved and hence, also the criterion for the interdependence between $\mathbf{x}$ and $\mathbf{y}$ is improved.

In the next section two new criteria are introduced for the detection of GS. They exploit the relationship between the geometric connection between both systems and their recurrences.

5.4 Generalized Synchronization and Recurrence

The connection between recurrences and GS is even more straightforward than the one between recurrences and PS. As we have mentioned in the last sections, when $\mathbf{x}(t)$ and $\mathbf{y}(t)$ are in GS, two close states in the phase space of $\mathbf{x}$ correspond to two close states in the space of $\mathbf{y}$ [78]. Hence, the "neighborhood identity" in phase space is preserved (see Fig. 5.13), i. e. they are topologically equivalent. Since the recurrence matrix $R_{i,j}^{(\varepsilon)}$ is nothing else as a record of the neighborhood of each point of the trajectory, one can conclude that two systems are in GS if their respective RPs are almost identical. Note, that it is possible to reconstruct the rank order of the time series considering only the information contained in the RP (see Sec. 2.4). Therefore, we can use the recurrence properties to detect and quantify GS.

However, in practice we note that the recurrence matrices of two systems in GS are very similar, but not identical. This can be due to many reasons: computational roundoff errors, measurements inaccuracies, etc. Hence, we construct an index that quantifies the degree of similarity between the respective recurrences of both systems. We propose two different indices in order to quantify GS based on the similarity of recurrences:
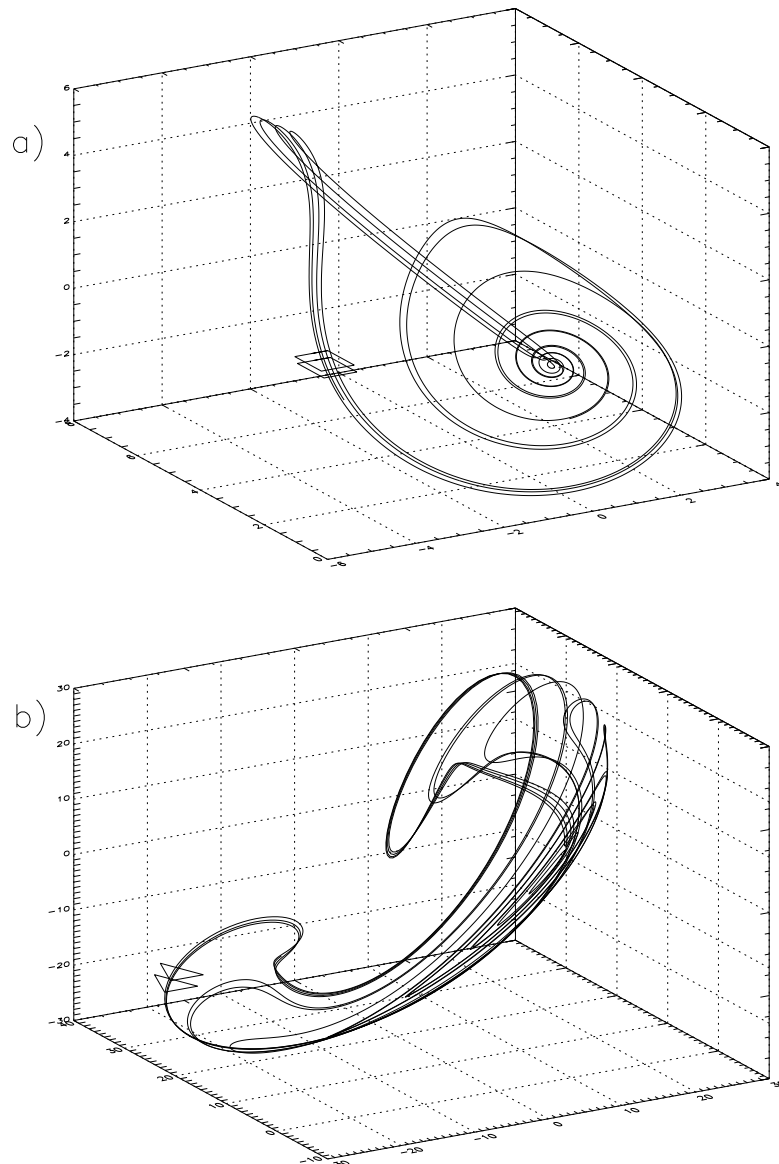
Figure 5.13: The systems represented in (a) and (b) (Eqs. 5.20 and 5.21) are in GS [38]. Two neighbors (i, j) in the system in (a) are marked with squares. The corresponding neighbors (i, j) in the system (b) are marked with triangles.

- The first approach compares the local recurrences of each point of the first system with the local recurrences of the second system. This index has the advantage, that it distinguishes rather well between non-PS, PS and GS or LS (we consider LS as an special case of GS [75]).

- The second index is again based on the probability of recurrence $P(\tau)$

(Eq. 5.8). But in contrast to the CPR index for PS, we do not only demand that the positions of the local maxima of $P(\tau)$ coincide for both systems, but also the height of the peaks of $P(\tau)$ must be equal, i. e. we demand that $P_1(\tau) \simeq P_2(\tau)$. This index has the advantage to be very robust against noise and non-stationarities.

The **first index** is based on the average probability of joint recurrence over time, given by

$$RR^{\mathbf{x,y}} = \frac{1}{N^2} \sum_{i,j=1}^{N} \Theta(\varepsilon^{\mathbf{x}} - ||\mathbf{x}_i - \mathbf{x}_j||)\Theta(\varepsilon^{\mathbf{y}} - ||\mathbf{y}_i - \mathbf{y}_j||). \qquad (5.14)$$

If both systems $\mathbf{x}$ and $\mathbf{y}$ are independent from each other, then the average probability of a joint recurrence [2] is given by $RR^{\mathbf{x,y}} = RR^{\mathbf{x}}RR^{\mathbf{y}}$ (see Sec. 3.3). If the oscillators are on the other hand in GS, we expect an approximate identity of their respective recurrences, and hence $RR^{\mathbf{x,y}} = RR^{\mathbf{x}} = RR^{\mathbf{y}}$ [78].
For the computation of the recurrence matrix in the case of essentially different systems that undergo GS, it is more appropriate to use a fixed number of nearest neighbors for each column in the matrix, following the idea presented in [6, 70, 81], than using a fixed threshold. That means, that the threshold is different for each column in the RP, but subjected to the following condition

$$\sum_{j=1}^{N} \Theta(\varepsilon^i - ||\mathbf{x}_i - \mathbf{x}_j||) = A \qquad \forall i, \qquad (5.15)$$

where A is the fixed number of nearest neighbors. We can automatically fix the RR by means of

$$RR = AN/N^2 = A/N,$$

and using the same A for each subsystem $\mathbf{x}$ and $\mathbf{y}$, $RR^{\mathbf{x}} = RR^{\mathbf{y}} = RR$.
Hence, the coefficient

$$S = \frac{RR^{\mathbf{x,y}}}{RR} \qquad (5.16)$$

is an index for GS that varies from RR to 1: it is approximately RR for independent systems, and it is close to 1 for systems in GS.
However, with the index S we would not detect lag synchronization ($\mathbf{y}(t + \tilde{\tau}) = \mathbf{x}(t)$). Since LS can be considered as an special case of GS [75], it would be desirable to have an index that also detects LS. For this reason, we include a time lag in the similarity and introduce the following quotient

$$S(\tau) = \frac{1/N^2 \sum_{i,j}^{N} \Theta(\varepsilon_{\mathbf{x}}^i - ||\mathbf{x}_i - \mathbf{x}_j||)\Theta(\varepsilon_{\mathbf{y}}^i - ||\mathbf{y}_{i+\tau} - \mathbf{y}_{j+\tau}||)}{RR}, \qquad (5.17)$$

---

[2]note that the average probability of a joint recurrence is the recurrence rate of the joint recurrence plot (JRP).

where the thresholds $\varepsilon_{\mathbf{x}}^i$ and $\varepsilon_{\mathbf{y}}^i$ are subjected to the following conditions:

$$\sum_{j=1}^{N} \Theta(\varepsilon_{\mathbf{x}}^i - ||\mathbf{x}_i - \mathbf{x}_j||) = A \qquad \forall i,$$

$$\sum_{j=1}^{N} \Theta(\varepsilon_{\mathbf{y}}^i - ||\mathbf{y}_i - \mathbf{y}_j||) = A \qquad \forall i.$$

Then, we choose the maximum value of $S(\tau)$ and normalize:

$$JPR = \max_{\tau} \frac{S(\tau) - RR}{1 - RR}. \qquad (5.18)$$

We denote this index by **JPR** because it is based on the average **joint probability of recurrence**. Since $S(\tau)$ varies between RR and 1, JPR ranges from 0 to 1. The value of RR is in principle a free parameter and its choice depends on the case under study. We consider rather low values of RR, e. g. 1% or 2% as appropriate.

The **second index** we propose, is based on the following idea: as we have mentioned above, the recurrence matrix contains only information about the neighborhood of each point of a time series. Hence, if two systems are in GS, their respective RPs must be almost identical. From this, it follows that also their respective probabilities of recurrence must coincide, as $P(\tau)$ is unambiguously given by $R_{i,j}$ (Eq. 5.8).

This suggests that the similarity coefficient between $P_{\mathbf{x}}(\tau)$ and $P_{\mathbf{y}}(\tau)$

$$SPR = 1 - \frac{< (\bar{P}_{\mathbf{x}}(\tau) - \bar{P}_{\mathbf{y}}(\tau))^2 >}{\sigma_{\mathbf{x}} \sigma_{\mathbf{y}}}, \qquad (5.19)$$

is of the order of 1 if $\mathbf{x}$ and $\mathbf{y}$ are in GS, and approximately zero or less than zero, if $P_{\mathbf{x}}(\tau)$ and $P_{\mathbf{y}}(\tau)$ are independent of each other ($\bar{P}(\tau)$ means that the mean value has been subtracted and $\sigma_{\mathbf{x}}$ and $\sigma_{\mathbf{y}}$ are the standard deviations of $P_{\mathbf{x}}(\tau)$ respectively. $P_{\mathbf{y}}(\tau)$) [75]. We call this index **similarity of probability of recurrence (SPR)**.

In the next sections, we show some examples and the advantages and disadvantages of these two recurrence based indices for GS.

5.4.1   Examples for GS

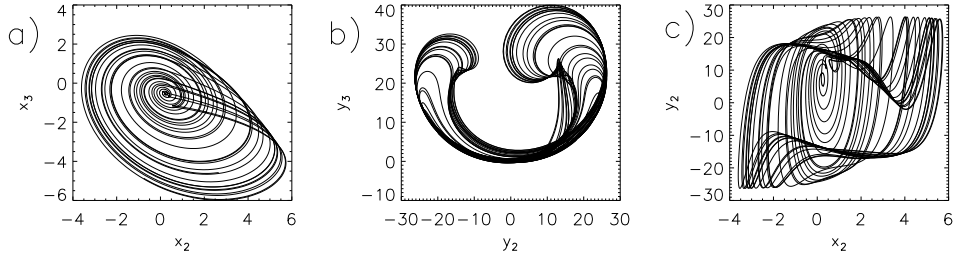In this section we show two examples of chaotic systems that undergo GS and compute for them JPR and SPR.

Figure 5.14: Projection of the Rössler driving system (a), the driven Lorenz system (b) and the diagram x_2 vs y_2 of Eqs. 5.20 and 5.21 (c).

- First we consider the **Lorenz system driven by a Rössler system**. The equations of the driving system are:

$$
\begin{aligned}
\dot{x}_1 &= 2 + x_1(x_2 - 4) \\
\dot{x}_2 &= -x_1 + x_3 \\
\dot{x}_3 &= x_2 + 0.45x_3,
\end{aligned}
\tag{5.20}
$$

and the equations of the driven system are the following:

$$
\begin{aligned}
\dot{y}_1 &= -\sigma(y_1 - y_2) \\
\dot{y}_2 &= ru(t) - y_2 - u(t)y_3 \\
\dot{y}_3 &= u(t)y_2 - by_3,
\end{aligned}
\tag{5.21}
$$

where $u(t) = x_1(t) + x_2(t) + x_3(t)$ and the parameters were chosen as follows: $\sigma = 10$, $r = 28$ and $b = 2.666$. In [38] it was shown, that the systems of Eqs. 5.20 and 5.21 are in GS, since the driven Lorenz system is asymptotically stable.

To demonstrate that they are completely different systems and that they are not in LS or CS, Fig. 5.14 shows the projections of the system 5.20 (a), of the system 5.21 (b) and the x_2 versus y_2 diagram (c).

Dealing with experimental time series, usually only one observable of the system is available. Hence, we perform the analysis with just one component of each system to illustrate the applicability of the proposed method (we use $10,000$ data points with a sampling time interval of 0.02 s). In this example, we take x_3, respectively, y_3 as observables. Then, we reconstruct
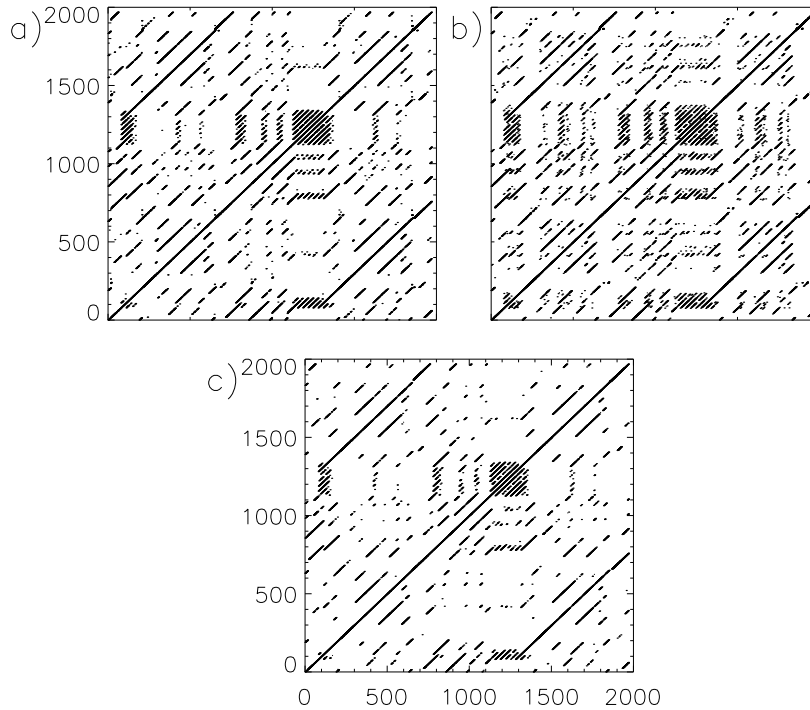
Figure 5.15: a) RP of the Rössler subsystem (Eqs. 5.20). b) RP of the driven Lorenz subsystem (Eqs. 5.21). c) JRP of whole system (Eqs. 5.20 and 5.21).

the phase space vectors using delay coordinates [87]. For the subsystem $\mathbf{x}$ we obtain the following embedding parameters [3]: delay time $\tau = 5$ and embedding dimension $m = 3$. For the subsystem $\mathbf{y}$ we find: $\tau = 5$ and $m = 7$. The corresponding RPs and JRP are represented in Fig. 5.15.

We see, that despite of the essential difference between both subsystems, their RPs are very similar (Fig. 5.15 a and b). Therefore, the structures are reflected also in the JRP and consequently, its recurrence rate is rather high. In this case, with the choice $RR = 0.02$ we obtain $JPR = 0.605$ (the value of JPR is similar for other choices of RR).

In order to show the contrary case, where both subsystems are independent (Fig. 5.16), we compute the RP of the Rössler system (Eq. 5.20) and of the independent Lorenz system [111], as well as their JRP (Fig. 5.17). We clearly see, that the mean probability over time for a joint recurrence is very small, as the JRP has almost no recurrence points. For this case, one obtains $JPR = 0.047$ using embedding parameters $\tau = 5$ and $m = 3$ for both systems, and $RR = 0.02$.

---

[3]see [29] for a detailed instructions
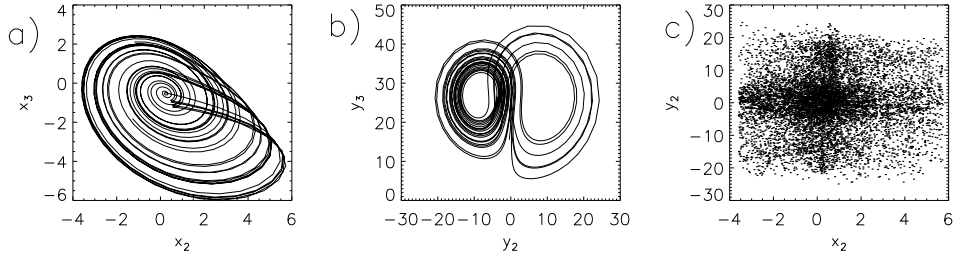
Figure 5.16: Projection of the Rössler system (Eqs. 5.20)(a), the independent Lorenz system [111] (b) and the diagram x_2 vs y_2, where x_2 is the second component of the Rössler system and y_2 is the second component of the independent Lorenz system (c).

Now, we compute the second index proposed SPR (Eq. 5.19) (5,000 data points were used and a sampling time interval of 0.02 s). We see in Fig. 5.18 a, that the probability of recurrence of both systems in GS nearly coincides. For comparison, $P(\tau)$ for a Lorenz system independent of a Rössler is represented in Fig. 5.18 b. In this case, the respective $P(\tau)$ are very different. For the GS case, we obtain $SPR = 0.934$ and for the independent case, $SPR = -0.196$. Here, we have used for the analysis the original components of Eqs. 5.20 and 5.21. Using embedding coordinates, the results are also convenient: $SPR = 0.832$ for the GS case, and $SPR = -0.365$ for the independent case.

- **Two mutually coupled Rössler systems** (Eqs. 5.12): for the coupling strength $\mu = 0.11$ both oscillators are in LS, as can be seen in Fig. 5.19. In this case, the RPs of both subsystems are obviously almost identical, except for a displacement on τ in the diagonal direction. Computing the index following Eqs. 5.17 and 5.18, we obtain the value $JPR = 0.988$ (JPR is in this case not exactly 1, because we do not have perfect LS, i. e. $\mathbf{x}(t+\tau) \simeq \mathbf{y}(t)$ [75]). For a smaller coupling strength $\mu = 0.02$ the oscillators are not in LS anymore. The obtained value is in this case $JPR = 0.014$. Computing the second proposed index SPR for this case, we obtain $SPR = 0.999$ for $\mu = 0.11$, as expected. And for $\mu = 0.02$, the result is $SPR = -0.657$.
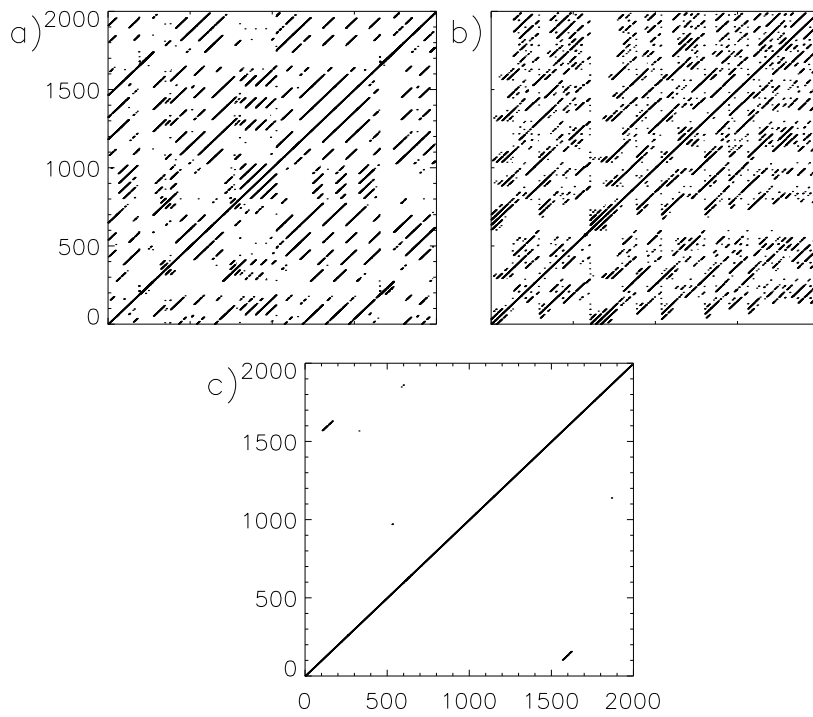
Figure 5.17: a) RP of the Rössler subsystem (Eqs. 5.20). b) RP of the indepen-
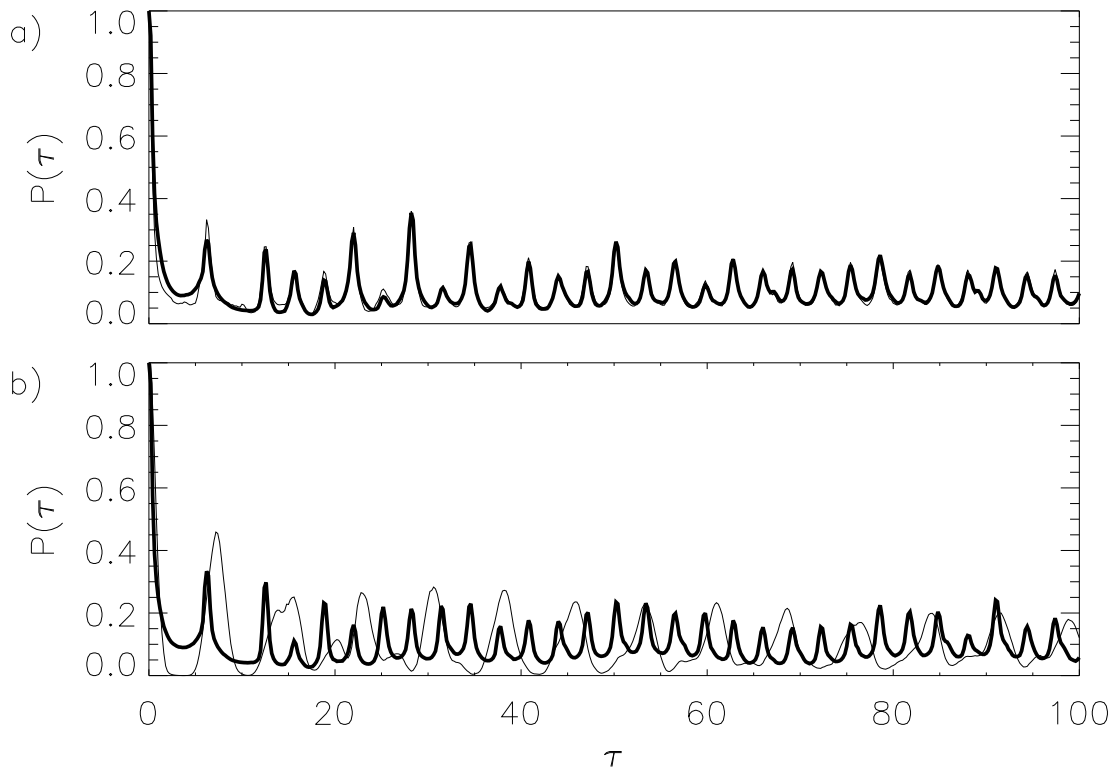dent Lorenz system [111]. c) JRP of whole system.

Figure 5.18: a) $P(\tau)$ for the Lorenz system driven by the Rössler (Eqs. 5.20 and 5.21). As both systems are in GS, their probabilities of recurrence almost coincide (solid line: driven Lorenz, bold line: Rössler). b) The same for a Lorenz system [111] independent of the Rössler system (Eqs. 5.20), for comparison.
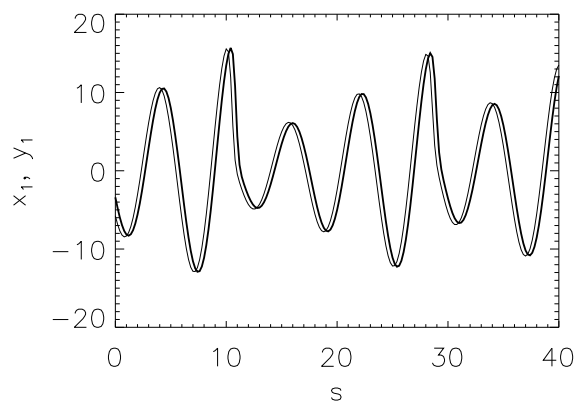

Figure 5.19: Example of lag synchronization: it is clearly seen that x_1 (bold line) goes behind y_1 (solid line). It holds: $x_1(t + \tau) = y_1(t)$, with $\tau = 4$.

Case	JPR(5% noise)	JPR(without noise)
GS	0.527	0.605
independent	0.0438	0.0470

Table 5.3: Index JPR calculated for Eqs. 5.20 and 5.21 with observational noise and without noise, for comparison.

Case	RR=0.02	RR=0.1	RR=0.2	RR=0.5
GS	0.107	0.191	0.213	0.120

Table 5.4: Index JPR calculated for the Lorenz system driven by the Rössler (Eqs. 5.20 and 5.21) with 20% observational noise and different choices of RR.

5.4.2   Influence of Noise

Analogously to Sec. 5.2.2, we analyze the influence of noise on the recurrence based indices for GS. We take as example the Lorenz system driven by the Rössler (Eqs. 5.20 and 5.21).

- First of all, we concentrate on JPR (Eq. 5.18). This index is not as robust as the index CPR to the influence of noise, i. e. with noise levels of 80%, the deviations of JPR from the noise free value are rather large, so that we cannot differentiate GS from independent systems. But for moderate noise levels, it yields rather good results (see Tab. 5.3).
  If we have higher noise levels, we can minimize the deviation of the value of JPR from the noise free case, choosing a higher RR. This corresponds to using higher thresholds ε_i in the computation of JPR [90]. The results for 20% noise and different values of RR are summarized in Tab. 5.4. We see, that if RR is chosen too high, then the deviation of JPR from the noise free becomes also large. This is because for $RR = 0.5$ half of the points in the RP are black and hence, spurious structures appear. The optimal choice of RR in this case, is about 0.2.

- Now, we analyze the influence of noise on SPR (Eq. 5.19). This index is based on the probability of recurrence $P(\tau)$, as well as CPR, and hence it is very robust against noise. We add to each component of Eqs. 5.20 and 5.21 80% independent noise and compute $P(\tau)$ for both subsystems (Fig. 5.20). We see, that although the peaks of $P(\tau)$ have become much smaller because of the high noise level (compared with the noise free case shown in Fig. 5.18), $P(\tau)$ of the driven Lorenz almost coincides with $P(\tau)$ of the driving Rössler system (Fig. 5.20 a). The results obtained with SPR
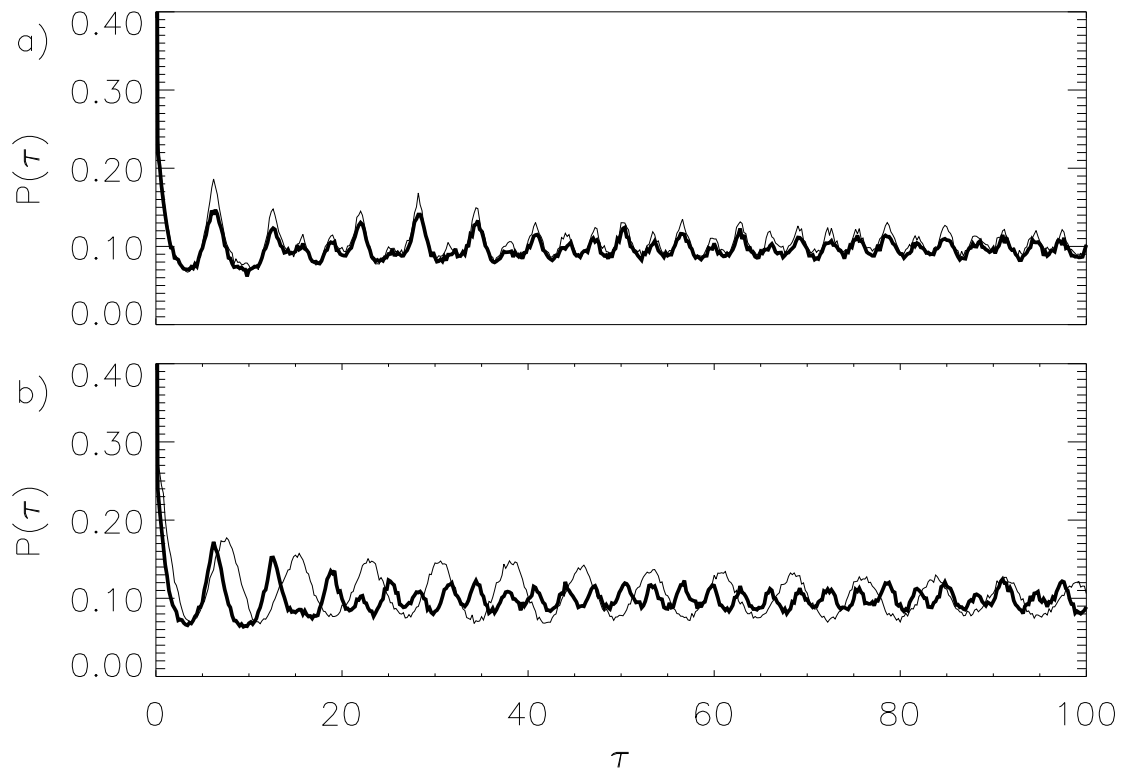
Figure 5.20: (a) $P(\tau)$ for the Lorenz system driven by the Rössler (Eqs. 5.20 and 5.21) with 80% observational noise (solid line: driven Lorenz, bold line: Rössler). (b) The same as in (a) for Lorenz independent of Rössler.

Case	SPR(80% **noise**)	SPR(**without noise**)
GS	0.968	0.934
independent	0.523	-0.196

Table 5.5: Index SPR calculated for Eqs. 5.20 and 5.21 with observational noise and without noise, for comparison.

Case	linear	periodic	nonlinear	without trend
GS	0.104	0.143	0.057	0.605
independent	0.136	0.137	0.094	0.0470

Table 5.6: Index JPR for GS calculated for the Lorenz system driven by the Rössler (Eqs. 5.20 and 5.21) with a linear trend, with a periodic trend and with a nonlinear trend. The values for JPR without trend are also given for comparison.

are summarized in Tab. 5.5. For the GS case, we see that there is almost no deviation of SPR from the free noise case. For the independent subsystems, we obtain a larger value of SPR with noise than without noise. At first, this may be surprising, but it is due to the fact that because of the high noise level, the peaks of both $P(\tau)$ become smaller. Hence, the difference between them is also smaller than in the case without noise.

5.4.3 Influence of Non-stationarity

We proceed in the same way as in Sec. 5.2.3 and take as example the Lorenz system driven by the Rössler (Eqs. 5.20 and 5.21). We add three different trends to the components of Eqs. 5.20 (linear, periodic and nonlinear) and compute both indices JPR and SPR.

In Tab. 5.6 the results for the index JPR are summarized. We see, that this index is not robust against non-stationarities. But as it is applicable to rather short time series, one can overcome this problem performing the analysis in windows.

In Tab. 5.7 the results for the index SPR are recapped. From this table, we see that SPR is rather stable against instationarities, similarly to the CPR index for PS. This is due to the averaging by computing the probability of recurrence $P(\tau)$ (Eq. 5.8).

Case	linear	periodic	nonlinear	without trend
GS	0.701	0.672	0.739	0.934
independent	-0.238	-0.191	-0.546	-0.196

Table 5.7: Index SPR for GS calculated for Eqs. 5.20 and 5.21 with a linear trend, with a periodic trend and with a nonlinear trend. The values for JPR without trend are also given for comparison.

5.5 Transition to Phase to Generalized Synchronization

We have seen in the previous sections, that the indices CPR, JPR and SPR clearly distinguish between oscillators in PS and oscillators which are not in PS, respectively GS. On the other hand, the synchronization indices should not only distinguish between synchronized and not synchronized regimes, but also indicate clearly the onset of PS, respectively of GS.

In order to demonstrate that the recurrence based indices fulfill this condition, we exemplify their application by two examples: two mutually coupled Rössler systems in a phase coherent regime (Eqs. 5.12), and in a non-phase coherent funnel regime (Eqs. 5.13). We increase in both cases the coupling strength μ continuously and compute for each value of μ the indices CPR, JPR and SPR. On the other hand, in the phase coherent case for a not too large but fixed frequency mismatch between both oscillators and increasing coupling strength, the transitions to PS and LS are reflected in the Lyapunov spectrum [66, 13] [4]. If both oscillators are not in PS, there are two zero Lyapunov exponents, that correspond to the (almost) independent phases. Increasing the coupling strength, the fourth Lyapunov exponent λ_4 becomes negative (see Fig. 5.21 d), indicating the onset of PS. For higher coupling strengths, the second Lyapunov exponent λ_2 crosses zero, which indicates the establishment of a strong correlation between the amplitudes (see Fig. 5.21 d). This last transition occurs almost simultaneously with the onset of LS [75]. Therefore, we compute for our two examples also λ_2 and λ_4 in order to validate the results obtained with CPR and JPR.

In Fig. 5.21 the indices CPR (a), JPR (b) and SPR (c) are represented for increasing coupling strength μ for the phase coherent case. In (d) λ_2 and λ_4 are also shown in dependence on μ. By means of CPR, the transition to PS is detected when CPR becomes of the order of 1. We see from Fig. 5.21 a, that the transition to PS occurs at approximately $\mu = 0.037$, in accordance with the transition of the fourth Lyapunov exponent λ_4 to negative values. The other two

---

[4]For other cases, e. g. for a fixed coupling strength and decreasing frequency mismatch, or for a large frequency mismatch and increasing coupling strength, the transition to PS is not always reflected in the Lyapunov spectrum (see Sec. 4.4).
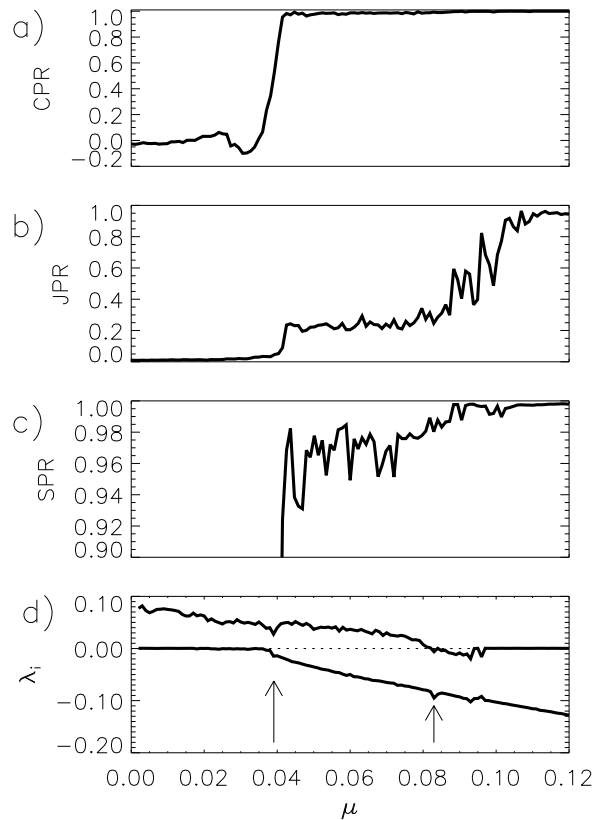
Figure 5.21: CPR (a), JPR (b), SPR (c)coefficients and λ_2 and λ_4 (d) in dependence of the coupling strength for two mutually coupled Rössler systems in the phase coherent regime. The dotted zero line in (d) is plotted to guide the eye. The arrows indicate the transition of λ_4 to negative values and the transition of λ_2 to zero.

criteria, JPR and SPR, also show the transition to PS, although they are indices for GS. The index JPR shows three plateaus in dependence on the coupling strength (Fig. 5.21 b), indicating the onset of PS at the beginning of the second one. The index SPR jumps from rather small values to values around 0.96 at the onset of PS (a magnification is shown in Fig. 5.21 c).

On the other hand, JPR clearly indicates the onset of LS because it becomes nearly one (third plateau) at approximately $\mu = 0.1$ (Fig. 5.21 b), after the transition from hyperchaoticity to chaoticity, which takes place at approximately $\mu = 0.08$ (Fig. 5.21 d). Between $\mu = 0.08$ and $\mu = 0.1$, the values of JPR have large fluctuations. This reflects the **intermittent lag synchronization** [75, 13], where LS is interrupted by intermittent bursts of no synchronization. The index SPR becomes nearly one at approximately $\mu = 0.08$, coinciding with the transition to LS according to the Lyapunov spectrum. The index SPR is based on the probability of recurrence, and hence, it is obtained by averaging over the time series. Therefore, the burst LS errors are averaged out and it does not detect the intermittent LS. The problem with SPR is that it does not distinguish between PS and LS as well as JPR: the values obtained with SPR for oscillators that are in PS but not yet in LS, are of the order of 0.96, whereas the values obtained with JPR for PS are of the order of 0.22. In this way, JPR has more power to detect LS than SPR.

Now we regard the more complex case of two coupled Rössler systems in the non-coherent funnel regime, where the direct application of the Hilbert transformation is not possible [53]. In Fig. 5.22 the coefficients CPR, JPR and SPR are represented for this case in dependence on the coupling strength μ. Again, λ_2 and λ_4 are also shown (Fig. 5.22 d).

First, we note that for $\mu > 0.02$, λ_4 has already passed to negative values (Fig. 5.22 d). However, CPR is still rather low, indicating that both oscillators are not in PS yet. CPR does not reveal the transition to PS until $\mu = 0.18$ (Fig. 5.22 a), as found with other techniques [53]. Furthermore, we see from Fig. 5.22 d, that λ_2 vanishes at $\mu \sim 0.17$. This transition indicates that the amplitudes of both oscillators become highly correlated. At approximately the same coupling strength, both indices JPR and SPR reach rather high values, indicating the transition to GS (Fig. 5.22 b, c). Then, according to the index CPR the transition to PS occurs after the onset of GS. This is a general result that holds for systems with a strong phase diffusion, as reported in [53]. For highly non-phase coherent systems, there exists more than one characteristic time scale. Hence, a high coupling strength is necessary in order to maintain the phase locking of both oscillators. Hence, PS is not possible without a strong correlation in the amplitudes.
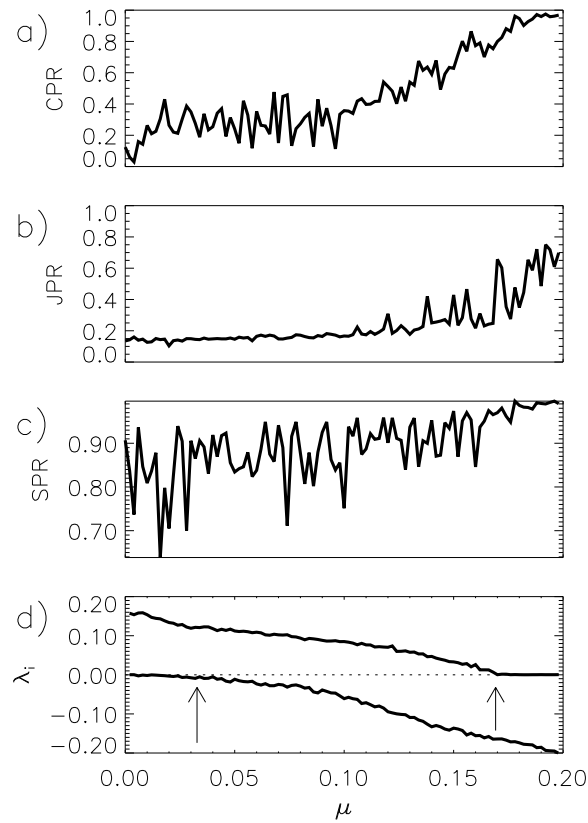
Figure 5.22: CPR (a), JPR (b), SPR (c)coefficients and λ_2 and λ_4 (d) in dependence on the coupling strength for two mutually coupled Rössler systems in the funnel regime. The dotted zero line in (d) is plotted to guide the eye. The arrows indicate the transition of λ_4 to negative values and the transition of λ_2 to zero.

5.6 Application to Experimental Data

5.6.1 Electrochemical Data

In order to test the applicability of the method to experimental data, we analyze time series from two globally coupled electrochemical oscillators.

The experiments were done with an electro-dissolution of iron in sulfuric acid in which non-phase coherent chaotic signals can be obtained and in which coupling strength μ can be varied. A standard three-compartment electrochemical cell consisting of an array of two iron working electrodes, a $Hg/Hg_2SO_4/K_2SO_4$ reference electrode and a Pt mesh counter electrode was used. The applied potentials of the two electrodes were held at the same value with a potentiostat and the experiments were performed in $0.5mol/dm^3 H_2SO_4$ solution at room temperature in stagnant solution. The currents of the electrodes were measured independently at a sampling rate of $2kHz$. The electrodes were connected to the potentiostat through two individual parallel resistors (R_{ind}) and through one series collective resistor (R_{coll}) which furnishes a global coupling of strength $\mu = R_{coll}/R_{tot}$, where $R_{tot} = R_{coll} + R_{ind}/2$ was kept constant. For $\mu = 0$, the external resistance furnishes no additional coupling and for $\mu = 1$, maximal external coupling is achieved [33]. Fig. 5.23 shows a segment of the time series of both electrochemical oscillators without coupling ($\mu = 0$). Two main different time scales are recognizable (small and large oscillations), indicating the non-phase coherency of both oscillators.

Now we compute the indices CPR (Eq. 5.9), JPR (Eq. 5.18) and SPR (Eq. 5.19) for six different coupling strengths $\mu = \{0.0, 0.2, 0.4, 0.6, 0.8, 1.0\}$.

We begin with the computation of the indices that are all based on the probability of recurrence $P(\tau)$ (Eq. 5.8). For the estimation of $P(\tau)$ of each oscillator, we choose $RR = 0.1$. Fig. 5.24 shows the probabilities of recurrence in dependence on the time lag for two different coupling strengths $\mu = 0$ (a) and 0.6 (b). It can be clearly recognized, that without coupling, the position of the maxima of $P(\tau)$ of both oscillators do not coincide (Fig. 5.24 a), whereas for $\mu = 0.6$, the probabilities of recurrence of both oscillators nearly coincide, indicating not only PS, but also GS (Fig. 5.24 b).

For the computation of JPR we choose also $RR = 0.1$. In Fig. 5.25 the RPs and JRPs of both electrochemical oscillators are shown for $\mu = 0$ and in Fig. 5.26 the corresponding plots are shown for $\mu = 0.6$. We see, that for $\mu = 0$ the JRP has almost no recurrence points, since both oscillators are independent (Fig. 5.25 c). In contrast, for $\mu = 0.6$ the RPs of both oscillators are very similar, and hence, also the JRP, indicating GS (Fig. 5.26).

The results of the computation of the three indices for the different coupling strengths $\mu = \{0.0, 0.2, 0.4, 0.6, 0.8, 1.0\}$ are represented in Fig. 5.27. We note, that the three synchronization indices have a similar course: the highest value is reached at $\mu = 0.6$ and for higher coupling strengths, the indices decrease.
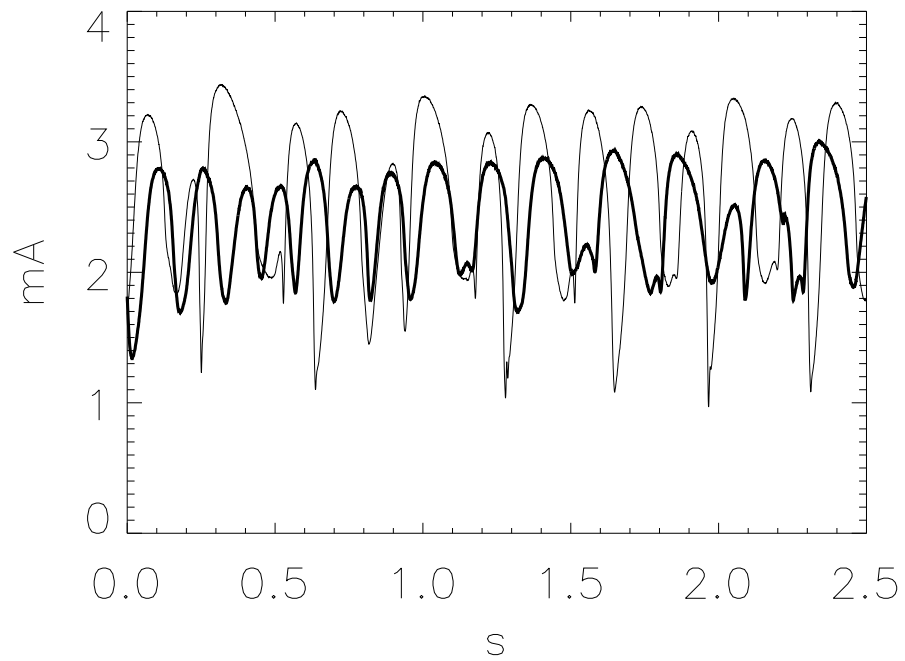
Figure 5.23: Time series of the current of two electrochemical oscillators for coupling strength $\mu = 0$ which display chaotic non-phase coherent signals. Solid line: oscillator 1, bold line: oscillator 2.
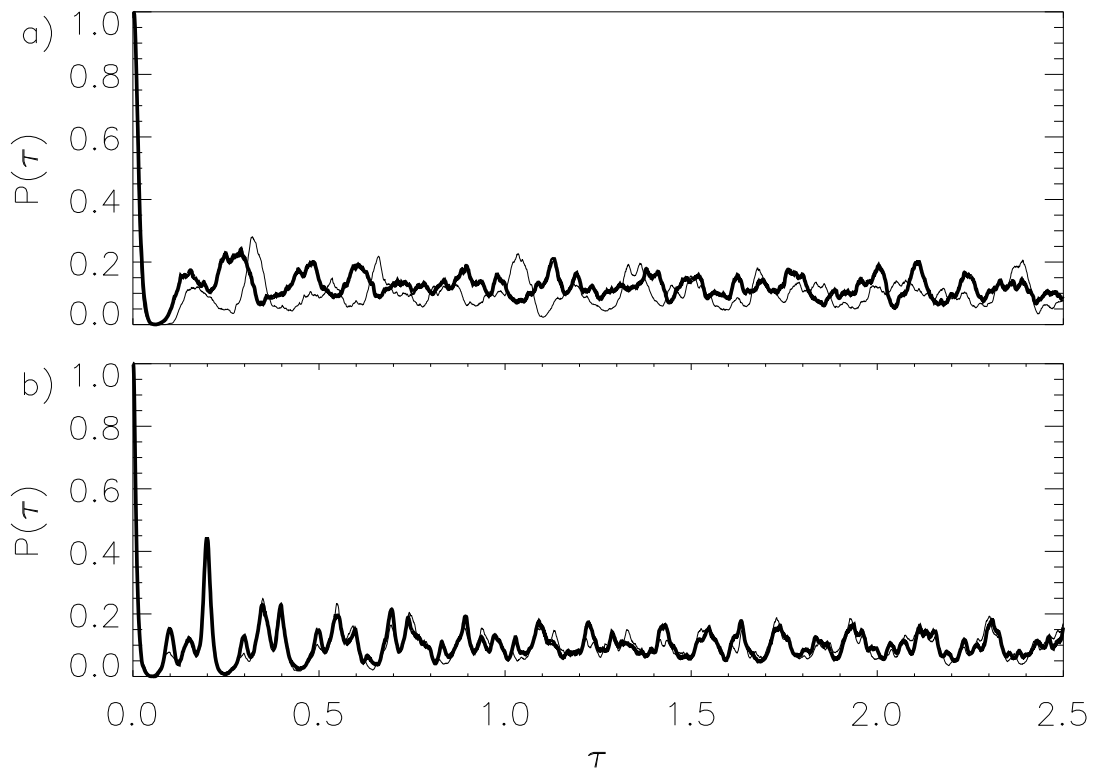
Figure 5.24: Probability of recurrence $P(\tau)$ (Eq. 5.8) for two non-phase coherent coupled electrochemical oscillators (solid line: oscillator 1, bold line: oscillator 2) for coupling strengths $\mu = 0$ (a) and $\mu = 0.6$ (b).
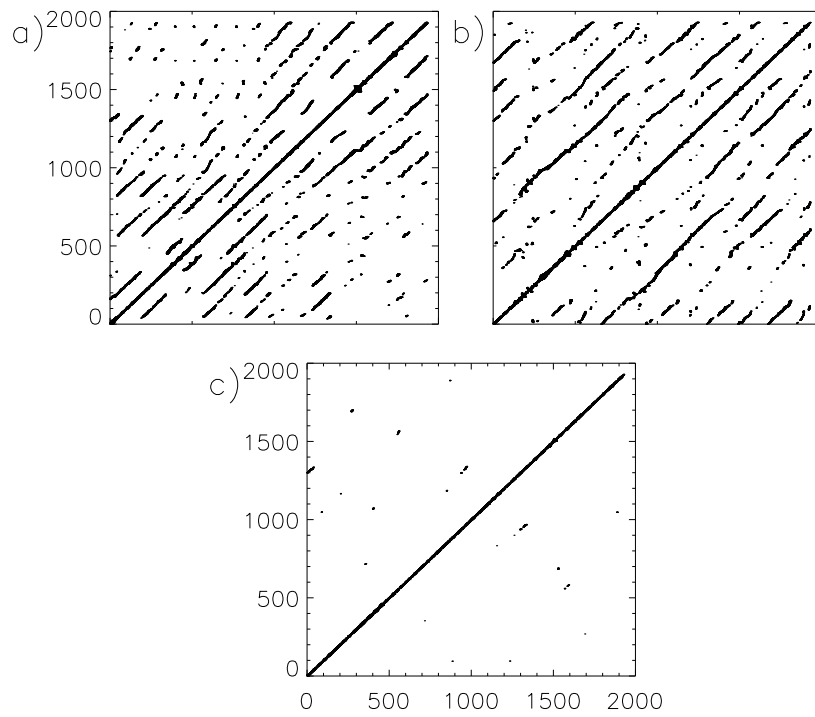
Figure 5.25: RP of the first electrochemical oscillator (a), RP of the second electrochemical oscillator (b) and JRP of both systems (c) (for $\mu = 0$).
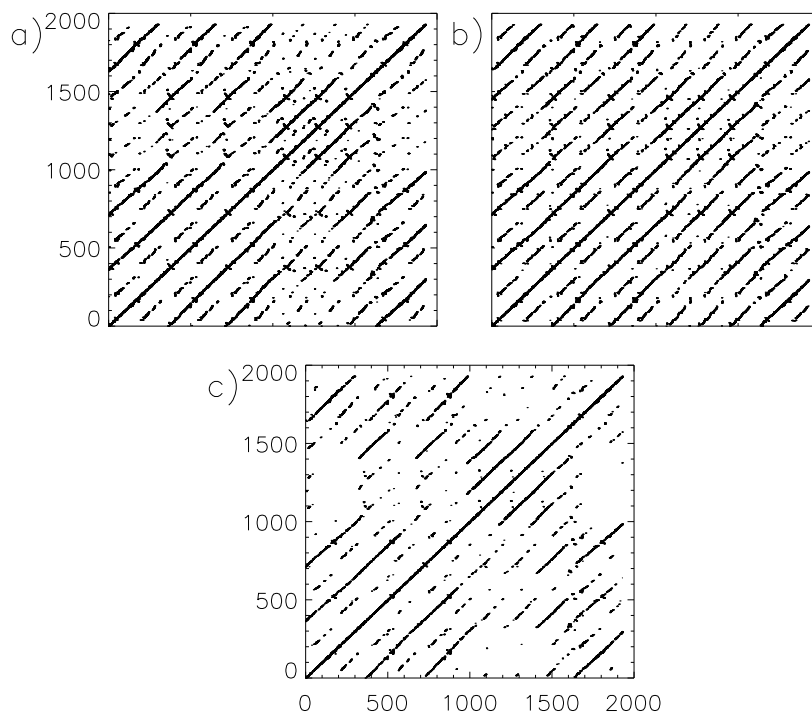
Figure 5.26: RPa of both electrochemical oscillators (a) and (b) for $\mu = 0.6$, and JRP of both systems (c).
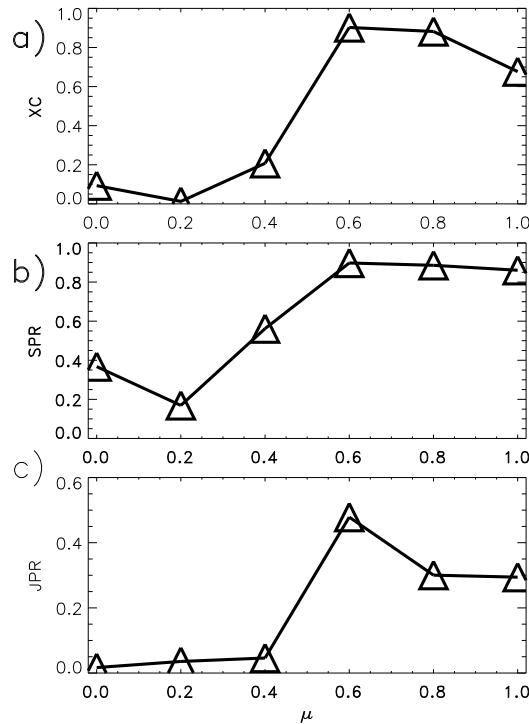
Figure 5.27: Synchronization indices CPR (a), SPR (b) and JPR (c) in dependence on the coupling strength for the non-phase coherent electrochemical oscillators.

We detect the transition to PS and GS simultaneously at the coupling strength $\mu = 0.6$, in accordance with theoretical results reported in [53]. As the electrochemical oscillators are highly non-coherent, a strong coupling strength is needed for the onset of PS, and hence, the amplitudes are already highly correlated.

Now we regard the more complicated case of non-stationary data, where the non-stationarity is imposed through a linear continuous change of a controllable parameter, namely the applied potential. In this case we consider two different values of the coupling strength: $\mu = 0.0$ and $\mu = 0.6$. We compute the indices CPR, SPR and JPR for both coupling strengths in dependence on time by choosing a window length of 20,000 data points and in each step shifting the window by 1,000 data points (Figs. 5.28 and 5.29). Again, we choose $RR = 0.1$ for the computation.   For $\mu = 0.0$ the values of CPR are rather low all the time. The maximum value that CPR reaches is 0.42, indicating the absence of PS, as expected (Fig. 5.28 a). Analogously, the values of SPR and especially the values of JPR are rather low in all windows, indicating also the absence of GS (Fig. 5.28b,c).
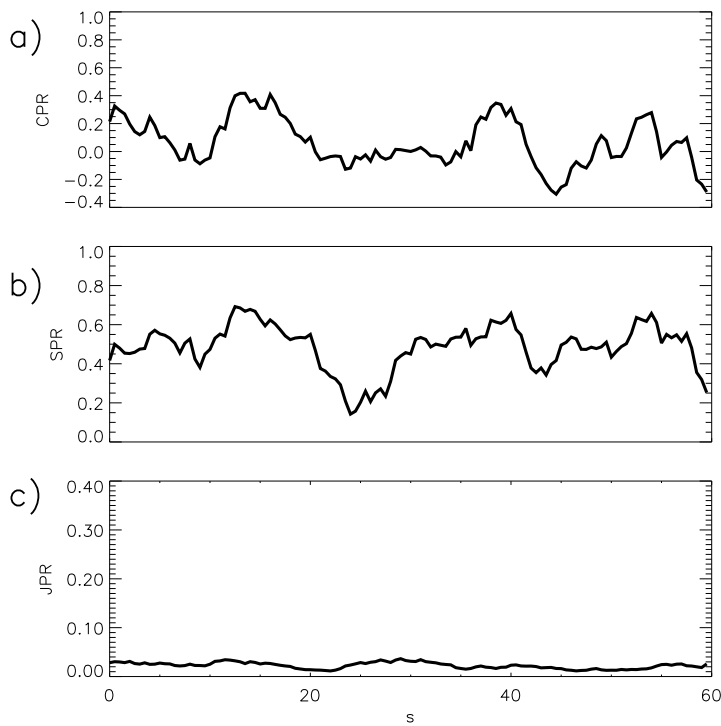
Figure 5.28: Synchronization indices CPR (a), SPR (b) and JPR (c) in dependence on time for coupling strength $\mu = 0$ for two non-phase coherent and non-stationary electrochemical oscillators.
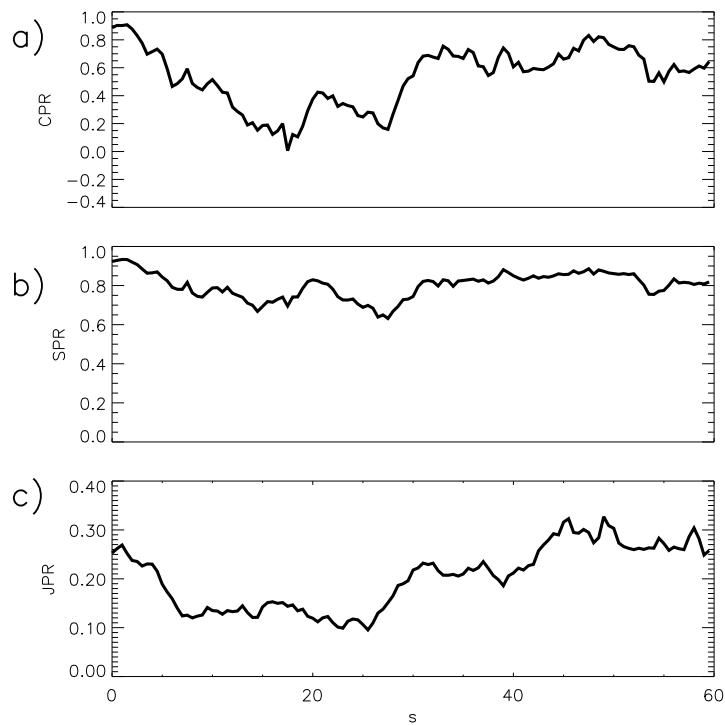
Figure 5.29: Synchronization indices CPR (a), SPR (b) and JPR (c) in dependence on time for coupling strength $\mu = 0.6$ for two non-phase coherent and non-stationary electrochemical oscillators.

For $\mu = 0.6$, we see a striking dependence on time: at the beginning and at the end of the data set, the values of CPR, SPR and JPR are rather high, indicating PS and GS, respectively (Fig. 5.29). However, in the middle of the data set, the synchronization indices are rather small, indicating the lack of PS and GS. Hence, due to the instationarity of the data, the synchronization degree between both oscillators changes in time. Furthermore, we see, according with the synchronization indices, that PS and GS sets on approximately at the same time, i. e. the index CPR for PS reaches its maximum value when the indices SPR and JPR also are maximal. This is again due to the strong non-coherence of the electrochemical oscillators.

5.7 Algorithm to Detect Clusters of PS

As we have seen in Sec. 5.2, it is possible to detect PS between two systems comparing the position of the local maxima in $P_1(\tau)$ and $P_2(\tau)$. In this section, we propose an algorithm for the quantification of PS extended to N oscillators that is rather useful for the detection of clusters of phase synchronized oscillators. We begin with the simpler algorithm to detect PS for two complex oscillators, and afterwards we extend it for the detection of clusters of oscillators in PS.

1. Compute $P_{1,2}(\tau)$ of both systems based on the RPs (Eq. 5.8).

2. Determine the times $\tau_{1,2}^i$, where $P_{1,2}(\tau)$ has local maxima.

$$\frac{dP_{1,2}(\tau^i)}{d\tau^i} = 0 \qquad (5.22)$$

3. Compute the difference between the times of maximum probability of recurrence

$$\Delta\tau^i = \tau_1^i - \tau_2^i, \qquad i = 1, \ldots, M, \qquad (5.23)$$

   where M is the number of local maxima.

If the systems are phase synchronized, the probability of recurrence is maximal at the same time. Therefore, $\Delta\tau^i$ versus i fluctuates about 0. In contrast to this, if the systems are not in PS, the maximum probability of recurrence does not occur simultaneously and we observe a drift (Fig. 5.30 c). Hence, the slope slp given by the linear regression of this curve can be used to quantify PS: $slp \simeq 0$ means PS and $slp > 0$ means non-PS.

Now we exemplify this algorithm in the case of two mutually coupled Rössler systems (Eqs. 5.12) in the phase coherent regime. For $\omega_1 = 0.98, \omega_2 = 1.02$ and $\mu = 0.05$ both systems are in PS [53]. If we compute $P(\tau)$ for both systems, we observe local maxima at $\tau = n \cdot T$, where T is the mean period of both Rössler systems (Fig. 5.30 a). In this case we obtain $slp = 0.0$ for $i = 0, \ldots, 20$ for
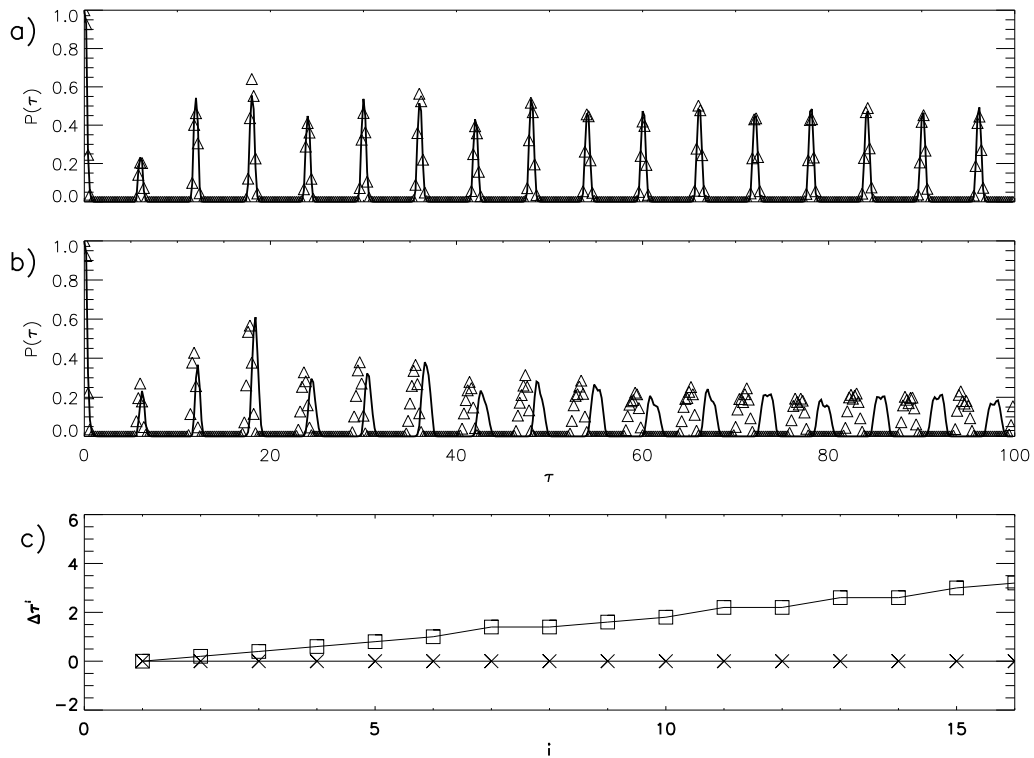
Figure 5.30: $P(\tau)$ for the two mutually coupled Rössler systems in phase coherent regime (Eqs. 5.12) for coupling strength $\mu = 0.05$ (a) and for $\mu = 0.02$ (b). Solid line: system 1, triangles: system 2. c) Difference of times of maximum probability of recurrence between both systems for $\mu = 0.05$ (crosses) and for $\mu = 0.02$ (squares).
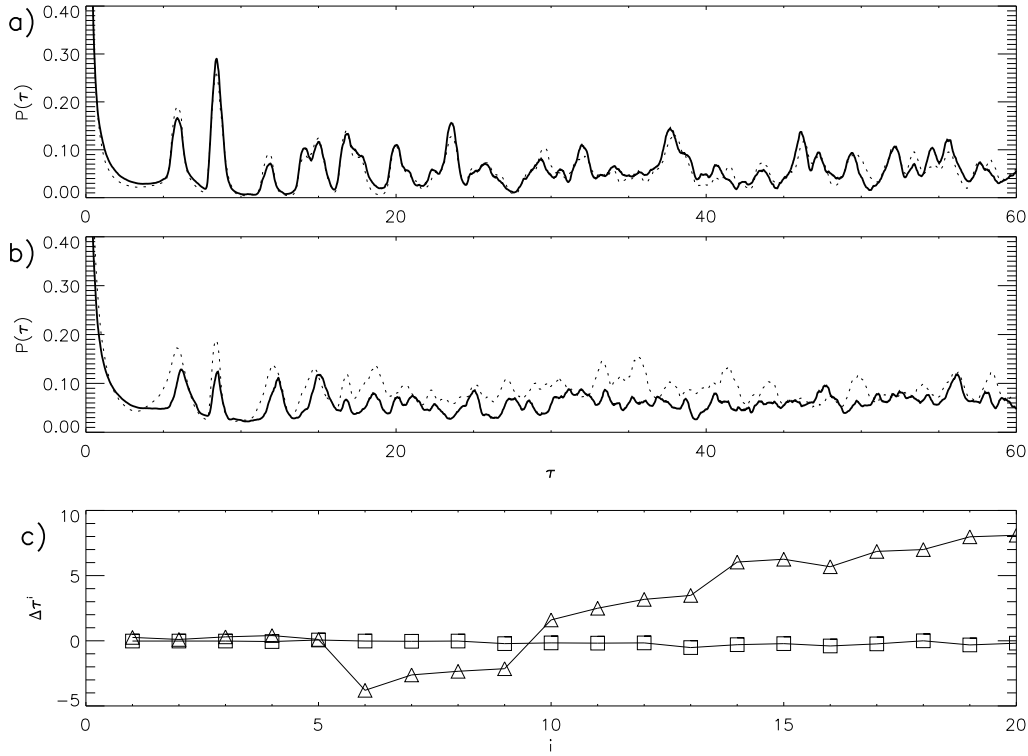
Figure 5.31: $P(\tau)$ for the two mutually coupled funnel systems (Eqs. 5.13) for coupling strength $\mu = 0.2$ (a) and for $\mu = 0.15$ (b). Solid line: system 1, dashed line: system 2. c) Difference of times of maximum probability of recurrence between the systems for $\mu = 0.2$ (triangles) and for $\mu = 0.15$ (squares).

coupling strength $\mu = 0.05$, with standard deviation $\sigma = 0.0$. For $\mu = 0.02$ we obtain $slp = 0.212$ for $i = 0, \ldots, 20$, with $\sigma = 0.068$. Under the assumption that the fluctuations about the regression lines are Gaussian distributed, an hypothesis test can be performed: if $slp > \frac{1.96 \cdot 2 \cdot \sigma}{M}$, then both systems are not in PS. Applying this criterion to the former cases, we confirm that for $\mu = 0.05$ the systems are in PS and for $\mu = 0.02$ the systems are not in PS, in accordance with [53].

Now we regard the more complex case of two coupled Rössler systems in the non-coherent funnel regime (Eqs. 5.13). In contrast to a direct use of the Hilbert transformation the proposed algorithm does detect PS for the coupling strength $\mu = 0.2$ and non-PS for $\mu = 0.15$: first we compute $P(\tau)$ for both systems for the two values of μ (Fig. 5.31). Also in this case, we see that for $\mu = 0.2$ the positions of the local maxima coincide for both oscillators (Fig. 5.31 a), whereas for $\mu = 0.15$ the positions of the local maxima do not coincide anymore (Fig. 5.31 b)

[5]. Again $\Delta\tau^i$ yields a clear distinction for both cases (Fig. 5.31 c). For $\mu = 0.2$ we obtain a mean slope $slp = -0.0159$ with $\sigma = 0.117$ for $i = 0, \ldots, 20$. For $\mu = 0.15$ we observe again a drift, analogously to Fig. 5.31 c, with $slp = 0.546$ with $\sigma = 1.97$ for $i = 0, \ldots, 20$. Applying the former hypothesis test to the obtained values for slp we confirm the results presented in [53]: for coupling strength $\mu = 0.2$ we detect PS and for $\mu = 0.15$ we detect non-PS.

The extension of this algorithm for the application to N oscillators is straight-forward: we compute $P_j(\tau)$ for each oscillator j (Eq. 5.8) and their respectively local maxima τ_j^i according to Eq. 5.22. Then we choose the set of times of local maxima τ_r^i of an arbitrary oscillator r as reference and compute $\Delta\tau_j^i = \tau_j^i - \tau_r^i$ for each oscillator j.

For the oscillators that are in PS with the reference oscillator, $\Delta\tau_j^i$ versus i fluctuates around zero. But for the oscillators that are in non-PS with the reference oscillator, $\Delta\tau_j^i$ versus i has mean slope greater than 0. Now even clusters of oscillators in PS are easily recognized, as the mean slope of $\Delta\tau_j^i$ versus i is equal for all oscillators j belonging to the same cluster.

To exemplify this algorithm we apply it first to a chain of coupled nonidentical Rössler oscillators with a nearest-neighbor diffusive coupling:

$$
\begin{aligned}
\dot{x}_j &= -\omega_j y_j - z_j, \\
\dot{y}_j &= \omega_j x_j + a y_j + \mu(y_{j+1} - 2y_j + y_{j-1}), \\
\dot{z}_j &= 0.4 + z_j(x_j - 8.5),
\end{aligned}
\tag{5.24}
$$

where the index $j = 1, \ldots, N$ denotes the position of an oscillator in the chain, μ is the coupling coefficient and ω_j corresponds to the natural frequency of each individual oscillator [52]. We consider a linear distribution of natural frequencies $\omega_j = \omega_1 + \delta(j-1)$, where δ is the frequency mismatch between neighboring systems. For coupling strength $\mu = 0.18$ and $\delta = 9 \times 10^{-3}$ we compute $P_j(\tau)$ for $j = 1, \ldots, 50$ and the positions of the local maxima τ_j^i for each oscillator. We choose the oscillator $j = 1$ as reference and compute $\Delta\tau_j^i$ for $j = 1, \ldots, 50$ (Fig. 5.32 a). Furthermore, we represent the slope of $\Delta\tau_j^i$ versus i computed by a linear regression for $j = 1, \ldots, 50$ in Fig. 5.32 b. We detect 9 clusters of oscillators in PS, in accordance with [52]. We have also analyzed this chain of Rössler oscillators with other values of the coupling strength and we obtain results in accordance with [52].

---

[5]In order to determine the local maxima of $P(\tau)$ in this case, a Butterworth filter was used to avoid the small statistical fluctuations.
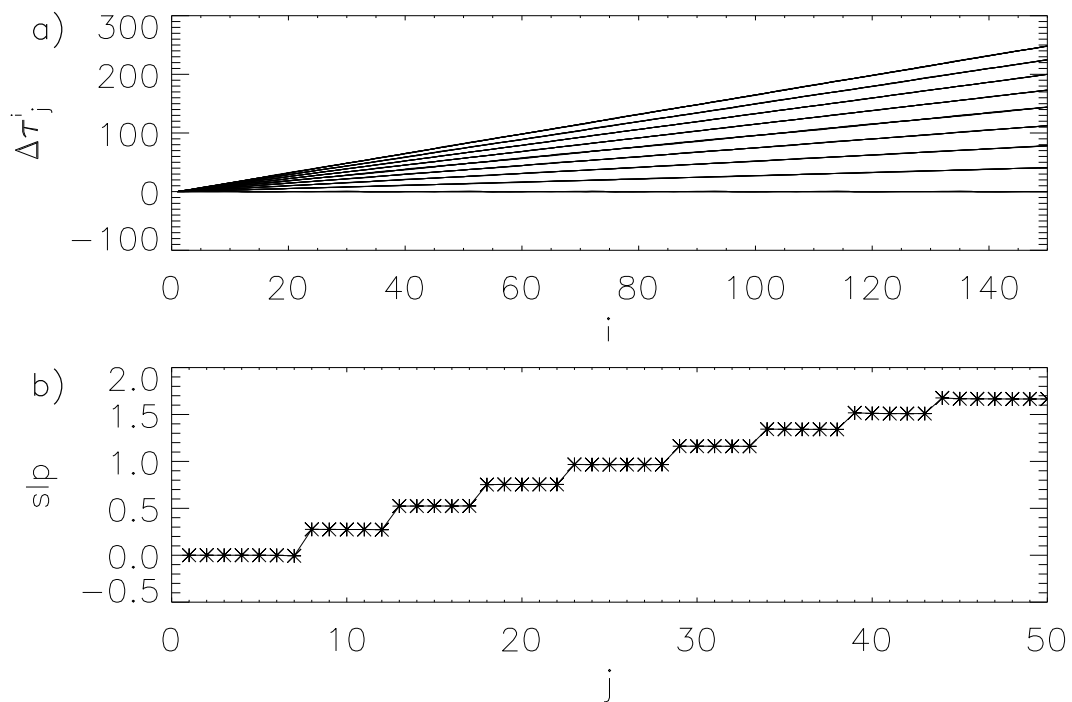
Figure 5.32: a) Difference between the local maxima of the probability of recurrence for a chain of 50 Rössler oscillators diffusively coupled for $\mu = 0.18$ and $\delta = 9 \times 10^{-3}$. b) Slope of $\Delta\tau_j^i$ versus i for $j = 1, \ldots, 50$ with $\mu = 0.18$ and $\delta = 9 \times 10^{-3}$

5.7.1   Application to a Population of Chaotic Electrochem- ical Oscillators

In order to show the applicability of the method to an experimental system we consider data from a population of 64 nonidentical chaotic electrochemical oscillators with weak global coupling. The electrochemical system is the electrodissolution of Ni in 4.5 mol/L sulfuric acid solution (see [31] for the details of the experiment). The electrochemical oscillators are electrically coupled with a combination of one series (R_s) and 64 parallel (R_p) resistors; a global coupling parameter can be defined as $\mu = R_s/(R_p N)$, where $N = 64$ is the number of elements.

We present here the results for three different coupling strengths: without ($\mu = 0.0$), with small ($\mu = 0.05$), and with relatively strong ($\mu = 0.1$) coupling. Without coupling the oscillators have an approximately unimodal frequency distribution with a mean frequency of 1.219 Hz and a standard deviation of 18 mHz.

After computing $P_j(\tau)$ for $j = 1, \ldots, 64$ we calculate $\Delta\tau_j^i$, where the oscillator $r = 1$ was chosen as reference (Fig. 5.33). We note that in the absence of coupling the slope of $\Delta\tau_j^i$ versus i is different for each oscillator (Fig. 5.33 a, b). Increasing the coupling strength to $\mu = 0.05$ we observe a main group of oscillators that have almost slope 0, but still many of them are spread out (Fig. 5.33 c, d). If we increase further the coupling strength to $\mu = 0.1$, we observe that all 64 oscillators have an approximately vanishing slope, and therefore they are in PS (Fig. 5.33 e, f), as reported in [31].

5.8   Discussion

In this chapter new indices to detect PS and GS (including LS) for chaotic and complex systems have been introduced, based on the fundamental idea of recurrences in phase space. They have been then applied to model systems and experimental data.

First, we have introduced the index CPR (Correlation of Probability of Recurrence) for the detection of PS, which is based on the probability of recurrence to the neighborhood of a former visited point in phase space (Eq. 5.8). We have shown, that this index is rather robust against noise: even for 80% observational noise, the method distinguishes rather well between PS and non-PS. Further, we have seen, that CPR is almost not influenced by non-stationarities. It also works for chaotic systems with a rather strong phase diffusion, as has been demonstrated for the funnel system and for non-phase coherent experimental data from electrochemical oscillators. It also detects rather well the onset of PS (Sec. 5.5). The robustness with respect to non-stationarities is due to the fact, that there is no need to choose an origin, about which all the trajectories of the system oscillate. Hence, CPR is not influenced if the "origin" wanders with time (by the
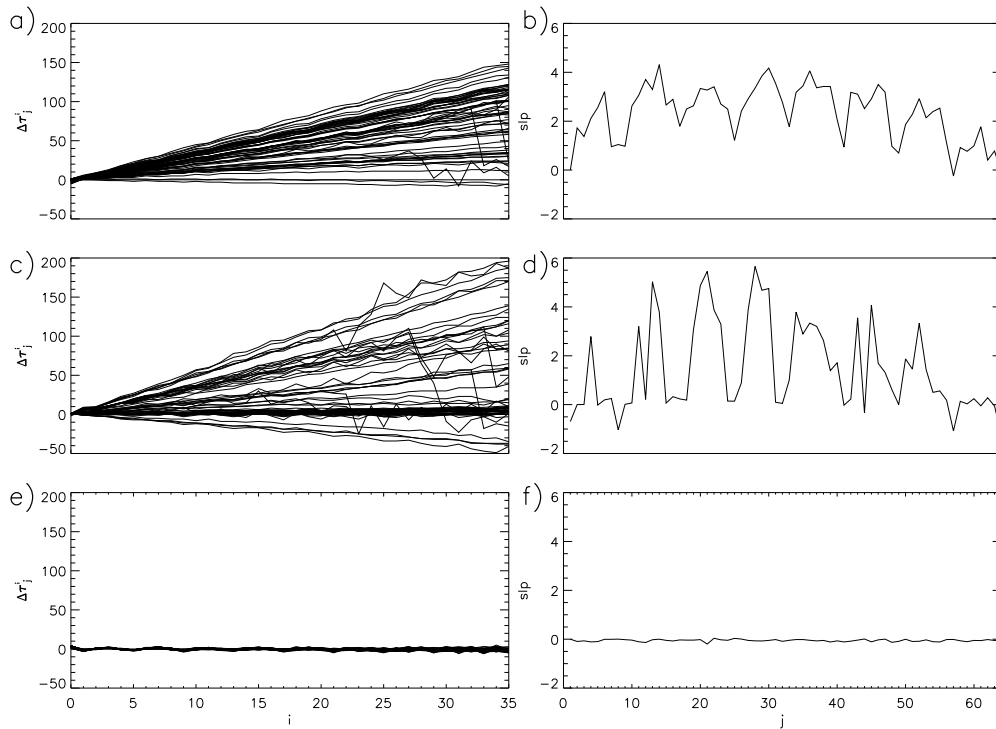
Figure 5.33: a) Difference between the local maxima of the probability of recurrence $\Delta\tau_j^i$ versus i (Eq. 5.23) for a population of 64 chaotic electrochemical oscillators and slope of $\Delta\tau_j^i$ versus j for $j = 1, \ldots, 64$ (j denotes the oscillator and i the time). (a) and (b) for coupling strength $\mu = 0$, (c) and (d) for $\mu = 0.05$, (e) and (f) for $\mu = 0.1$.

definition of the phase based on the Hilbert transformation, difficulties appear with non-stationary time series, as the the origin varies with time [66]).

The robustness with respect to noise, is due to the fact that considering the probability of recurrence (Eq. 5.8) we average out synchronization errors induced by the present noise.

As we have mentioned in Sec. 5.2, the probability of recurrence (Eq. 5.8) can be considered as a generalized autocorrelation function, because it takes moments of higher order into account. Simulations show that the linear autocorrelation function can detect PS in rather "simple" cases (e. g. a periodically driven Rössler system), but it fails in the more complex ones (e. g. if rather high levels of noise, non-stationarities or strong non-phase coherent attractors are present).

The disadvantage of others techniques proposed so far for the synchronization analysis of complex chaotic signals, e. g. in [53], is that the derivative of the time series has to be computed. This can be problematic in the presence of noise. Furthermore, for higher dimensional systems, the approach presented in [53] does not always work, as the definition of the phase is based on an appropriate projection, and this cannot be always found. With the index CPR we overcome all these problems.

Secondly, two different indices for GS (including LS) have been introduced. The first one, JPR (Joint Probability of Recurrence), compares the local recurrences of each point in phase space with the ones of the interacting (sub)system. It has the advantage, that it recognizes very well the transition between PS and GS (see Sec. 5.5). The other proposed index for GS, is SPR (Similarity of Probability of Recurrence) and it is based on the probability of recurrence (Eq. 5.8), as well as CPR. It does not distinguish between PS and GS as well as JPR, but it is extremely robust against noise and instationarities for the same reason mentioned above. Hence, depending on the case one is faced with, one has to choose the most appropriate of them, or even use both and compare the results.

Furthermore, an alternative algorithm has been proposed, that allows to identify clusters of PS in populations of weakly coupled oscillators. It has been successfully applied to simulated, as well as experimental data.

All the different indices proposed here do not require a large computational effort and the number of data points needed for the analysis is rather low. They are based on the fundamental relationship between recurrences and synchronization. However, a correct synchronization analysis should be accompanied always by an hypothesis test. Thiel et al. [94] have recently proposed an algorithm to generate surrogates, which allows to test for PS. Hence, the next steps to complete the methods presented in this work for the synchronization detection of complex signals, will be to apply them together with the surrogates technique presented in [94].

Chapter 6

Conclusions and Outlook

In this work the relationship between recurrences and synchronization of chaotic and complex systems has been investigated.

First (Chap. 3), a new method for the computation of multivariate recurrence plots has been proposed (joint recurrence plots), which considers joint or simultaneous recurrences in the respective phase spaces of the coupled subsystems. It differs from the former technique to compute recurrence plots of bivariate data, since it does not "mix" the phase spaces of both subsystems, but it considers each one separately.

Furthermore, it has been shown, that by means of the new joint recurrence plots it is possible to estimate the joint Rényi entropy of second order JK_2. Then it has been focused on the synchronization analysis by means of JK_2, and its application has been exemplified for the two bidirectionally coupled Rössler systems. There, we have found new characteristics of the transition to phase synchronization and lag synchronization (Chap. 4). Some of them are:

- The transition to phase synchronization for intermediate and large coupling strengths can be a chaos-period-chaos one.

- For intermediate and large coupling strengths the whole system is more chaotic inside than outside the Arnold tongue , i. e. the whole system is more chaotic when the subsystems synchronize. This seems to be at a first counterintuitive.

- For large frequency mismatch and increasing coupling strength, a direct transition from non-phase synchronized regime to lag synchronized regime is observed. In the course of this transition, the amplitudes become strongly correlated, but the phases do not lock.

Furthermore, the sum of the positive Lyapunov exponents has been compared with JK_2, and we have concluded, that one obtains more information about the transition to PS by means of JK_2 than by means of the sum of the positive Lyapunov exponents. This is due to the nonhyperbolicity of the system

under consideration. Hence, JK_2 may be a more appropriate measure for the predictability of the system under consideration than the sum of the positive Lyapunov exponents [72].

Moreover, a detailed analysis of the Lyapunov spectrum in the parameter space has revealed that there is region for intermediate coupling strengths, where the transition to phase synchronization is not given anymore by the zero crossing of the fourth Lyapunov exponent, as the latter is already negative outside of the Arnold tongue. That means, that because of the strong coupling, the phases have established a correlation also outside the synchronization region.

In the last part of this work (Chap. 5), a more direct and pragmatic relationship between recurrences and synchronization of chaotic systems has been developed [42]. Then, four different indices have been proposed that quantify phase and generalized synchronization. The major advantage of these indices with respect to the ones introduced in the literature so far, is their robustness against noise and instationarity, as well as their applicability to systems with a strong phase diffusion. This has been demonstrated for the Rössler system in funnel regime and for experimental non-phase coherent data from electrochemical experiments, which were also subjected to instationarity [73].

The next steps to be undertaken, are the application of the method to physiological or geophysical data, where it is difficult to define directly a phase. Furthermore, the performance of an hypothesis test is necessary to complete the synchronization analysis and test the power and specificity of the proposed indices. The application of the method of surrogates proposed in [94] seems to be very promising. Moreover, the recurrence based indices introduced in this work indicate the onset of PS and GS rather well. Hence, they are especially appropriate for the performance of the hypothesis test.

The analysis of generalized synchronization in structurally nonequivalent systems is still cumbersome. The recurrence based indices for GS may be more appropriate for the analysis of this kind of systems.

Furthermore, the automatic detection of $n : m$ phase synchronization of complex systems is still an open question. The relationship between recurrences and synchronization can eventually be exploited to develop suitable algorithms to tackle this task.

Acknowledgments

Bibliography

[1] H. D. I. Abarbanel, Analysis of observed chaotic data, Springer, (1995).

[2] V. S. Afraimovich, N. N. Verichev, M. I. Rabinovich, Izvestiya Vysshikh Uchebnykh Zavedenii Radiofizika **29 (9)**, 1050 (1986).

[3] E. Allaria, F. T. Arecchi, A. Di Garbo, R. Meucci, Phys. Rev. Lett. **86**, 701 (2001).

[4] K. Alligood, T. Sauer, and J. A. Yorke, Chaos an introduction to dynamical systems, Springer, (1996).

[5] V. S. Anishchenko, T. E. Vadivasova, J. Kurths, G. Okrokvertskhov, and G. I. Strelkova, Phys. Rev. E **69**, 036215 (2004).

[6] J. Arnhold, P. Grassberger, K. Lehnertz, C. E. Elger, Physica D **134**, 419 (1999).

[7] N. Asghari, C. Broeg, L. Carone, R. Casas-Miranda, J.C. Castro Palacio, I. Csillik, R. Dvorak, F. Freistetter, G. Hadjivantsides, H. Hussmann, A. Khramova, M. Khristoforova, I. Khromova, I. Kitiashivilli, S. Kozlowski, T. Laakso, T. Laczkowski, D. Lytvinenko, O. Miloni, R. Morishima, A. Moro-Martin, V. Paksyutov, A. Pal, V. Patidar, B. Pečnik, O. Peles, J. Pyo, T. Quinn, A. Rodriguez, M. C. Romano, E. Saikia, J. Stadel, M. Thiel, N. Todorovic, D. Veras, E. Vieira Neto, J. Vilagi, W. von Bloh, R. Zechnervand E. Zhuchkova, Astronomy and Astrophysics (in press).

[8] F. M. Atay, and Y. Altıntaş, Phys. Rev. E **59 (6)**, 6593 (1999).

[9] C. Bandt, G. Keller, and B. Pompe, Nonlinearity **15**, 1595 (2002).

[10] C. Beck and F. Schlögl, Thermodynamics of chaotic systems an introduction, Cambridge Nonlinear Science Series, (1992).

[11] B. Blasius, A. Huppert, and L. Stone, Nature **399**, 354 (1999).

[12] S. Boccaletti, D. L. Valladares, J. Kurths, D. Maza, and H. Mancini, Phys. Rev. E, **61 (4)**, 3712 (2000).

[13] S. Boccaletti, J. Kurths, G. Osipov, D. L. Valladares, and C. S. Zhou, Physics Reports **366**, 1 (2002).

[14] R. Brown, N. F. Rulkov, and E. R. Tracy, Phys. Lett. A **194**, 71 (1994).

[15] T. L. Carroll, and L. M. Pecora, Physica D **67**, 126 (1993).

[16] M. C. Casdagli, Physica D **108**, 12 (1997).

[17] K. M. Cuomo, and A. V. Oppenheim, Phy. Rev. Lett **71**, 65 (1993).

[18] J.-P. Eckmann, S. O. Kamphorst and D. Ruelle, Eur. Phys. Lett. **4**, 973 (1987).

[19] P. Faure, H. Korn, Physica D **122**, 265 (1998).

[20] H. Fujisaka, and T. Yamada, Prog. Theor. Phys., **69 (1)**, 32 (1983).

[21] D. Gabor, J. IEE London **93**, 429 (1946).

[22] J. Gao and H. Cai, Physics Letters A **270**, 75 (1999).

[23] C. G. Gilmore, Int. J. Bif. Chaos **3 (3)**, 583 (1993).

[24] P. Grassberger and I. Procaccia, Phys. Rev. Lett. **50**, 346 (1983).

[25] P. Grassberger and I. Procaccia, Physica D **9**, 189 (1983).

[26] P. Grassberger, Physics Letters A **97**, 227 (1983).

[27] P. Grassberger and I. Procaccia, Physica D **13**, 34 (1984).

[28] M. Itoh, T. Yang, L. O. Chua, Int. J. Bifurc. Chaos **9,** 1393 (1999).

[29] H. Kantz and T. Schreiber, Nonlinear Time Series Analysis, University Press, Cambridge, (1997).

[30] I. Z. Kiss, J. L. Hudson, Phys. Rev. E **64** 046215 (2001).

[31] I. Z. Kiss, Y. Zhai, and J. L. Hudson, Phys. Rev. Lett. **88**, 238301 (2002).

[32] I. Z. Kiss, Y. Zhai, and J. L. Hudson, Science **296**, 1676 (2002).

[33] I. Z. Kiss, Q. Lv, and J. L. Hudson, submitted to Phys. Rev. Lett.

[34] A. Kittel, A. Parisi, K. Pyragas, Physica D **112**, 459 (1998).

[35] L. Kocarev, K. S. Halle, K. Eckert, L. O. Chua, and U. Parlitz, Int. J. Bif. Chaos **2 (3)**, 709 (1992).

[36] L. Kocarev, U. Parlitz, and T. Stojanovski, Proccedings of the Symposium NOLTA (1995).

[37] L. Kocarev, and U. Parlitz, Phys. Rev. Lett. **74 (25)**, 5028 (1995).

[38] L. Kocarev, and U. Parlitz, Phys. Rev. Lett. **76**, 1816 (1996).

[39] M. Koebbe, and G. Mayer-Kress, Nonlinear modeling and forecasting -in: Proceedings of SFI Studies in the Science of Complexity, XXI, Eds.: M. Casdagli and S. Eubank, Addison-Wesley, Redwood City, 361 (1992).

[40] Y. Kuramoto, Chemical Oscillations, Waves and Turbulence, Springer, Berlin (1984).

[41] J. Kurths, U. Schwarz, C.P. Sonett, and U. Parlitz, Nonlinear Processes in Geophysics **1**, 72 (1994).

[42] J. Kurths, M. C. Romano, M. Thiel, G. V. Osipov, and M. V. Ivanchenko, proceedings of the 12th International IEEE, NDES in Evora (Portugal) (2004).

[43] E. N. Lorenz, J. Atmos. Sci. **20**, 130 (1963).

[44] E.N. Lorenz, J. Atmos. Sci. **26**, 636 (1969).

[45] N. Marwan, N. Wessel, U. Meyerfeldt, A. Schirdewan, and J. Kurths, Phys. Rev. E **66**, 026702 (2002).

[46] N. Marwan, M. Thiel, and N. R. Nowaczyk, Nonlinear Processes in Geophysics **9 (3-4)**, 325 (2002).

[47] N. Marwan, and J. Kurths, Phys. Lett. A **302 (5-6)**, 299 (2002).

[48] N. Marwan, Encounters With Neighbours - Current Developments Of Concepts Based On Recurrence Plots And Their Applications.- Ph.D. Thesis, Institute of Physics, University of Potsdam, ISBN 3-00-012347-4, (2003).

[49] N. Marwan, M. H. Trauth, M. Vuille, and J. Kurths, Climate Dynamics **21 (3-4)**, 317 (2003).

[50] N. Marwan, and A. Meinke, Int. J. Bif. Chaos, **14 (2)**, 761 (2004).

[51] N. Marwan, and J. Kurths, Cross Recurrence Plots and Their Applications, in Mathematicall Physics Research at the Cutting Edge, Nova Science Publishers, Hauppauge (2004).

[52] G. V. Osipov, A. Pikovsky, M. Rosenblum, and J. Kurths, Phys. Rev. E **55**, 2353 (1997).

[53] G. V. Osipov, B. Hu, C. Zhou, M. V. Ivanchenko, and J. Kurths, Phys. Rev. Lett. **91**, 024101 (2003).

[54] K. Otsuka, R. Kawai, S.-L. Hwong, J.-Y. Ko, J.-L. Chern, Phys. Rev. Lett. **84**, 3049 (2000).

[55] E. Ott, Chaos in Dynamical Systems, Cambridge University Press, (1993).

[56] E.-H. Park, M. Zaks, and J. Kurths, Phys. Rev. E **60**, 6627 (1999).

[57] U. Parlitz, L. Junge, and L. Kocarev, Phys. Rev. E **54 (6)**, 6253 (1996).

[58] U. Parlitz, L. Junge, W. Lauterborn, and L. Kocarev, Phys. Rev. E **54 (2)**, 2115 (1996).

[59] U. Parlitz, L. Kocarev, T. Stojanovski, and H. Preckel, Phys. Rev. E **53 (5)**, 4351 (1996).

[60] U. Parlitz, and L. Kocarev, Synchronization of Chaotic Systems, in Handbook of Chaos Control, Ed. H.G. Schuster, Wiley-VCH (1999).

[61] L. M. Pecora, and T. L. Carroll, Phys. Rev. Lett. **64**, 821 (1990).

[62] A. Pikovsky, Z.Physik B **55 (2)**, 149 (1984).

[63] A. S. Pikovsky, M. G. Rosenblum, G. V. Osipov, and J. Kurths, Physica D, **104**, 219 (1997).

[64] A. S. Pikovsky, G. V. Osipov, M. G. Rosenblum, M. Zaks, and J. Kurths, Phys. Rev. Lett. **79**, 47 (1997).

[65] A. S. Pikovsky, M. Zaks, M. G. Rosenblum, G. V. Osipov, and J. Kurths, Chaos **7**, 680 (1997).

[66] A. S. Pikovsky, M. G. Rosenblum, and J. Kurths, Synchronization, Cambridge University Press, (2001).

[67] H. Poincarè, Acta Math. **13**, 1 (1890).

[68] B. Pompe, J. Stat. Phys. **73**, 587 (1993).

[69] B. Pompe, P. Blidh, D. Hoyer and M. Eiselt, IEEE Engineering in Medicine and Biology, Magazine **17**, 32 (1998).

[70] R. Q. Quiroga, J. Arnhold, P. Grassberger, Phys. Rev. E **61**, 5142 (2000).

[71] A. Rényi, Probability theory, North-Holland, (1970) (appendix).

[72] M. C. Romano, M. Thiel, J. Kurths, and W. von Bloh, Phys. Lett. A (in press).

[73] M. C. Romano, M. Thiel, J. Kurths, I. Z. Kiss, and J. L. Hudson, submitted to Phys. Rev. Lett.

[74] M. G. Rosenblum, A. S. Pikovsky, and J. Kurths, Phys. Rev. Lett. **76**, 1804 (1996).

[75] M. G. Rosenblum, A. S. Pikovsky, and J. Kurths, Phys. Rev. Lett. **78**, 4193 (1997).

[76] M. G. Rosenblum, A. S. Pikovsky, J. Kurths, G. V. Osipov, I. Z. Kiss, and J. L. Hudson, Phys. Rev. Lett. **89 (26)**, 2641021 (2002).

[77] D. Ruelle, Bol. Soc. Brass. Mat. **9**, 83 (1978).

[78] N. F. Rulkov, M. M. Sushchik, L. .S. Tsimring, and H. D. I. D. Abarbanel, Phys. Rev. E, **51** 2, 980 (1995).

[79] C. Schaefer, M. G. Rosenblum, J. Kurths, and H. H. Abel, Nature **392**, 239 (1998).

[80] S. J. Schiff, P. So, T. Chang, R. E. Burke, T. Sauer, Phys. Rev. E **54**, 6708 (1996).

[81] A. Schmitz, Phys. Rev. E **62**, 7508 (2000).

[82] K. Shockley, M. Butwill, J. P. Zbilut and C. L. Webber Jr., Phys. Lett. A **305**, 59 (2002).

[83] O. V. Sosnovtseva, A. G. Balanov, T. E. Vadisova, V. V. Asthakov, and E. Mosekilde, Phys. Rev. E, **60**, 6560 (1999).

[84] M. de Sousa Vieira, P. Khoury, A. J. Lichtenberg, M. A, Lieberman, W. Wonchoba, J. Gullicksen, Y. J. Huang, R. Sherman, and M. Steinberg, Int. J. Bifurc. Chaos **2**, 645 (1992).

[85] H. Späth, Cluster Dissection and Analysis, Horwood, Chichester (1992).

[86] F. Strozzi, J.-M. Zaldivar, and J. P. Zbilut, Physica A **312 (3-4)**, 520 (2002).

[87] F. Takens, Detecting strange attractors in turbulence, in: Dynamical Systems and Turbulence, eds. D. A. Rand and L.-S. Young, Lecture Notes in Mathematics, Vol. 898, Springer, Berlin, (1980).

[88] P. Tass, M. G. Rosenblum, M. G. Weule, J. Kurths, A. Pikovsky, J. Volkmann, A. Schnitzler, H. J. Freund, Phys. Rev. Lett. **81**, 3291 (1998).

[89] J. Theiler, Phys. Rev. A **34 (3)**, 2427 (1986).

[90] M. Thiel, M. C. Romano, J. Kurths, R. Meucci, E. Allaria, T. Arecchi, Physica D **171 (3)**, 138 (2002).

[91] M. Thiel, M. C. Romano and J. Kurths, Applied Nonlinear Dynamics **11 (3)**, 20 (2003)

[92] M. Thiel, M. C. Romano, P. Read, and J. Kurths, Chaos **14 (2)**, 234 (2004).

[93] M. Thiel, M. C. Romano and J. Kurths, Phys. Lett. A (in press).

[94] M. Thiel, M. C. Romano, and J. Kurths, submitted to PRL.

[95] C. M. Ticos, E. Rosa Jr., W. B. Pardo, J. A. Walkenstein, M. Monti, Phys. Rev. Lett. **85**, 2929 (2000).

[96] M. H. Trauth, B. Bookhagen, N. Marwan, and M. R. Strecker, Palaegeography Palaeclimatology Palaeoecology, **194(1-3)**, 109 (2003).

[97] L. L. Trulla, A. Giuliani, J. P. Zbilut, and C. L. Webber Jr., Physics Letters A, **223 (4)**, 255 (1996).

[98] C. L. Webber Jr., and J. P. Zbilut, J. Appl. Physiol. **76**, 965 (1994).

[99] C. L. Webber Jr., M. A. Schmidt, and J. M. Walsh, Journal of Applied Physiology **78 (3)**, 814 (1995).

[100] M. Wiesenfeldt, U. Parlitz, and W. Lauterborn, Int. J. Bifurc. Chaos **11**, 2217 (2001).

[101] G. D. Van Wiggeren, R. Roy, Science **279**, 1198 (1998).

[102] C. W. Wu, L. O. Chua, Int. J. Bifurc. Chaos **4**, 979 (1994).

[103] T. Yamada, and H. Fujisaka, Prog. Theor. Phys. **70 (5)**, 1240 (1983).

[104] Y. Yuan Zhao, Int. J. Bifurc. Chaos **7**, 1401 (1992).

[105] M. Zaks, E.-H. Park, M. G. Rosenblum, and J. Kurths, Phys. Rev. Lett. **82**, 4229 (1999).

[106] J. P. Zbilut, and C. L. Webber Jr., Physics Letters A **171 (3-4)**, 199 (1992).

[107] J. P. Zbilut, A. Giuliani, and C. L. Webber Jr., Physics Letters A **246**, 122 (1998).

[108] J. P. Zbilut, M. Thomasson, and C. L. Webber Jr., Medical Engineering and Physics **24 (1)**, 53 (2002).

[109] J. P. Zbilut, D. D. Dixon, and M. Zak, Physics Letters A **304**, 95 (2002).

[110] G. Zimatore, S. Hatzopoulos, A. Giuliani, A. Martini, and A. Colosimo, Journal of Applied Physiology **92 (6)**, 2521 (2002).

[111] The Lorenz equations are given by

$$
\begin{aligned}
\dot{x} &= -\sigma x + \sigma y \\
\dot{y} &= -xz + rx - y \\
\dot{z} &= xy - bz
\end{aligned}
$$

For $\sigma = 10$ and $b = 8/3$ they display chaotic behavior.

Automatization of the Algorithm to Compute JK_2

To compute the joint Rényi entropy JK_2 (Eq. 3.12) in the whole range of parameters $\nu \in [-0.04, 0.04]$ and $\mu \in [0.0, 0.12]$, the algorithm based on JRPs (Eq. 3.10) has to be automated. First, the distribution of diagonal lines for different thresholds ε has to be computed, as the entropy is only well defined when a scaling region with ε is found. In the case of JRPs we have in general two thresholds ε_x and ε_y. We compute these two thresholds fixing the value of RR (Eq. 2.2) and applying the algorithm presented in Sec. 2.3. The crucial point in the automatization is the estimation of the scaling region of $\ln P_{RR}(l)$ vs. l and the plateau in $JK_2(RR)$ vs. RR. In both cases we apply a cluster dissection algorithm [85]. The algorithm divides the set of points into distinct clusters. In each cluster a linear regression is performed. The algorithm minimizes the sum of all square residuals in order to determine the scaling region and the plateau. To find both regions automatically, we use the following parameters:

- We consider only diagonal lines up to length $l_{max} = 400$. Longer lines are excluded because of finite size effects.

- We consider only values of $P_{RR}(l)$ with $P_{RR}(l) > 500$ for the same reason as in the last item.

- We use 40 different values for ε_x and ε_y, corresponding to 40 equally spaced recurrence rates RR between 1% and 95%, to have a good defined plateau in $K_2(RR)$ vs. RR.

- We use $10,000$ data points of each simulated trajectory. The more data points one uses, the more pronounced the scaling regions. Note that the computation time increases approximately with N^2.

- We have to specify for the applied cluster dissection algorithm the number of clusters in each run: for the detection of the scaling region in $\ln P_{RR}(l)$ vs. l, we choose 2 different clusters and use the slope of the largest cluster. For the detection of the plateau in $K_2(RR)$ vs. RR, we choose 3 clusters and use the value of the cluster with the minimum absolute slope.

These choices have proven to be rather appropriate for the estimation of the scaling regions. All these parameters are defaults of the computer program we have used. Furthermore, this automatization of the algorithm has been already successfully applied to the computation of the stability of trajectories of extrasolar planetary systems [7].